THESIS

EFFECT OF TAILINGS COMPOSITION ON THE SHEAR STRENGTH BEHAVIOR OF MINE WASTE ROCK AND TAILINGS MIXTURES

Submitted by

Megan M. Jehring

Department of Civil & Environmental Engineering

In partial fulfillment of the requirements

For the Degree of Master of Science

Colorado State University

Fort Collins, Colorado

Fall 2014

Master's Committee:

Advisor: Christopher A. Bareither

Charles D. Shackelford
Sally J. Sutton

ABSTRACT

EFFECT OF TAILINGS COMPOSITION ON THE SHEAR STRENGTH BEHAVIOR OF MINE WASTE ROCK AND TAILINGS MIXTURES

The objective of this study was to evaluate the effect of mine tailings composition on the shear behavior and shear strength of co-mixed mine waste rock and tailings (WR&T). Crushed gravel was used as a synthetic waste rock and mixed with four types of tailings: (1) fine-grained garnet, (2) coarse-grained garnet, (3) copper, and (4) soda ash. Co-mixed WR&T specimens were prepared to target mixture ratios of mass of waste rock to mass of tailings (*R*) such that tailings "just filled" inter-particle void space of the waste rock (R_{opt}) prepared at the maximum void ratio of waste rock alone. Triaxial compression tests were conducted on waste rock, tailings, and co-mixed specimens at effective confining stresses (σ'_c) of approximately 5, 10, 20, and 40 kPa. Low σ'_c were selected to assess performance of co-mixed WR&T in final earthen cover applications for waste containment facilities. Waste rock and co-mixed WR&T specimens were 150-mm in diameter by 300-mm tall, whereas tailings specimens were 38-mm in diameter by 76-mm tall. Waste rock was tested with drained and undrained conditions, whereas undrained conditions were used for tailings and co-mixed specimens to reduce testing duration.

Shear strength of the WR&T mixtures was comparable to that of waste rock alone. The effective stress friction angle (ϕ') of waste rock was 41°, whereas ϕ' of the tailings ranged from 34° (copper) to 41° (soda ash). The WR&T mixtures had an average ϕ' = 40° for fine-garnet mixtures and 39° for coarse-garnet and copper mixtures, which are similar to waste rock alone and suggests that the waste rock skeleton controlled shear strength of these mixtures. The soda ash mixtures had a slightly lower ϕ' of 38° compared to waste rock alone, which was attributed to clay-sized tailings particles lubricating contacts between waste rock particles.

Shear behavior of co-mixed WR&T was controlled by the tailings fraction when tailings were composed of silt and mixed to a ratio of $R < R_{opt}$. Waste rock controlled shear behavior of co-mixed WR&T when tailings were composed of sand or clay and mixed to a ratio of $R \geq R_{opt}$. At σ'_c = 5 kPa, the waste rock was entirely dilative, and transitioned to entirely contractive behavior at σ'_c = 40 kPa. In WR&T mixtures, potential contraction of the waste rock skeleton will transfer normal and shear stress to the tailings fraction within the waste rock void space. Thus, shear behavior of co-mixed WR&T specimens were dependent on composition of the tailings and the overall soil structure, which is a function of *R*.

The actual *R* for fine-garnet, copper, and soda ash mixtures was lower than the target ratio ($R < R_{opt}$) and corresponded to higher tailings content. An increase in tailings content creates a soil structure where tailings exist between inter-particle waste rock contacts and cause waste rock particles to “float” in a tailings matrix. Shear behavior of this co-mixed WR&T structure was dependent on composition of the tailings. Fine-garnet and copper mixtures expressed stronger dilative tendencies compared to tailings alone at all σ'_c, which was attributed to interlocking between waste rock and tailings particles. Soda ash tailings alone were purely contractive, and combining two contractive materials resulted in a contractive WR&T mixture.

The coarse-garnet tailings alone expressed strong dilative tendencies for all σ'_c, whereas coarse-garnet mixtures exhibited similar shear behavior to waste rock alone. The contractive tendencies of coarse-garnet mixtures was attributed to specimens prepared at $R > R_{opt}$, which likely prevented involvement of the tailings fraction in transferring normal and shear stresses.

The equivalent granular void ratio (e^*), based on the global void ratio (e_g) and tailings content, accurately characterized the soil structure of co-mixed WR&T by accounting for the contribution of tailings particles in transferring stress. The equivalent granular state parameter (ψ^*), determined using e^*, was able to capture the shear behavior of all waste mixtures. Shear strength behavior of co-mixed WR&T can be predicted using ψ^* provided *R*, e_g, and the steady state line of the WR&T mixture are known.

ACKNOWLEDGEMENTS

I would like to express my sincere gratitude to all those who have aided and guided me during my time at Colorado State University.

First, I would like to thank my advisor, Dr. Christopher Bareither, who provided constant support and guidance throughout my Master's program. His enthusiasm for geotechnical engineering was contagious and he kept me focused on the larger picture and avoided becoming lost in the minor details. I would also like to extend my thanks to Dr. Charles Shackelford and Dr. Sally Sutton for serving on my graduate committee.

Second, I am grateful to my fellow Master's student, Mohammad Gorakhki, for providing findings from his work on soda ash tailings which aided me during the analysis of my data. I also greatly appreciate him for putting up with my frequent interruptions and willingness to bounce ideas off each other. I would also like to thank Risa Benvenga for her assistance during triaxial testing and helpful comments on the initial draft of this thesis.

Last, but not least, I wish to thank my family for their continuous love and support throughout my entire academic career. My many siblings inspired me to be slightly different and study geotechnical engineering instead of electrical or chemical engineering. In particular, I would like to thank my sister, Kristin, who encouraged me to pursue a graduate education. I am deeply indebted to my parents without whom I would not be where I am today. I would especially like to thank my father who always reminded me that rocks are hard.

TABLE OF CONTENTS

LIST OF TABLES

LIST OF FIGURES

LIST OF SYMBOLS

A	Skempton's pore pressure parameter	e_r	waste rock void ratio
A_c	corrected specimen cross sectional area	e_{SS}	steady state void ratio
A_{ce}	final cross sectional area of the shear plane	e_t	tailings void ratio
A_f	specimen cross sectional area at formation of the shear plane	e^*	equivalent granular void ratio
b	fraction of fines active in transferring forces	$e_{\lambda,SS}$	fitting constant to determine location of the steady state line
C_c	compression index	f	friction between the membrane and the soil
c'	effective cohesion	f_c	fines content
c_v	coefficient of consolidation	f_{thres}	threshold fines content
D_{10}	coarse fraction particle diameter at 10% finer	G_s	specific gravity
d_{50}	fine fraction particle diameter at 50% finer	$G_{s,c}$	specific gravity of coarse fraction
d_a	final specimen diameter and major axis of an ellipse	$G_{s,f}$	specific gravity of fines fraction
d_b	minor axis of an ellipse	$G_{s,r}$	specific gravity of waste rock
d_{im}	initial inner diameter of the membrane	$G_{s,t}$	specific gravity of tailings
d_{max}	maximum particle size	H:D	specimen height-to-diameter ratio
d_o	initial specimen diameter	h_o	initial specimen height
E	modulus of elasticity of the membrane	K_f line	failure line in p'-q space
e	void ratio	k	hydraulic conductivity
e_g	global void ratio	LL	liquid limit
e_i	initial void ratio	M_r	mass of waste rock
e_{max}	maximum void ratio	M_t	mass of tailings
e_{min}	minimum void ratio	$M_{w,r}$	mass of water in waste rock

PI	plasticity index	Δh	change in height
p'	mean effective stress	Δh_t	total change in height
p_{om}	additional lateral stress applied by the membrane	ΔV	change in volume
R	mixture ratio	$\Delta\sigma_d$ or q	deviator stress
R_{opt}	optimum mixture ratio	$\Delta\sigma_{d,corr}$	corrected deviator stress
SL	shrinkage limit	$\Delta\sigma_{d,max}$	maximum deviator stress
t	membrane thickness	δ	strain developed along the shear plane
u_e	excess pore pressure	δ_e	final strain developed along the shear plane
$u_{e,max}$	maximum excess pore pressure	ε_a	axial strain
V_a	volume of air	ε_{ae}	axial strain at critical state
V_o	initial volume	ε_{af}	axial strain at failure
V_s	volume of solids	ε_v	volumetric strain
V_{slurry}	volume of tailings slurry	λ	slope of the steady state line
$V_{s,r}$	volume of waste rock	$\rho_{s,r}$	density of waste rock particles
$V_{s,t}$	volume of tailings	$\rho_{s,t}$	density of tailings particles
V_v	volume of voids	ρ_{slurry}	density of tailings slurry
$V_{v,r}$	volume of voids in waste rock	ρ_w	density of water
V_w	volume of water	σ'_o	initial effective stress
$V_{w,r}$	volume of water in waste rock	σ'_1	effective major principle stress
w	water content	σ_{1corr}	corrected major principle stress
w_r	waste rock water content	σ_{1m}	additional major principle stress contributed by the membrane
w_t	tailings water content	σ'_3	effective minor principle stress
Δd	length the shear plane extends beyond the specimen	σ_{3corr}	corrected minor principle stress

σ_{3m}	additional minor principle stress contributed by the membrane	ϕ'	effective friction angle
$(\sigma'_1/\sigma'_3)_{max}$	maximum principle stress ratio	ϕ'_{cs}	effective critical state friction angle
σ'_c	effective confining stress	ψ	state parameter
σ_v	vertical stress	ψ^*	equivalent granular state parameter

CHAPTER 1: INTRODUCTION

1.1 Problem Statement

Mine operations generate vast amounts of waste materials as a result of ore extraction and refining processes. Two types of mine waste that require short- and long-term management are tailings and waste rock (Bussière 2007; Blight 2010). Tailings typically are composed of fine-grained particles (≤ 0.075 mm) and disposed as a slurry (i.e., high water content) in impoundment facilities. Waste rock usually is managed in piles and predominantly contains gravel-sized particles with some sand and fines (Bussière 2007). Management of tailings and waste rock requires large areas of land and potentially can generate acid rock drainage (ARD) if sulfide minerals are present. Management of tailings also includes challenges related to high compressibility potential and low shear strength, which are typical engineering characteristics of mine tailings (Qiu and Sego 2001; Bussière 2007; Wickland et al. 2010).

Co-disposal of waste rock and tailings (WR&T) has been proposed as an alternative mine waste management approach to address impoundment stability and ARD concerns as well as reduce storage volume and land required for waste management facilities (e.g., Williams et al. 2003; Wickland and Wilson 2005; Li et al. 2011). Co-mixed WR&T enhances strength and reduces compressibility of tailings, while decreasing the permeability of waste rock to improve overall impoundment stability and limit infiltration and migration of water and oxygen (Bussière 2007, Wickland et al. 2010). Alternatively, WR&T can be reused in geoengineering applications, and in particular, in water-balance covers for waste containment facilities (e.g., Fines et al. 2003; Williams et al. 2003). In a water-balance cover system, co-mixed WR&T can serve as a water storage layer that limits infiltration of water and oxygen to reduce mine waste leachate and generation of ARD. Beneficial reuse of mine waste also reduces the final mine waste volume for disposal and long-term management (Wilson et al. 2003; Wilson et al. 2009).

Knowledge of geotechnical properties of mine waste, including moisture retention and shear strength, is necessary to design and optimize performance of water-balance covers. Shear strength parameters (e.g., friction angle and cohesion intercept) are necessary for final cover design and slope stability analysis. A limited number of laboratory- and field-scale studies (e.g., Leduc et al. 2004; Khalili et al. 2010; Wickland et al. 2010) have been conducted to characterize the geotechnical properties of co-mixed WR&T (e.g., permeability and shear strength). Results from these studies indicate that shear strength of co-mixed WR&T is dominated by the waste rock when waste rock particles form a skeleton with continuous inter-particle contacts throughout the mixed material. As tailings content of a given mixture increased, shear strength decreased and approached comparable shear strength of the tailings. However, studies have been limited to evaluation of a single source of waste rock and tailings (Khalili et al. 2010; Wijewickreme et al. 2010) and varying material characteristics of waste rock and tailings likely yield different geotechnical behavior and properties.

1.2 Research Objectives and Tasks

The objective of this study was to evaluate shear strength of co-mixed WR&T and to assess the effect of tailings composition on shear behavior of mine waste mixtures. A synthetic waste rock composed of crushed gravel was used as a control during testing, which also negated acid generation from oxidation of sulfide minerals commonly present in mine waste rock. Waste rock was mixed with four different types of tailings: (1) fine-grained garnet tailings, (2) coarse-grained garnet tailings, (3) copper tailings, and (4) soda ash tailings. These mine tailings represent a broad range in mineralogical composition, particle size, and soil plasticity.

The following research tasks were completed as part of this study:

1. Identified an optimum mixture ratio of waste rock to tailings where tailings “just fill” the waste rock void space for each tailings source and created homogeneous mixtures;
2. Developed specimen preparation procedures for waste mixtures and tailings slurries to create uniform, repeatable specimens for triaxial (TX) testing at low effective confining stresses (σ'_c);
3. Evaluated shear strength behavior of waste rock and tailings separately to establish a baseline for comparison with mixture materials;
4. Evaluated shear strength behavior of co-mixed WR&T; and
5. Compared shear strength properties and behavior to literature on other mine waste mixtures and soil mixtures to evaluate the effect of tailings composition on shear strength and shear behavior.

Triaxial compression testing was used to measure shear strength parameters and shearing behavior of waste rock, tailings, and co-mixed WR&T. Consolidated drained (CD) and consolidated undrained (CU) triaxial tests were conducted on waste rock, whereas only CU tests were conducted on tailings and WR&T mixtures due to anticipated low permeability of the tailings. Tailings specimens were formed from slurries to represent deposition conditions in impoundment facilities. Waste rock and WR&T were tested with waste rock near the maximum void ratio. In the mixture specimens, tailings “just filled” the void space of the waste rock skeleton, which represents an ideal, homogeneous mixture of WR&T (Wickland et al. 2006). Triaxial compression tests on all materials were conducted at σ'_c = 5, 10, 20, and 40 kPa to capture anticipated effective stresses in water-balance covers under saturated conditions (Albright et al. 2010).

CHAPTER 2: BACKGROUND

This study primarily focused on the shear strength behavior of hard rock tailings mixed with waste rock. Description of mine waste properties, mine waste management, and field and laboratory case studies are provided to capture the state-of-art- and state-of-practice of co-mixed WR&T. A discussion on shear strength considerations and behavior also is included to describe shear strength of waste rock and gravel, shear behavior of silt, and fundamental soil mechanics relationships used throughout this study.

2.1 Mine Waste

2.1.1 Typical Characteristics and Properties

A compilation of geotechnical characteristics and engineering properties of common mine wastes is in Table 2.1. A range and average particle-size distribution (PSD) for waste rock and tailings are shown in Fig. 2.1. Mine waste rock typically is composed of coarse-grained angular rock particles as a result of ore extraction, and is characterized by low compressibility, high shear strength, and high permeability (Wilson et al. 2003; Khalili et al. 2010; Wickland et al. 2010). Waste rock generally has effective stress friction angles (ϕ') greater than 40° and saturated hydraulic conductivity (k) on the order of 10^{-3} cm/s (Table 2.1). Tailings are composed of sand-, silt-, and clay-sized particles and frequently are deposited as a slurry at high water contents (e.g., 120 – 300 %). Hard rock mine tailings generally classify as low plasticity materials, with liquid limit (*LL*) ranging from 20 to 40 % and plasticity index (*PI*) ranging from 1.5 to 16 % (Table 2.1). The slurry nature of tailings can lead to high compressibility and low shear strength (Bussière 2007; Wickland et al. 2010). Tailings generally have lower shear strength ($30° \leq \phi' \leq 35°$) and lower k (10^{-5} to 10^{-7} cm/s) compared to waste rock (Table 2.1.)

2.1.2 Overview of Mine Waste Management and Co-Disposal

Geotechnical properties of waste rock and tailings create challenges for management and storage of mine waste. The high shear strength of waste rock facilitates disposal in large piles; however, high permeability and low water retention of waste rock create an environment conducive to acid rock drainage (ARD) when sulfide minerals are present (Wilson et al. 2000; Wickland et al. 2006). Tailings usually are stored in impoundment facilities that can occupy considerable areal extent when disposed as a slurry. High compressibility, low *k*, and low shear strength of tailings render impoundment facilities prone to liquefaction and potential failure (Williams and Kuganathan 1993; Wickland and Wilson 2005; Bussière 2007). Co-disposal of waste rock and tailings (WR&T) is a mine waste management alternative to mitigate risks associated with impoundment stability and ARD (Wilson et al. 2003; Wickland and Wilson 2005; Wickland et al. 2006; Khalili et al. 2010; Wickland et al. 2010).

Waste rock and tailings can be co-disposed through layering, co-mingling, or co-mixing (Wickland et al. 2006; Bussière 2007; Li et al. 2011). Layering involves placing thin layers of tailings (≤ 1 m) over lifts of waste rock. A capillary barrier effect develops at the waste rock-tailings interface, which limits ingress of water and oxygen to reduce ARD (Williams et al. 2003; Wilson et al. 2003; Wickland and Wilson 2005; Bussière 2007). Co-mingling can be achieved by constructing waste rock embankments and dikes within a tailings impoundment. The waste rock increases pore water drainage from the tailings to accelerate tailings consolidation and strength gain (Wickland et al. 2006; Bussière 2007). Co-mixing tailings and waste rock such that tailings fill the void space of waste rock yields a more homogenous waste mixture compared to other co-disposal methods. Co-mixed WR&T combines high strength and low compressibility of waste rock with low permeability and high water retention of tailings to improve stability and reduce ARD (Wickland et al. 2006).

Field-scale experiments have been conducted to evaluate the performance of layered co-disposal and co-mixed WR&T (e.g., Morris and Williams 1997; Leduc et al. 2004; Li et al.

2011). Layered co-disposal was shown feasible at the Cerro de Maimón mine in the Dominican Republic. Placement of tailings between lifts of waste rock expedited tailings consolidation and increased strength and stability of the storage facility (Li et al. 2011). Creation of co-mixed WR&T at field-scale can be achieved via injection of tailings into waste rock, blending waste materials at an active disposal area, pumping waste materials together to a storage facility, or mixing with a dozer or excavator (Morris and Williams 1997; Leduc et al. 2004; Bussière 2007). Mixing and placement of mine waste in small volumes has been effective in creating homogenized WR&T mixtures (Wickland and Wilson 2005; Khalili et al. 2010; Wickland et al. 2010); however, field-scale techniques still are evolving and in need of future research to facilitate adoption in practice.

2.1.3 Previous Studies on Co-Mixed WR&T

A limited number of laboratory studies have been conducted on co-mixed WR&T. Wickland and Wilson (2005) and Wickland et al. (2010) performed experiments to determine compression and hydraulic properties of waste rock and tailings from a gold mine in Papua New Guinea. Hydraulic conductivity of the mixtures was 4×10^{-6} cm/s one order of magnitude lower than waste rock alone (3×10^{-3} cm/s) and more comparable with k of the tailings (3×10^{-6} cm/s). The waste rock and co-mixed WR&T had comparable settlement for similar applied vertical stress, and the presence of waste rock in the mixtures suppressed the magnitude and duration of consolidation settlement relative to that of the tailings. These results suggest that k of the WR&T mixtures is controlled by the tailings and compression behavior is controlled by the waste rock.

The waste rock-to-tailings mixture ratio (R) is defined as the ratio of dry mass of waste rock (M_r) to dry mass of tailings (M_t) (Wickland et al. 2006):

$$R_{opt} = \frac{M_r}{M_t} \tag{2.1}$$

Relationships between ϕ' and *R* from Leduc et al. (2004) and Khalili et al. (2010) are shown in Fig. 2.2. The same mine waste materials from Wickland et al. (2005, 2010) were used by Khalili et al. (2010) and Wijewickreme et al. (2010) to evaluate static and cyclic shear behavior. The effective peak friction angle of the mixture (40.5°) was similar to that of waste rock alone (41.7°), whereas tailings alone had ϕ' = 30.6° (Fig. 2.2). Leduc et al. (2004) observed that shear strength of co-mixed WR&T transitioned from being controlled by tailings at low R-ratios to controlled by waste rock at high *R* ratios. This transition occurred as waste rock particles formed continuous inter-particle contacts throughout the mixture and ultimately controlled ϕ' (Fig. 2.2).

Field-scale experiments have been performed on co-mixed WR&T used as a water balance cover (e.g., Eger et al. 1984; Wilson et al. 2003; Wilson et al. 2009). These studies demonstrated that layers of mixed WR&T can retain water and act as a water storage layer to decrease infiltration through a cover system. Eger et al. (1984) constructed bins of mixed WR&T and measured metal concentrations in effluent. Co-mixed WR&T had a 33 to 66 % reduction in metal concentration compared to control bins constructed only from waste rock. Wilson et al. (2003) reported that co-mixed WR&T has suitable *k* (10^{-6} to 10^{-7} cm/s) and air entry pressure (30 to 100 kPa) to reduce desiccation and oxygen infiltration, but noted that both waste rock and tailings may require additional treatment to remove sulfide minerals (e.g., desulfurization) to effectively prevent ARD. Wilson et al. (2009) constructed water-balance covers from uncompacted and compacted co-mixed mine waste over a copper tailings impoundment and measured cumulative infiltration using field lysimeters. The compacted cover had no measureable infiltration and the uncompacted cover limited cumulative infiltration to 125 mm, which was 75 % less than uncovered tailings.

2.1.4 Mixture Theory

Designing mixtures of WR&T requires the PSD and water content (w) of waste rock and tailings as well as R. Schematics of different particle structures for co-mixed WR&T are shown in Fig. 2.3. The optimum mixture ratio (R_{opt}) is defined as the ratio where tailings "just fill" void space of the waste rock skeleton. This optimum mixture ratio can provide the necessary shear strength and hydraulic properties for use in final cover systems that are designed on water balance principles (e.g., Wilson et al. 2003; Kahlili et al. 2010). As the mixture ratio increases ($R > R_{opt}$), the particle structure becomes increasingly dominated by waste rock particles with tailings contained within the void space of the waste rock skeleton. As the mixture ratio decreases ($R < R_{opt}$), the amount of tailings increases and waste rock particles transition to acting as inclusions in a matrix of tailings (Fig. 2.3).

A phase diagram of co-mixed WR&T is shown in Fig. 2.4. The phase diagram can be used to determine void ratio (e) for a given R provided mass and volume of each phase are known. Three void ratios can be defined for co-mixed WR&T: (1) e_g = global void ratio, (2) e_r = void ratio of the waste rock skeleton, and (3) e_t = void ratio of the tailings matrix. These void ratios are used to characterize particle structure and density of a mixture (Thevanayagam 1998; Wickland et al. 2006). Using the phase diagram from Fig. 2.4, the void ratios are obtained as follows:

$$e_g = \frac{V_v}{V_s} = \frac{V_a + V_w}{V_{s,r} + V_{s,t}} \tag{2.2}$$

$$e_r = \frac{V_a + V_w + V_{s,t}}{V_{s,r}} \tag{2.3}$$

$$e_t = \frac{V_a + V_w}{V_{s,t}} \tag{2.4}$$

where V_v = volume of voids, V_a = volume of air, V_w = volume of water, V_s = volume of solids, $V_{s,r}$ = volume of waste rock, and $V_{s,t}$ = volume of tailings. Development of these void ratio definitions is based on assumptions that (i) waste rock, tailings, and water are incompressible, (ii) the mass of air is negligible, and (iii) waste rock void spaces have larger average diameters than tailings solids such that tailings are retained within the waste rock void space.

The volumetric proportions of water, air, tailings solids, and waste rock solids as well as e_g, e_r, and e_t as a function of R are shown in Fig. 2.5 for the fine-garnet tailings and waste rock used in this study. Properties of these materials are discussed in Chapter 3. The R_{opt} coincides with saturated tailings that completely fill void space of the waste rock such that V_a = 0 (Fig. 2.5a). At a mixture ratio of R_{opt}, e_g is a minimum, which indicates maximum density of the mixture occurs at R_{opt}. Increasing the volumetric contribution of either tailings or waste rock solids will increase e_g (Fig. 2.5b). The waste rock void ratio is at the maximum void ratio (e_{max}) when tailings "just fill" the waste rock void space and all larger R. As R decreases below R_{opt}, e_r becomes greater than e_{max}, which only is possible if tailings and corresponding air and water phases are considered to remain within the waste rock void space. The actual soil fabric for this condition corresponds to waste rock particles "floating" in a tailings matrix (Fig. 2.3 for $R < R_{opt}$). Increasing R above R_{opt} causes an increase in e_t due to a decrease in $V_{s,t}$ and an increase in V_a and V_w (Eq. 2.4). For this condition, the air and water phase partially will be retained between waste rock particles rather than completely within the tailings.

The optimum mixture ratio can be determined based on phase relationships using e_r, waste rock water content (w_r), tailings water content (w_t), specific gravity of waste rock ($G_{s,r}$), and specific gravity of tailings ($G_{s,t}$). The optimum mixture ratio determined for each tailings source is summarized in Table 2.2. Assuming a unit volume of waste rock particles (i.e., $V_{s,r}$ = 1 m^3) and density of water (ρ_w) = 1000 kg/m^3, the volume of voids of the waste rock skeleton ($V_{v,r}$) and M_r can be found using Eqs. 2.5 and 2.6:

$$M_r = V_{s,r} \cdot G_{s,r} \cdot \rho_w = V_{s,r} \cdot \rho_{s,r} \tag{2.5}$$

$$V_{v,r} = V_{s,r} \cdot e_r \tag{2.6}$$

where $\rho_{s,r}$ = density of waste rock particles. The mass ($M_{w,r}$) and volume ($V_{w,r}$) of water contained in the waste rock can be calculated using Eqs. 2.7 and 2.8.

$$M_{w,r} = w_r \cdot M_r \tag{2.7}$$

$$V_{w,r} = \frac{M_w}{\rho_w} \tag{2.8}$$

The density of the tailings slurry (ρ_{slurry}) can be derived from w_t, $G_{s,t}$, and density of tailings particles, $\rho_{s,t}$ (= $G_{s,t} \cdot \rho_w$) as shown in Eq. 2.9.

$$\rho_{slurry} = \frac{(1+w_t)\rho_{s,t}}{1+w_t \cdot G_{s,t}} \tag{2.9}$$

The volume of tailings slurry (V_{slurry}) required to fill the waste rock void space is the difference between $V_{v,r}$ and $V_{w,r}$. Mass of tailings can be calculated using V_{slurry}, ρ_{slurry}, and w_t as in Eq. 2.10.

$$M_t = \frac{\rho_{slurry} \cdot V_{slurry}}{1+w_t} = \frac{\rho_{slurry} \cdot (V_{v,r} - V_{w,r})}{1+w_t} \tag{2.10}$$

Equations 2.5 through 2.10 can be combined to determine R_{opt} as shown in Eq. 2.11.

$$R_{opt} = \frac{M_r}{M_t} = \frac{\rho_{s,r} \cdot V_{s,r}}{\dfrac{\rho_{slurry} \cdot V_{slurry}}{1+w_t}} = \frac{\rho_{s,r} \cdot V_{s,r}}{\dfrac{\rho_{slurry} \cdot (V_{v,r} - V_{w,r})}{1+w_t}} \tag{2.11}$$

Assuming no water is contained in the waste rock void space (i.e., $V_{w,r}$ = 0 and $V_{slurry} = V_{v,r} = V_{s,r} \cdot e_r$), Eq. 2.11 is simplified to Eq. 2.12.

$$R_{opt} = \frac{M_r}{M_t} = \frac{\rho_{s,r} \cdot V_{s,r}}{\dfrac{\rho_{slurry} \cdot e_r \cdot V_{s,r}}{1+w_t}} = \frac{\rho_{s,r}}{\dfrac{\rho_{slurry} \cdot e_r}{1+w_t}} \tag{2.12}$$

2.2 Shear Strength Behavior

2.2.1 Shear Strength and Parallel Gradation of Gravel and Waste Rock

Testing materials with large particles sizes can be challenging due to specimen diameter-to-particle size constraints. Triaxial testing standards (e.g., ASTM D 4767) specify a specimen diameter-to-d_{max} ratio of at least 6:1. Waste rock can have particles with d_{max} > 100 mm (Fig. 2.1), which requires large, specially designed laboratory equipment for strength evaluation. Waste rock specimens can be scalped to remove larger particles to facilitate testing in traditional-sized laboratory equipment (Khalili et al. 2010). However, scalping changes the PSD of the material. Marachi et al. (1972) showed the parallel gradation can be an effective method to prepare and test materials with large particle sizes at laboratory scale. In the parallel gradation technique, a scale factor is applied to a given PSD to shift the PSD to smaller particle diameters while maintaining the original gradation of the material. Marachi et al. (1972) report that triaxial compression tests performed on the same material with varying d_{max} yielded similar ϕ'. The technique also has been applied to waste rock and similar shear strength was measured for large scale (150-mm-diameter) and conventional scale (70-mm-diameter) triaxial compression specimens (Stoeber et al. 2012).

2.2.2 Shear Behavior of Nonplastic Silts

The shear behavior of nonplastic silt is different from the shear behavior of sand and clay. Sand and clay will contract when prepared loosely or normally consolidated and dilate when prepared dense or over-consolidated; however, nonplastic silt tends to dilate during shear and develop negative excess pore pressures (u_e) with increasing axial strain (ε_a) regardless of whether the silt is normally or over-consolidated (Brandon et al. 2006). The tendency for dilation is controlled by e and the initial effective stress (σ'_o). Specimens at a higher density generally have a greater tendency to dilate at a given effective stress (Penman 1953).

The dilative tendencies of nonplastic silt pose a variety of challenges in triaxial compression testing. Cavitation may occur as ε_a increases and u_e becomes increasingly negative, particularly for tests conducted at low effective confining stress (σ'_c). During cavitation, air will come out of solution in the pore water and cause the specimen to desaturate. Desaturation will increase total specimen volume and increase effective stress due to soil suction, which will cause failure to occur at a higher strength with an apparent cohesion intercept (*c*) (Penman 1953). Brandon et al. (2006) recommended using higher than necessary back-pressures to saturate silt specimens to ensure a sufficient pore pressure to maintain specimen saturation.

The dilative behavior of nonplastic silt can make defining failure difficult and a variety of failure criteria are identified in Fig. 2.6 on an idealized effective stress path for silt in triaxial compression. Brandon et al. (2006) outlined the following six criteria to define failure in triaxial testing: (1) maximum deviator stress, $\Delta\sigma_{d,max}$; (2) maximum principle stress ratio, $(\sigma'_1/\sigma'_3)_{max}$; (3) maximum excess pore pressure, $u_{e,max}$; (4) Skempton's pore pressure parameter (A) equal to zero; (5) stress path reaches the failure (K_f) line in p'-q space; and (6) limiting axial strain (e.g., ε_a = 5 or 10 %). Failure criterion of A = 0 yielded consistent values for ϕ' from triaxial tests conducted on Yazoo silt and Lower Mississippi Valley Division silt by Brandon et al. (2006). Wang and Luna (2012) performed triaxial tests on Mississippi River Valley silt and reported similar ϕ' using failure criteria of $\Delta\sigma_{d,max}$, $(\sigma'_1/\sigma'_3)_{max}$, and ε_a = 15 %.

2.2.3 State Parameter

The state parameter (ψ) was introduced by Been and Jefferies (1985) to describe the shear behavior of sand and is useful at extreme values of σ'_c, e.g., dense sands tested at high enough σ'_c can contract and behave similarly to a loose sand. A schematic showing the definition of ψ in void ratio-stress space is presented in Fig. 2.7. The state parameter considers the effects of specimen density and σ'_c and is defined as the difference between the initial void ratio (e_i) and the void ratio at steady state (e_{SS}) for a given σ'$_c$. Been and Jefferies (1985) identified steady state when there was no additional change in volume, pore pressure, and deviator stress with continued specimen deformation. The state parameter can also be viewed as the vertical difference between the normally consolidated line (NCL) and the steady state line (SSL), which are parallel in void ratio-stress space (Fig. 2.7). The specimen will dilate during shear for ψ < 0 (NCL is below SSL) and will contract for ψ > 0 (NCL is above SSL).

Determining ψ for undrained conditions is more challenging since the void ratio is constant during shear. The initial mean effective stress (p') is used to predict e_{SS}, which then is used to calculate ψ. The mean effective stress is defined as:

$$p' = \frac{\sigma_1' + 2\sigma_3'}{3} \tag{2.13}$$

where σ'$_1$ = major effective principle stress and σ'$_3$ = minor effective principle stress. The state parameter for an undrained test can be denoted as ψ(0), where (0) reflects the basis on initial conditions (Rahman and Lo 2014). Predicting e_{SS} requires an e-p' relationship to characterize the SSL. This relationship can be derived by fitting a logarithmic function to steady state points obtained from a series of undrained tests performed at varying e and σ'$_c$ (Schofield and Wroth 1968; Been and Jefferies 1985).

The state parameter initially was developed for clean sands but also can be applied to sands containing fines. Been and Jefferies (1985) conducted a series of undrained tests on a uniform, medium sand with fines contents (f_c) between 0 and 10 % and demonstrated that the slope of the SSL increases with increasing f_c. A small change in f_c can alter the location of the SSL, and thus, the SSL must be defined for each f_c (Rahman and Lo 2014; Rahman et al. 2014). Additionally, e_g for sand-fines mixtures may not accurately characterize the specimen density (Chu and Leong 2002; Carraro et al. 2009; Rahman et al. 2014). Rahman et al. (2014) introduced the equivalent granular state parameter (ψ*) to avoid determining the SSL for each

f_c. The equivalent granular void ratio (e^*) is used in place of e_g to calculate ψ using an equation proposed by Thevanayagam et al. (2002) that assumes equal G_s for coarse and fine fractions:

$$e^* = \frac{e_g + f_c(1-b)}{1-f_c(1-b)} \tag{2.14}$$

where b = fraction of fines active in transferring forces, which ranges from 0 to 1.

The materials tested in this study had a broad range in G_s (2.51 to 3.07, discussed in Chapter 3); therefore, the assumption of equal G_s for coarse and fine fractions proposed by Thevanayagam et al. (2002) could not be applied. When accounting for different G_s, Eq. 2.14 becomes,

$$e^* = \frac{e_g \cdot G_{s,c} + \left[f_c(1-b)\right]\left(G_{s,f} + e_g \cdot G_{s,f} - e_g \cdot G_{s,c}\right)}{G_{s,c}\left[1-f_c(1-b)\right]} \tag{2.15}$$

where $G_{s,c}$ = specific gravity of the coarse fraction (e.g., waste rock) and $G_{s,f}$ = specific gravity of the fine fraction (e.g., tailings).

Rahman et al. (2008, 2009) developed an empirical equation for determining b based on PSDs of the coarse and fine materials:

$$b = \left[1-\exp\left(-0.3\frac{(f_c / f_{thres})}{k}\right)\right]\cdot\left(r\frac{f_c}{f_{thres}}\right)^r \tag{2.16}$$

where f_{thres} = threshold fines content where the soil structure changes from a coarse-grained skeleton filled with fines to coarse particles in a fine-grained matrix, $k = 1 - r^{0.25}$, $r = (D_{10}/d_{50})^{-1}$, D_{10} = coarse particle diameter at 10 % passing, and d_{50} = fines particle diameter at 50 % passing. The threshold fines content also can be defined as the fines content corresponding to R_{opt}. These two parameters are related through Eq. 2.17.

$$f_{thres} = \frac{1}{1+R_{opt}} \tag{2.17}$$

The SSL can be characterized in terms of e^* by converting the global void ratio at the end of consolidation to e^* and following the procedure for CU tests discussed previously.

Table 2.1. Compilation of geotechnical characteristics and engineering properties of mine waste rock and tailings.

Material	G_s	*LL* (%)	*PI* (%)	*SL* (%)	USCS	*k* (cm/s)	C_c	c_v (m^2/yr)	ϕ'^{a} (°)	c'^{a} (kPa)	Reference
Uranium tailings	2.77 – 2.81	25-40	0-10	NR	SM – ML	1.0×10^{-8} – 1.0×10^{-3}	0.05 – 0.48	NR	34 – 46	NA	Matyas et al. (1984)
Coal tailings	1.69 – 2.28	NR	NR	NR	NR	NR	NR	NR	NR	NR	Morris and Williams (1995)
Coal waste rock	1.92 – 2.59	N/A	N/A	N/A	NR	NR	NR	NA	NR	NR	
Hard rock tailings	2.78 – 2.87	18	0	NR	SM – ML	1.3×10^{-5} – 2.1×10^{-4}	0.05 – 0.13	3.44 – 50.8	NR	NR	Aubertin et al. (1996)
Coal tailings	1.94	40	16	21.1	CL	4.0×10^{-7} – 1.1×10^{-5}	0.37 – 0.40	1.48 – 17.3	32	10	Qiu and Sego (2001)
Copper tailings	2.75	N/A	N/A	24.4	SM	4.5×10^{-5} – 9.8×10^{-5}	0.06 – 0.09	22.3 – 104	34	0	
Oil sand tailings	2.60	N/A	N/A	25.2	SM	2.2×10^{-7} – 6.3×10^{-7}	0.27 – 0.32	0.310 – 8.46	30	3	
Gold tailings	3.17	N/A	N/A	21.6	ML	2.7×10^{-5} – 6.7×10^{-5}	0.08 – 0.16	13.6 – 80.1	33	0	
Gold tailings	2.89	33	12	NR	CL	3.0×10^{-6}	0.53 – 1.9	6.30 – 30.0	30.6	0	Wickland and Wilson (2005); Wickland et al. (2010); Khalili et al. (2010)
Gold waste rock	2.70	NA	NA	NA	GW	3.0×10^{-3}	NA	NA	41.7	0	
Bauxite residue	3.05	54	14	NR	MH	NR	0.41	NR	42.0	10 – 20	Newson et al. (2006)
Gold tailings	2.89	23	1.5	18	ML	NR	NR	NR	31.9	0	Dailiri et al. (2014)

Note: G_s = specific gravity; *LL* = liquid limit; *PI* = plasticity index; *SL* = shrinkage limit; USCS = Unified Soil Classification System; *k* = saturated hydraulic conductivity; C_c = compression index; c_v = coefficient of consolidation; ϕ' = effective stress friction angle; *c'* = effective stress cohesion intercept; NR = not reported; NA = not applicable.

[a] Shear strength parameters obtained from undrained triaxial compression tests.

Table 2.2. Optimum mixture ratio and corresponding fines content for each mine tailings used in this study.

Tailings	Optimum Mixture Ratio (R_{opt})	Fines Content (%)
Fine-Garnet	2.45	29.0
Coarse-Garnet	2.12	32.0
Copper	3.04	24.8
Soda Ash	5.75	14.8

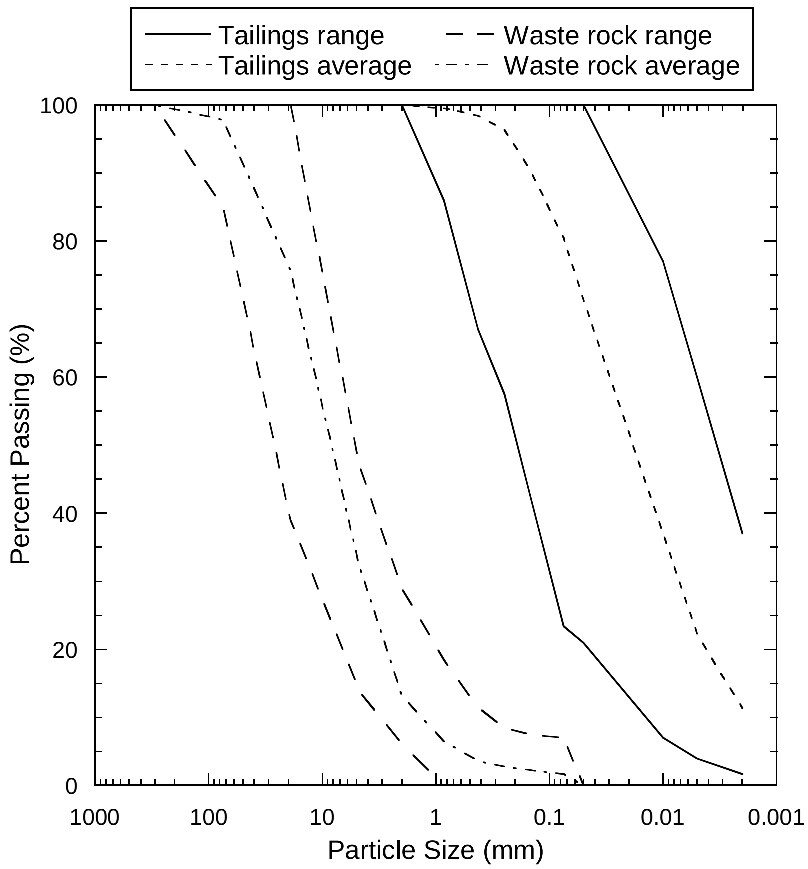

Fig. 2.1. Range and average particle-size distributions for mine tailings and waste rock compiled from Qiu and Sego (2001), Morris and Williams (2005), Khalili et al. (2005), Wickland and Wilson (2005), Wickland et al. (2006) Bussière (2007), Khalili et al. (2010), and Wickland et al. (2011).

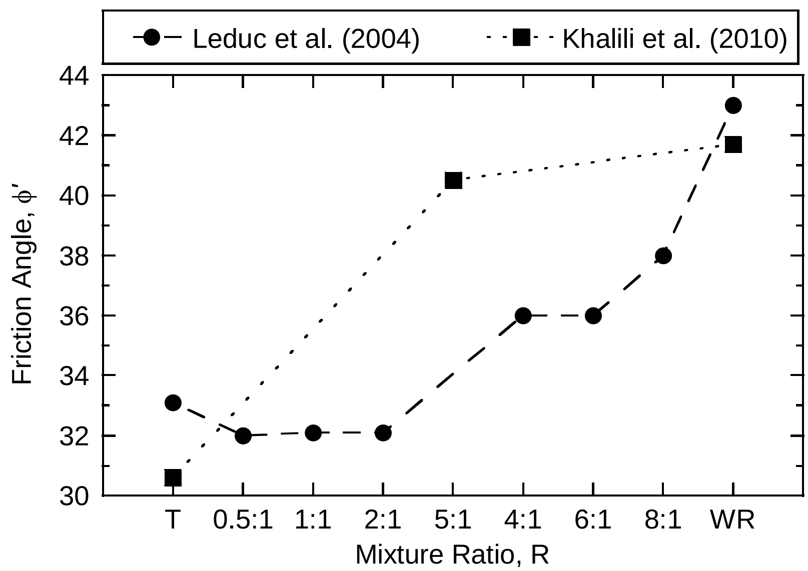

Fig. 2.2. Relationship between effective stress friction angle (ϕ') and mixture ratio (*R*) of waste rock (WR) to tailings (T), based on dry mass. Data obtained from Leduc et al. (2004) and Khalili et al. (2010).

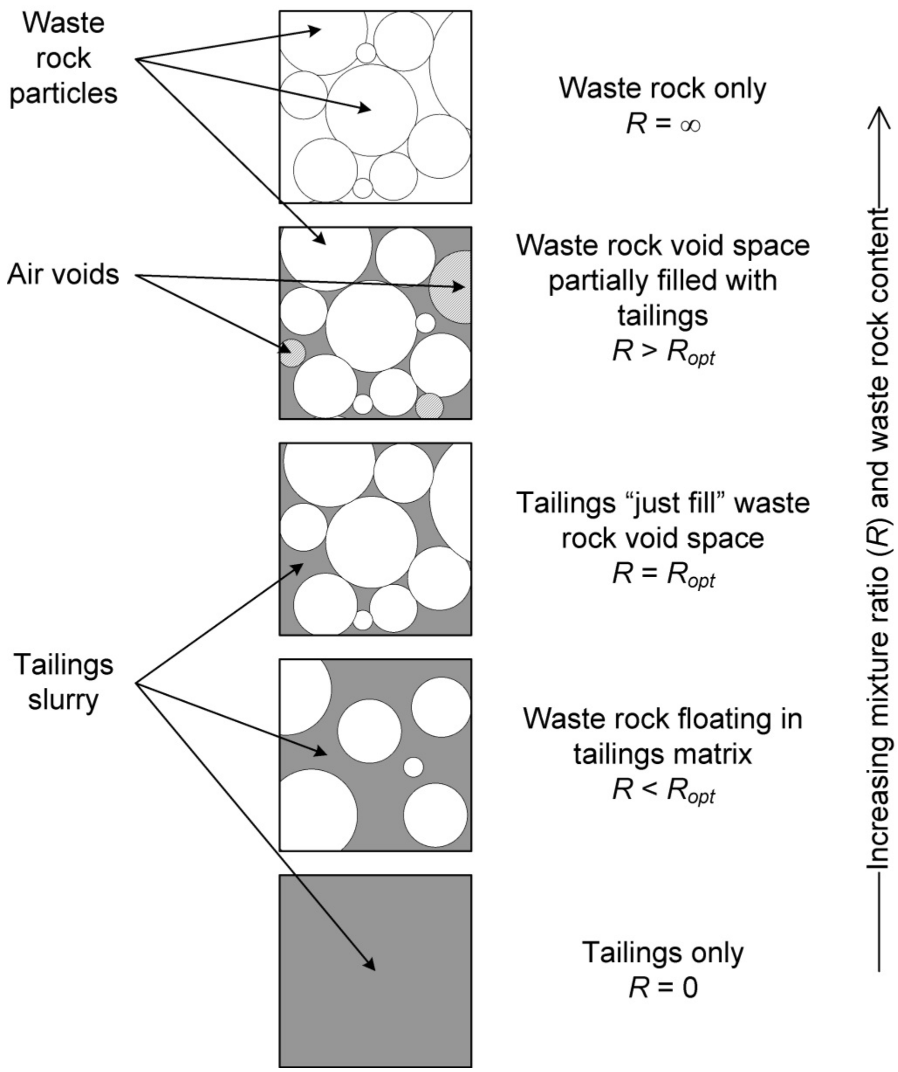

Fig. 2.3. Particle structure of co-mixed waste rock and tailings for different mixture ratios, R. Adapted from Wickland et al. (2006).

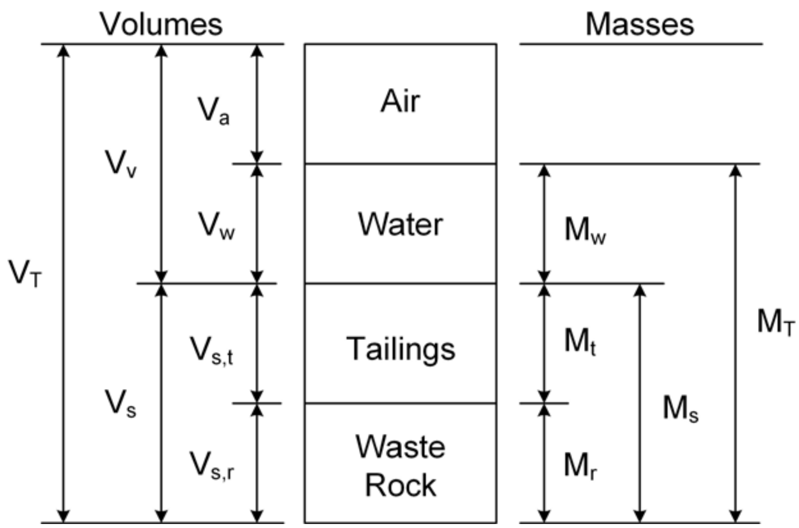

Fig. 2.4. Phase diagram for mixtures of waste rock and tailings. Adapted from Wickland et al. (2006). Definitions: V_T = total volume, V_v = volume of voids, V_s = volume of solids, V_a = volume of air, V_w = volume of water, $V_{s,t}$ = volume of tailings solids, $V_{s,r}$ = volume of waste rock particles, M_T = total mass, M_w = mass of water, M_s = mass of solids, M_t = mass of tailings solids, and M_r = mass of waste rock particles.

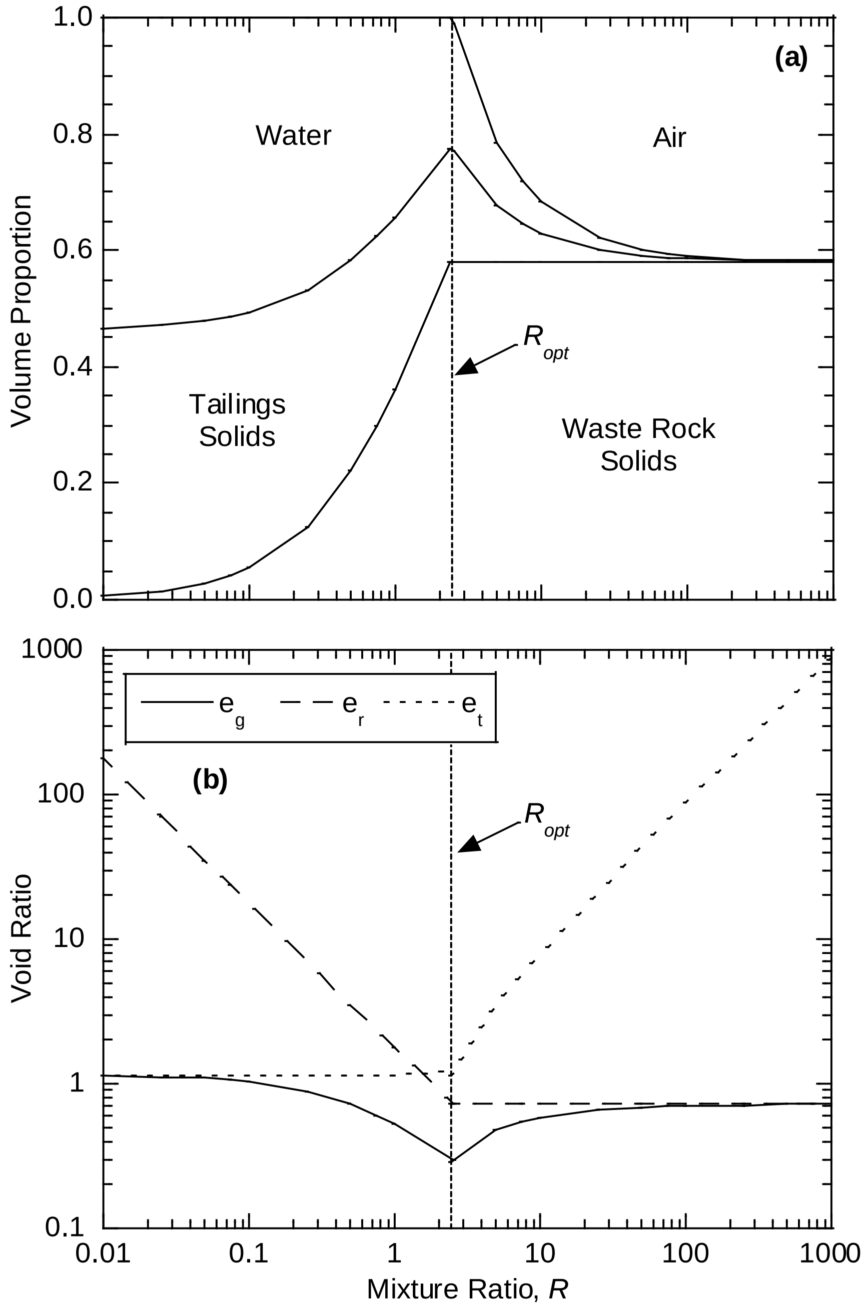

Fig. 2.5. Relationships of (a) volume proportions of waste rock, tailings, water, and air phases and (b) void ratios of the mixture (e_g), waste rock skeleton (e_r), and tailings (e_t) versus mixture ratio (R), where R_{opt} = optimum mixture ratio. Volume proportions and void ratios determined for waste rock mixed with fine-garnet tailings.

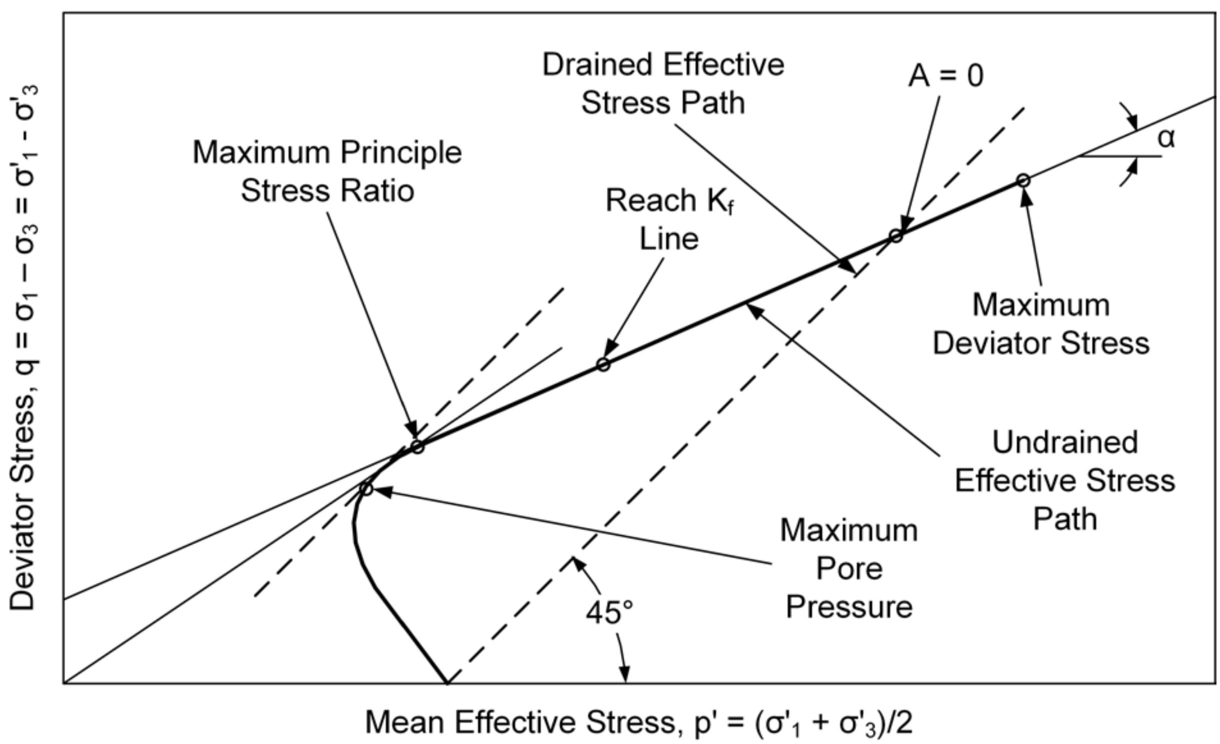

Fig. 2.6. Schematic of an idealized effective stress path in *p*'-*q* space for nonplastic silt during triaxial compression (adapted from Brandon et al. 2006). Failure criteria definitions: (1) maximum deviator stress ($\Delta\sigma_{d,max}$); (2) maximum principle stress ratio (σ'_1/σ'_3); (3) maximum excess pore pressure ($u_{e,max}$); (4) Skempton's pore pressure parameter (A) is zero; and (5) stress path reached the failure (K_f) line identified on the stress path. The slope of the K_f line is given by tan (α).

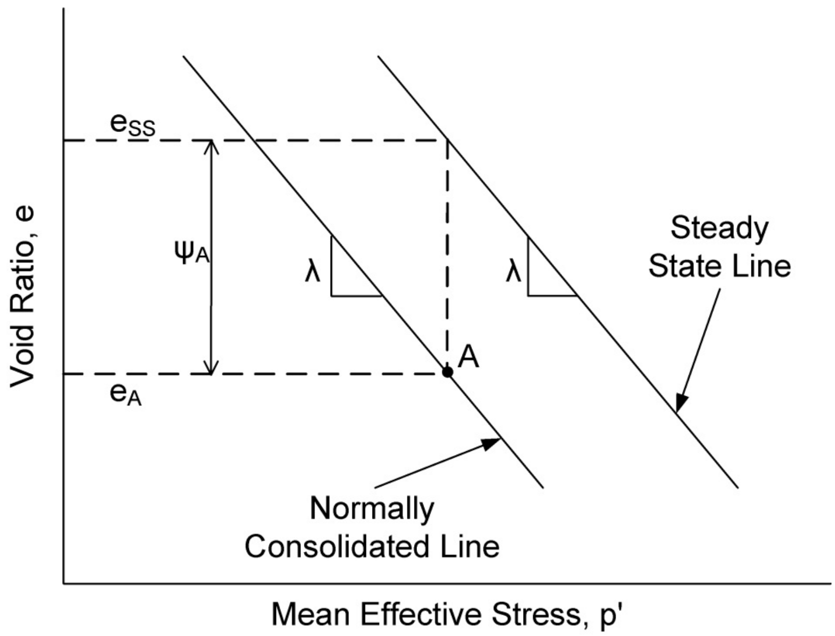

Fig. 2.7. Schematic showing definition of the state parameter (ψ) in void ratio-stress space; e_{SS} = void ratio at steady state, e_A = void ratio for a specimen consolidated to point A, λ = slope of the normally consolidated and steady state lines, and ψ_A = state parameter for a specimen consolidated to point A. Adapted from Been and Jefferies (1985).

CHAPTER 3: MATERIALS AND METHODS

Mine waste materials included crushed gravel used as a synthetic waste rock and three different sources of tailings: (1) garnet (fine and coarse grained), (2) copper, and (3) soda ash. Two fractions of garnet tailings, fine-garnet and coarse-garnet, were collected as a hydrocyclone was used at the garnet mine to fractionate tailings for subsequent management and disposal. Triaxial compression tests were conducted on each material alone as well as on mixed waste rock and tailings (WR&T) to evaluate shearing behavior and determine shear strength parameters.

3.1 Synthetic Waste Rock

Synthetic waste rock was prepared from crushed gravel to create the target particle size distribution (PSD) shown in Fig. 3.1. The target PSD was based on parallel gradation of the average PSD of waste rock compiled from literature (Fig. 2.1). The maximum particle size was 25.4 mm, which was the maximum allowable size for 150-mm-diameter triaxial specimens based on specimen diameter-to-d_{max} requirements stipulated in ASTM D 4767. The target PSD was truncated on the No. 4 sieve (d = 4.75 mm) to provide a clear distinction between the synthetic waste rock and mine tailings, and also to maximize tailings storage capacity in the waste rock skeleton. Synthetic waste rock created at the target PSD classified as poorly graded gravel (GP) according to the Unified Soil Classification System (USCS) (ASTM D 2487).

Physical characteristics of the synthetic waste rock are summarized in Table 3.1. Waste rock particles were visually identified as sub-angular to angular and composed primarily of sandstone and limestone. Specific gravity (G_s) was measured using the buoyant weight method described in ASTM C 127, and G_s = 2.51 refers to an oven-dried specific gravity (Table 3.1).

The maximum void ratio (e_{max}) was determined according to Methods A and B in ASTM D 4254. Oven-dried waste rock was placed in a 14,200-cm^3 mold via hand scoop (Method A) and by extracting a soil-filled, 200-mm-diameter tube (Method B). The minimum void ratio (e_{min}) was measured by vibrating oven-dried waste rock in a 14,200-cm^3 mold at a frequency of 60 Hz for 15 min (ASTM D 4253-Method 2A). The e_{max} from Method A was 0.72 and from Method B was 0.76; e_{min} was 0.48.

3.2 Mine Tailings

3.2.1 Characterization and Classification

The characterization and classification of each tailings material are in Table 3.1. Particle-size distributions for all materials determined via mechanical sieve and hydrometer tests (ASTM D 422) are shown in Fig. 3.2. Atterberg limits were obtained following ASTM D 4318. The fine-garnet and soda ash tailings classified as fine-grained materials, whereas the copper and coarse-garnet tailings classified as coarse-grained materials (Table 3.1). The soda ash tailings classified as low plasticity clay (CL) with a liquid limit (*LL*) of 33.5 % and plasticity index (*PI*) of 16.1 %. Fine-garnet tailings classified as low plasticity silt (ML) with *LL* = 18.8 % and *PI* = 0.4 %. Copper tailings classified as clayey sand (SC) with *LL* = 25.2 % and *PI* = 17.4 %. Atterberg limits were not measured for the coarse-garnet tailings as this material contained 10.1 % < 0.075 mm; coarse-garnet tailings classified as poorly graded sand (SP).

Maximum void ratio of the coarse-garnet tailings was determined following Method B in ASTM D 4254, whereby a 100-mm-diameter tube filled with oven-dried tailings was extracted to deposit tailings into a 2830-cm^3 mold. An e_{max} of 0.82 was determined for the coarse-garnet tailings and is used in subsequent discussions on mixture behavior. The water pycnometer method outlined in ASTM D 854 was used to measure G_s for each tailings material, which ranged from 2.55 for soda ash to 3.07 for fine-garnet tailings (Table 3.1).

The pore fluid of the soda ash tailings was saline and contained 7.6 % sodium carbonate, by dry weight. This high salt content required corrections for hydrometer and G_s tests. A material-specific hydrometer correction factor was developed for the soda ash tailings to account for the increase in pore fluid density. The presence of soluble salts in the G_s test can lead to an overestimation of G_s. Thus, total dissolved solids in the pore fluid was measured and used to correct G_s. Details on the laboratory procedures and correction factors can be found in Gorakhki and Bareither (2014).

3.2.2 Mineralogy

Mineralogical composition of all tailings is summarized in Table 3.2. Mineralogy was determined using X-ray diffraction (XRD) and X-ray fluorescence (XRF) performed by Mineralogy, Inc. in Tulsa, OK. Clay minerals mainly were qualitatively identified as illite and chlorite in copper tailings and illite with mixed-layered illite and smectite in soda ash tailings. The clay mineral composition of copper and soda ash tailings agree with the measured Atterberg limits. Clay minerals were not detected for fine-garnet tailings, which had low plasticity behavior. Images of fine-garnet, copper, and soda ash tailings were obtained using a scanning electron microscope (SEM) and are included in Appendix C.

3.3 Triaxial Compression Testing

Synthetic waste rock and co-mixed WR&T were tested in a large scale triaxial (LSTX) apparatus that contained a 150-mm-diameter specimen to allow testing of particles up to 25 mm in diameter. A linear variable displacement transducer (LVDT) was used to measure vertical displacement (Macro Sensors Model PR 750 2000, 100 ± 0.07 mm) and a load cell was used to measure axial load (Tovey Engineering, Inc. Model SW20-25K-B00, 110 ± 0.29 kN). Pressure transducers were used to measure cell and pore pressures (Omega Engineering, Inc. Model SR-PR-OM-1000, 1000 ± 0.1 kPa) and a differential pressure transducer was used to measure volume change in drained tests (Validyne Engineering, Inc. Model SR-VC-VAL-DP15-30, 500 ± 1 mm of water).

Conventional 38-mm-diameter triaxial (TX) specimens were used for testing mine tailings since d_{max} was ≤ 2 mm for all materials (Table 3.1). Axial load was measured using a load cell (Artech Industries, Inc., 8900 ± 0.4 N) and axial displacement was measured with an LVDT (NOVOtechnik, 50 ± 0.003 mm). Cell and pore pressure were monitored with pressure transducers (GeoTac, 1378 ± 0.07 kPa; ELE International, Ltd., 700 ± 0.07 kPa).

Consolidated undrained (CU) triaxial tests were conducted on the synthetic waste rock, tailings, and waste mixtures in accordance with ASTM D 4767. Consolidated drained (CD) tests also were performed on the synthetic waste rock following ASTM D 7181. Triaxial tests were conducted at target σ'_c = 5, 10, 20, and 40 kPa. All CU and CD specimens were back-pressure saturated to achieve a *B*-value ≥ 0.95. Consolidated undrained tests were sheared at an axial strain rate of 1 %/h, and CD tests were sheared at an axial strain rate of 20 %/h. Pore water pressures were measured in all tests. The strain rate for CU testing was selected based on time required to reach 50 % primary consolidation of the soda ash tailings as described in ASTM D 4767; however, the time to reach 50 % primary consolidation was determined for one-dimensional consolidaton instead of isotropic consolidation. The soda ash tailings exhibited the slowest rate of consolidation and a single strain rate was based on this material for consistency among all CU triaxial compression tests. All triaxial tests were conducted to an axial strain of at least 20 %. Bladder accumulators were used with soda ash tailings alone and soda ash tailings mixed with waste rock to isolate the saline pore fluid from de-aired water in the panel board and also to avoid potential pore fluid chemistry changes during testing.

3.3.1 Tailings Specimen Preparation

Tailings specimens were prepared following a modified version of the slurry deposition method described by Wang et al. (2011). A schematic of the tailings specimen preparation apparatus is shown in Fig. 3.3. Tailings slurries were poured into a 38-mm-diameter by 101-mm-tall split mold lined with a 0.25-mm-thick latex membrane. The fine-garnet and copper tailings slurries were prepared at twice the *LL* with de-aired water and allowed to hydrate for 24 h prior to specimen preparation. Soda ash tailings were mixed at the natural water content (125.8 %) to avoid salt precipitation and changes in pore fluid chemistry. Coarse-garnet tailings were prepared at a water content of 27.4 %, which corresponds to 100 % saturation at e_{max}. Oven-dried coarse-garnet tailings were deposited into de-aired water by extracting a 20-mm-diameter soil-filled tube placed within the split mold. The tube extraction method was used to consistently create coarse-garnet specimens at e_{max}.

A 0.05-mm-thick paper mold was placed around the outside of the latex membrane prior to assembling the split mold and depositing the tailings slurry. The paper mold aided in maintaining a cylindrical shape of the tailings specimen following removal of the split mold. The paper mold fell apart during filling of the triaxial cell with water and lost all strength prior to shear testing.

Tailings specimens were consolidated via vertical stress application in two steps prior to applying the cell confining pressure in the triaxial test. Specimens initially were allowed to self-consolidate for three hours and subsequently were consolidated under application of a vertical stress in the consolidation frame (Fig. 3.3). Vertical stress was applied via dead weights such that the vertical stress (σ_v) was equivalent to the target σ'_c. A single load increment was used to achieve a σ_v = 5 kPa, whereas multiple loadings were used to achieve a σ_v = 10, 20, and 40 kPa; e.g., a final σ_v = 20 kPa required three daily loadings to target stresses of 5, 10, and 20 kPa.

Vertical deformation was monitored during consolidation using a dial gage. Completion of consolidation was identified using the square root of time method outlined in ASTM D 4186. Plots of axial strain versus square root of time were used to determine completion of consolidation for the fine-garnet, copper, and soda ash tailings and are presented in Appendix

D. The split mold was removed and triaxial cell assembled following completion of the vertical consolidation stage to achieve the target σ'_c.

Three CU tests were conducted on soda ash tailings at σ'_c = 10 kPa to evaluate repeatability of the specimen preparation technique. Relationships of u_e and $\Delta\sigma_d$ versus ε_a for these tests are shown in Fig. 3.4. Similar u_e and $\Delta\sigma_d$ versus ε_a trends are observed for all three tests, which demonstrate the repeatability of the slurry specimen preparation and CU testing procedure. The tailings void ratio during shear ranged from 1.33 to 1.31 and the higher $\Delta\sigma_d$ for the third test is attributed to a lower e_t.

3.3.2 Waste Rock and Waste Mixture Specimen Preparation

Synthetic waste rock and co-mixed WR&T were prepared in a 300-mm-tall by 150-mm-diameter split mold lined with a 2-mm-thick rubber membrane. The membrane thickness was necessary for LSTX testing to avoid membrane puncture due to the large, angular waste rock particles. A membrane correction was applied to triaxial test data to account for additional resistance and strength contributed by the membrane. The membrane correction procedure is in Appendix A.

Triaxial compression specimens composed of WR&T were prepared following the slurry displacement method developed by Khalili and Wijewickreme (2008). Waste mixtures were created by incrementally mixing waste rock into a given tailings slurry to achieve the target mixture ratio (Table 2.2). The membrane-lined split-mold cavity was filled to a height of 100 mm with the same tailings slurry used to create a given waste mixture. The waste mixture was then deposited incrementally into the mold in six layers, which displaced the tailings slurry as filling progressed. A 25-mm-diameter rod was used to gently tamp each layer. Tamping was completed to create a level surface for each subsequent layer and was not intended to densify the specimen. A filter paper, porous stone, and top platen were placed on top of the specimen after filling was complete.

The specimen was allowed to consolidate under self-weight for 1 d. Specimen consolidation was performed within the split mold to mirror preparation of tailings only specimens (described previously). Dead weights were placed directly on the top platen such that the vertical stress (σ_v) was equivalent to the target σ'_c. A single load increment was used to reach σ_v = 5 kPa and multiple load increments were used to achieve σ_v = 10, 20, and 40 kPa (i.e., similar to the method applied to tailings specimens). Following consolidation for 1 d under the final target σ_v, the split mold was removed and triaxial cell assembled. Synthetic waste rock specimens were prepared in a similar manner with the exception that de-aired water was used instead of tailings slurry.

Waste rock and tailings mixtures were prepared at the optimum mixture ratio, which corresponds to the ratio of mass of waste rock to mass of tailings where tailings “just fill” the waste rock void space. Tailings were mixed with waste rock at water contents discussed in the previous section.

Table 3.1. Summary of waste rock and tailings physical characteristics and classification.

Material	*LL* (%)	*PI* (%)	USCS	d_{max} (mm)	Sand Content (%)	Fines Content (%)	Clay Content (%)	As-Collected Water Content (%)	G_s	e_{max}	e_{min}
Waste Rock	-	-	GP	25.4	-	-	-	-	2.51	0.72[b], 0.76[c]	0.48
Soda Ash[a]	33.5	16.1	CL	2.00	26.5	73.5	18.0	124	2.55	-	-
Copper	25.2	13.7	SC	0.85	54.7	45.3	7.0	238	2.72	-	-
Fine Garnet	18.8	0.4	ML	2.00	36.7	63.3	6.6	13.1	3.07	-	-
Coarse Garnet	-	-	SP	2.00	89.9	10.1	-	-	2.99	0.82[b]	-

Note: *LL* = liquid limit; *PI* = plasticity index; USCS = Unified Soil Classification System; d_{max} = maximum particle size; G_s = specific gravity; e_{max} = maximum void ratio; and e_{min} = minimum void ratio.

[a]Test results for soda ash tailings with original saline pore water. Corrections applied to particle-size distribution and G_s.

[b]Measured according to Method A in ASTM D 4254.

[c]Measured according to Method B in ASTM D 4254.

Table 3.2. Mineralogical composition by percent (%) mass for fine-garnet, coarse-garnet, copper, and soda ash tailings based on X-ray diffraction and X-ray fluorescence analysis.

Mineral	Fine-Garnet	Coarse-Garnet	Copper	Soda Ash
Quartz	-	-	34	11
Plagioclase Feldspar	69	62	23	trc
K-Feldspar	-	-	22	8
Calcite	-	-	1	2
Dolomite	-	-	-	46
Shortite	-	-	-	26
Magnetite	-	-	trc	-
Hematite	-	-	1	-
Ilmenite	2	3	-	-
Ferroan Fassaite	-	-	2	-
Ferroan Pargasite	19	18	-	-
Almandine	10	16	-	-
Clay/Mica	trc	1	17	7

Note: trc = trace amounts

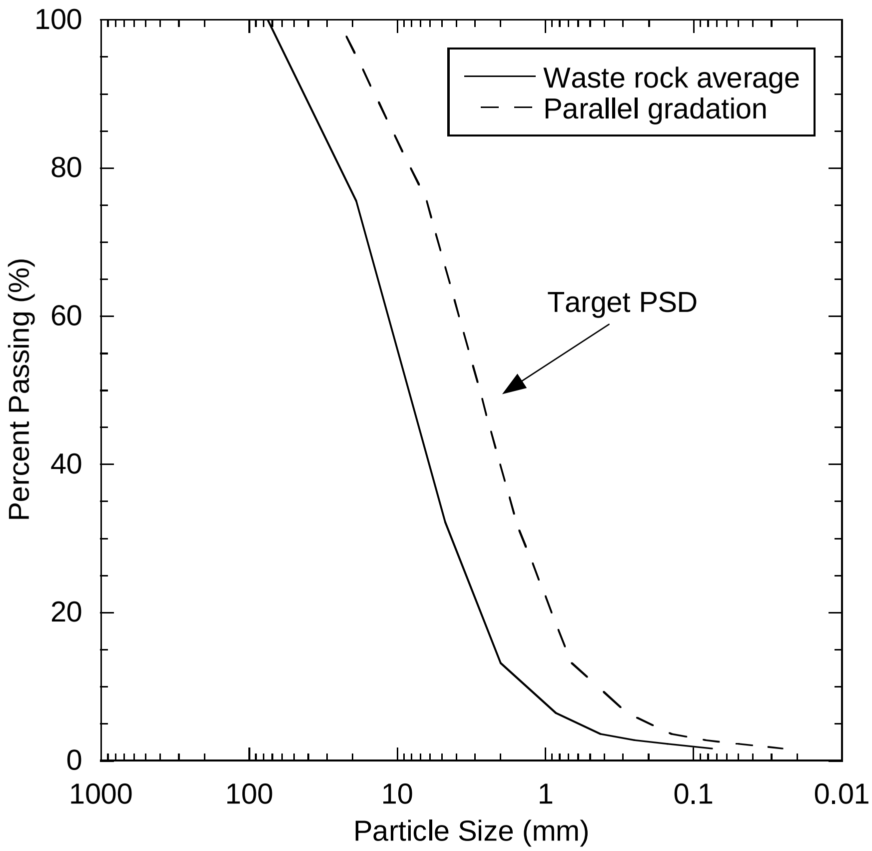

Fig. 3.1. Parallel gradation and average particle-size distribution (PSD) of waste rock from literature.

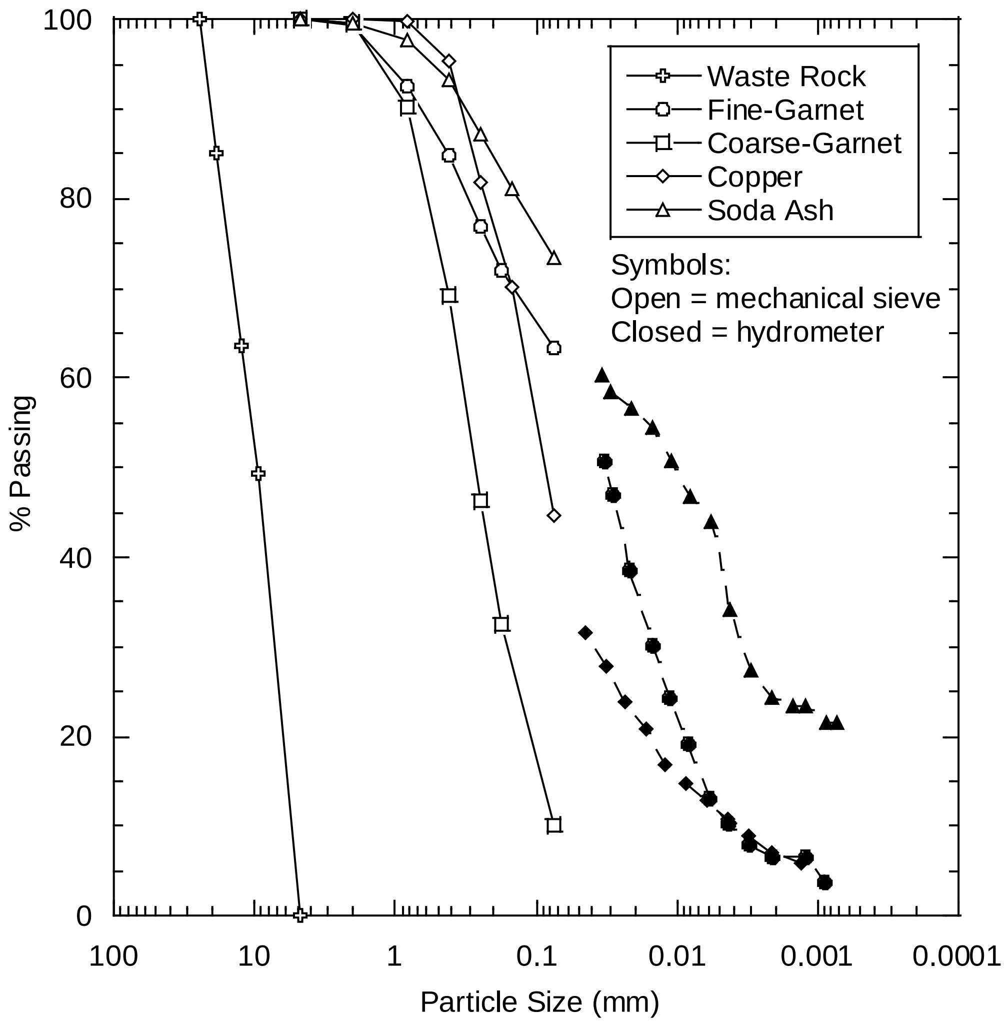

Fig. 3.2. Particle-size distributions for synthetic waste rock, fine-garnet tailings, coarse-garnet tailings, copper tailings, and soda ash tailings.

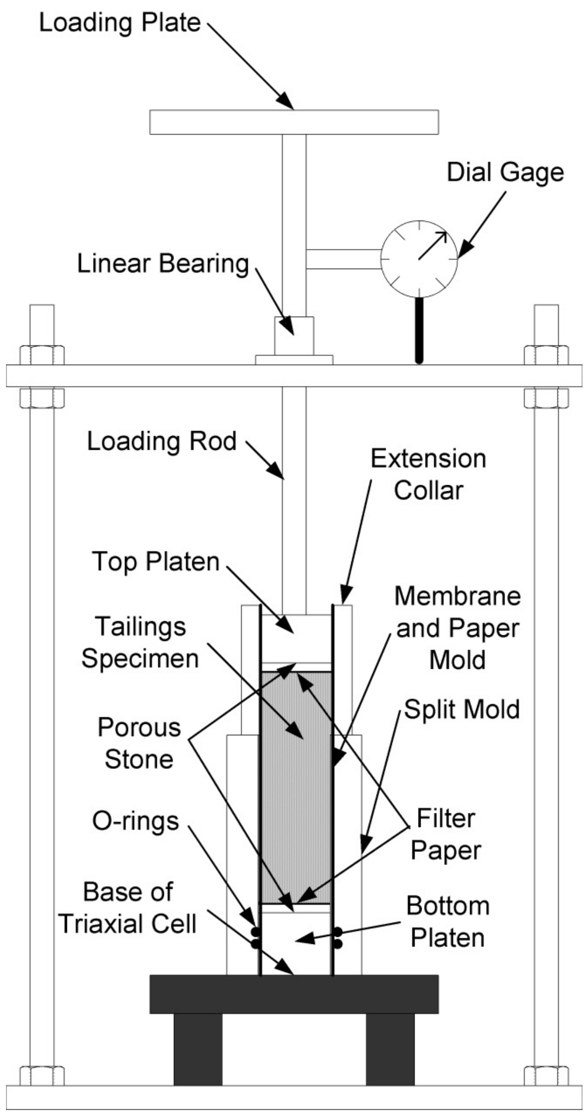

Fig. 3.3. Schematic of the consolidation frame used for preparation of tailings specimens for triaxial compression testing.

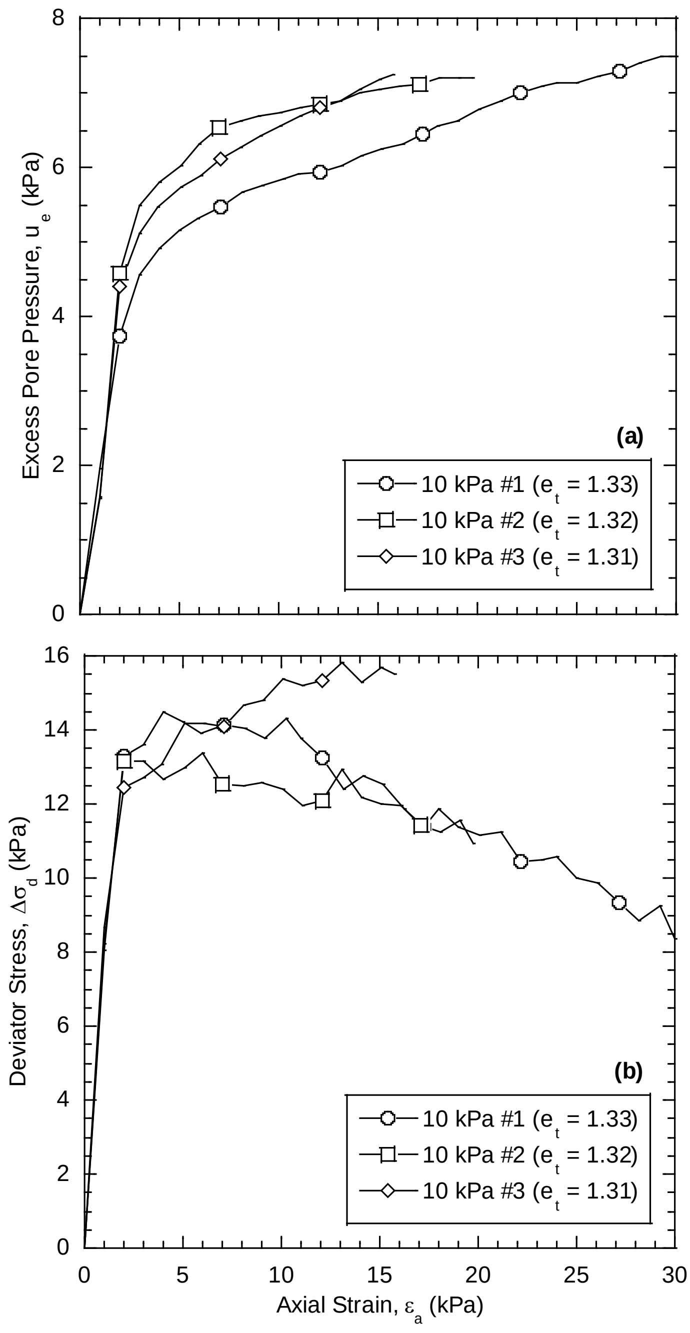

Fig. 3.4. Relationships of (a) excess pore pressure and (b) deviator stress versus axial strain for experiments conducted on soda ash tailings at an effective confining pressure of 10 kPa. The initial void ratio during shear for each test is given in parentheses in the legend.

CHAPTER 4: RESULTS AND DISCUSSION

A summary of triaxial tests conducted on each material for this study is in Table 4.1. The data compilation in Table 4.1 includes σ'_c, effective major principle stress at failure (σ'_{1f}), effective minor principle stress at failure (σ'_{3f}), ϕ', axial strain at failure (ε_{af}), initial and final e_r and e_t, actual R achieved for a given waste mixture, and R_{opt}. A compilation of experimental data from all triaxial compression tests on all materials is in Appendix E, which includes relationships between $\Delta\sigma_d$ and u_e versus ε_a for CU tests, and $\Delta\sigma_d$ and ε_v versus ε_a for CD tests. Plots of Mohr's circles that represent failure conditions and stress paths for each material are also included in Appendix E.

4.1 Shear Behavior

4.1.1 Waste Rock

Relationships of ε_v and $\Delta\sigma_d$ versus ε_a for CD tests and u_e and $\Delta\sigma_d$ versus ε_a for CU tests on the synthetic waste rock are shown in Fig. 4.1. In both CD and CU tests the waste rock became increasingly contractive as σ'_c increased (Fig. 4.1). At σ'_c = 5 kPa, the waste rock displayed dilative behavior and transitioned to purely contractive behavior at σ'_c = 40 kPa. Deviator stress increased with increasing σ'_c in CD tests (Fig. 4.1) due to additional external work necessary for volume change to occur (Rowe et al. 1964). In CU tests, $\Delta\sigma_d$ increased with increasing σ'_c until σ'_c = 40 kPa. During this test, waste rock displayed entirely contractive tendencies, which decreased the effective stress and caused failure to occur at a lower $\Delta\sigma_d$ compared to other CU tests (Fig. 4.1). The higher $\Delta\sigma_d$ in CD tests compared to CU tests is attributed to additional energy required to rearrange particles causing volume change (Rowe 1962; Rowe et al. 1964; Bolton 1986). This drained and undrained behavior of the synthetic waste rock is comparable to drained and undrained behavior of sands reported in Seed and Lee (1967) and Lee and Seed (1967).

4.1.2 Fine-Garnet Tailings and Mixtures

Relationships of $\Delta\sigma_d$ and u_e versus ε_a for fine-garnet tailings and WR&T mixtures are shown in Fig. 4.2. The tailings alone and co-mixed WR&T displayed a tendency to dilate during shear (i.e., developed negative u_e). Tailings expressed contractive tendencies (positive u_e) as shear initiated and then became increasingly dilative as ε_a increased, which is typical behavior for nonplastic silts (e.g., Brandon et al. 2006; Wang and Luna 2012). The magnitude of u_e during initial contraction and subsequent dilation increased with increasing σ'_c. The more pronounced tendency to dilate as σ'_c increased was attributed to increased consolidation during specimen preparation that reduced e_t (Table 4.1). At σ'_c = 40 kPa, fine-garnet tailings had the lowest e_t and displayed the greatest tendency to dilate compared to other σ'_c (Fig. 4.2a).

Similar to tailings alone, mixtures of fine-garnet and waste rock displayed increasing dilative tendencies as σ'_c increased (Fig. 4.2b). The strongest tendency to dilate occurred at σ'_c = 40 kPa. Waste rock alone was entirely contractive at σ'_c = 40 kPa (Fig. 4.1b); however, contraction of waste rock particles in the mixture was prevented by the presence of fine-garnet tailings in the void space. The contractive nature of the waste rock was over-compensated by the dilative nature of the fine-garnet tailings and the overall mixture exhibited dilative behavior. The fine-garnet mixture at σ'_c = 10 kPa displayed greater dilation (more negative u_e) and higher $\Delta\sigma_d$ compared to 20 kPa (Fig. 4.2b and 4.2d). These two specimens had similar e_r and e_t (Table 4.1) and the dilative tendency of the mixture at σ'_c = 20 kPa likely was suppressed by the increase in σ'_c.

The dilative behavior expressed by the fine-garnet mixtures was comparable to the behavior of tailings alone (Fig. 4.2a and Fig. 4.2b); however, the tendency to dilate in the mixtures was more pronounced. At σ'_c = 10 kPa, tailings in the mixture and prepared alone had a similar e_t (Table 4.1). A more negative u_e was measured in the mixture, which may be attributed to interlocking and development of friction between waste rock and tailings particles (Thevanayagam et al. 2002). Carraro et al. (2009) observed greater dilatancy in sand mixed with nonplastic silt compared to sand mixed with clay. The increase in dilatancy was attributed to greater angularity in the silt particles which increased the potential for interlocking with defects on the surface of the sand grains. Both the fine-garnet tailings and waste rock particles were angular indicating the greater tendency for dilation may be an effect of particle interlocking.

4.1.3 Coarse-Garnet Tailings and Mixtures

Relationships of u_e and $\Delta\sigma_d$ versus ε_a for coarse-garnet tailings alone and mixed with waste rock are shown in Fig. 4.3. In general, tailings alone exhibited strong dilative tendencies and strain-hardening behavior, whereas mixed WR&T only exhibited modest volumetric deformation tendencies and attainment of an ultimate $\Delta\sigma_d$ during continued deformation. With exception of tests at σ'_c = 20 kPa for the tailings alone, the tendency for coarse-garnet tailings to dilate increased with increasing σ'_c (Fig. 4.3a) even though specimens were prepared at $e > e_{max}$ (Table 4.1). The maximum void ratio was determined by depositing tailings in a dry environment; however, triaxial specimens were prepared by depositing tailings into deaired water, which may have created a different soil fabric (Kuerbis and Vaid 1988; Carraro and Prezzi 2008). Net pore pressure, taken as the sum of backpressure and excess pore pressure, approached zero during the 20 kPa tests and may have allowed cavitation to occur. Penman (1953) and Brandon et al. (2006) reported an increase in dilation with cavitation, which agrees with behavior observed in the coarse-garnet tailings at σ'_c = 20 kPa.

The increase in dilatancy with increasing σ'_c exhibited by the coarse-garnet tailings for σ'_c = 5, 10, and 40 kPa (Fig. 4.3a) is comparable to behavior of the fine-garnet mixtures (Fig. 4.2d). Coarse-garnet tailings contained approximately 90 % sand and 10 % fines, which likely resulted in the material behaving as a silty sand mixture as opposed to a pure sand. The mixture theory that has been applied to WR&T mixtures subsequently is applied to coarse-garnet tailings alone to explain the effect of the fines content on shear behavior.

In contrast with the tailings alone, coarse-garnet tailings mixed with waste rock exhibited increasing contractive tendencies as σ'_c increased (Fig. 4.3b). The waste rock void ratio of all coarse-garnet mixtures was less than $e_{r,max}$, which suggests that waste rock particles were in continuous contact throughout the specimen. As shearing proceeded in the CU tests, deformation and strength behavior was comparable to the waste rock alone (Figs. 4.1b and 4.1d), implying that the waste rock controlled shear behavior of the mixture. The coarse-garnet mixture at σ'_c = 20 kPa had the smallest tailings fraction and yielded a lower $\Delta\sigma_d$ and comparable u_e to the test at σ'_c = 10 kPa. Thus, as the tailings fraction decreased, strength decreased and was more comparable to strength of the waste rock (Fig. 4.1d).

4.1.4 Copper Tailings and Mixtures

Relationships of u_e and $\Delta\sigma_d$ versus ε_a for copper tailings and mixed WR&T are shown in Fig. 4.4. The $\Delta\sigma_d$ at failure and strain-hardening behavior of the copper tailings increased with increasing σ'_c. This behavior agrees with increasing specimen density of the copper tailings as σ'_c increased (i.e., decrease in e_t, Table 4.1). Although copper tailings initially contracted more as σ'_c increased, the propensity to dilate also increased (Fig. 4.4a). This behavior is similar to that observed for the fine-garnet tailings (Figs. 4.2a and 4.2c). These two tailings had comparable particle size distribution and Atterberg limits, which supports the similarity in shear behavior between the two materials.

Copper tailings mixtures displayed dilative tendencies at all σ'_c (Fig. 4.4b) and stiffer response to loading compared to the tailings alone (Fig. 4.4d). The tendency to dilate initially increased with increasing σ'_c (5 kPa to 10 kPa) then became less dilative with further increase in σ'_c (10 to 40 kPa). The behavior of copper tailings mixed with waste rock was more comparable with the behavior of copper tailings alone relative to waste rock (Fig. 4.4a and Fig. 4.4b), which also was observed for waste rock mixed with fine-garnet tailings. The waste rock void ratio of the copper tailings mixtures was greater than $e_{r,max}$, and suggests that waste rock particles were not in continuous contact. This mixture state and shear behavior response is comparable to the fine-garnet mixtures and suggests that as e_r increases above $e_{r,max}$ the tailings matrix has a more pronounced influence on shear behavior of mixed WR&T.

4.1.5 Soda Ash Tailings and Mixtures

Relationships of u_e and $\Delta\sigma_d$ versus ε_a for soda ash tailings and mixed WR&T are shown in Fig. 4.5. Soda ash tailings were the only material to exhibit completely contractive behavior during shear (Fig. 4.5a). These tailings had the highest clay content of all materials evaluated (Tables 3.1 and 3.2), and the clay content likely contributed to the contractive tendencies (Qiu and Sego 2001; Newson et al. 2006). Although soda ash tailings were contractive, they also were stiff during initial loading that was followed by attainment of an ultimate strength at small ε_a (Fig. 4.5c). The high stiffness at low ε_a for the soda ash tailings may be an effect of saline pore fluid causing clay particle flocculation that created a stiff material at small strains. The effects of pore fluid salinity and strength gain in the soda ash tailings are discussed subsequently.

Mixtures of soda ash tailings and waste rock yielded a considerable increase in $\Delta\sigma_d$ for a given σ'_c and exhibited modest dilative tendencies relative to the tailings alone (Figs. 4.5b and 4.5d). Similar to soda ash tailings alone, mixture specimens became more contractive as σ'_c increased (Fig. 4.5b). The soda ash mixtures was dominantly dilative at σ'_c = 5 kPa and transitioned to more contractive behavior as σ'_c increased. The overall trend in u_e as a function of σ'_c is comparable to the waste rock behavior (Fig. 4.1b). Waste rock void ratios of the mixtures were close to $e_{r,max}$ for all tests (Table 4.1), but slightly higher, suggesting that some tailings were present between waste rock particles that may have contributed to the modest dilative tendencies of the mixtures.

4.2 Shear Strength

4.2.1 Evaluation and Definition of Failure

Defining failure for the fine-grained garnet, coarse-grained garnet, and copper tailings, which all contained ≥ 10 % silt content, required an evaluation of failure criteria outlined in Brandon et al. (2006). Effective stress friction angles determined from all individual triaxial tests with each of the six failure criteria in Brandon et al. (2006) are shown in Fig. 4.6a. Considerable scatter (> 10°) is observed for all materials and is attributed to both failure criteria and the effect of σ'_c on ϕ'. Friction angles equal to 0° plotted in Fig. 4.6a represent failure criteria that could not be applied to a given material. Only the failure criterion of A = 0 could not universally be applied to all materials as this criterion is not applicable for materials that exhibited purely contractive behavior.

Average ϕ' for each failure criterion are shown in Fig. 4.6b and a summary of ϕ' determined with each criterion at each σ'_c for copper tailings is in Table 4.2. Although Brandon et al. (2006) recommended the failure criterion of A = 0 for silty soils, this method could not be universally applied to all triaxial test data in this study and was not selected for defining failure. Wang and Luna (2012) recommended $\Delta\sigma_{d,max}$, $(\sigma'_1/\sigma'_3)_{max}$, or limiting ε_a to 15% as failure criteria for silty soils. The $\Delta\sigma_{d,max}$, ε_a = 15%, and K_f line criteria yielded comparable ϕ' for copper tailings with low standard deviation between tests conducted at different σ'_c (Table 4.2). Furthermore, these failure criteria also yielded consistent ϕ' for all materials (Fig. 4.6). Failure criteria of $(\sigma'_1/\sigma'_3)_{max}$ and $u_{e,max}$ yielded higher and lower ϕ' for copper tailings with a considerable increase in standard deviation between tests at different σ'_c (Table 4.2), and were omitted from defining failure in this study. Average values of ϕ' for each of the three consistent failure criteria and a practical estimate of ϕ' are listed in Table 4.3. The practical estimate was determined by averaging ϕ' determined using the $\Delta\sigma_{d,max}$, ε_a = 15%, and K_f line failure criteria and rounding down.

4.2.2 Shear Strength of Waste Materials

Average ϕ' based on $\Delta\sigma_{d,max}$, ε_a = 15%, and K_f line failure criteria as well as a single ϕ' estimate based on these methods for each material are summarized in Table 4.3. The synthetic waste rock had an average ϕ' = 41° when tested under drained conditions and average ϕ' = 37° for undrained conditions. The higher friction angle from CD tests compared to CU tests was attributed to the ability of the specimen to dilate during drained shear (Seed and Lee 1967). Lee and Seed (1967) report that the ability for coarse-grained soils to dilate during drained shear contributes to increased shearing resistance that can increase ϕ' at low σ'_c.

The ϕ' for pure mine tailings evaluated in this study ranged from 34° to 41° (Table 4.3) Fine-garnet tailings (ϕ' = 35°) and copper tailings (ϕ' = 34°) had comparable ϕ', which can be attributed to similarity in composition between the two materials (Table 3.1). These tailings agree with ϕ' = 34° – 37° for similar silty, hard rock mine tailings reported by Matyas et al. (1984) and Qiu and Sego (2001). Friction angles for hard rock mine tailings generally are higher compared to natural silts ($\phi' \approx$ 30° to 35°, Brandon et al. 2006; Wang and Luna 2012) due to greater particle angularity (Bussière 2007). Coarse-garnet tailings had ϕ' = 38°, which was higher than the fine-garnet tailings and attributed to a greater sand content.

The ϕ' of soda ash tailings was the largest (41°) among the tailings evaluated in this study (Table 4.3). Shear behavior of this material was similar to typical behavior of normally consolidated clays, and the high ϕ' is not consistent with typical ϕ' for soils containing clay (Lambe and Whitman 1969). The high ϕ' of the soda ash tailings potentially is due to saline pore fluid that caused clay particle flocculation during formation of the specimen from slurry (discussed subsequently). Although soda ash tailings were the most compressible of all tailings (see Appendix D), the specimen height-to-diameter ratio (H:D) prior to initiating shear ranged from 1.98 to 2.33 (i.e., ≥ 2 required by ASTM D 4767), which suggests that the shear plane did not intersect the top or bottom platen.

In general, WR&T mixtures displayed similar shear strength to waste rock alone. Effective friction angles for the mixtures with fine-garnet, coarse-garnet, and copper tailings ranged from 39° to 40° (Table 4.3). Waste rock particles were in continuous contact in the coarse-garnet mixtures; thus, the waste rock skeleton controlled shear strength. Although shear behavior of the fine-garnet and copper mixtures was similar to the tailings and waste rock particles were not in continuous contact, the waste rock increased shear strength relative to the tailings alone via interparticle reinforcing effects. Shear strength observed for the fine-garnet, coarse-garnet, and copper mixtures agrees with the shear strength observed by Khalili et al. (2010) for waste rock and gold tailings mixtures.

Soda ash mixtures exhibited the lowest shear strength of all mixtures with $\phi' = 38°$ (Table 4.3). The e_r of the soda ash mixtures was greater than $e_{r,max}$, indicating that some tailings were present between waste rock particles. The clay content of the soda ash tailings (18.0 %) may have reduced interparticle friction and prevented interlocking between waste rock particles that created a lubrication effect (Holtz and Ellis 1961; Carraro et al. 2009). This lubrication effect was absent in the silty tailings due to greater particle angularity as shown in SEM images in Appendix C. The reduced shear strength for soda ash mixtures agrees with shear strength of clay-gravel mixtures reported in Holtz and Ellis (1961).

4.2.3 State Parameter

The state parameter (ψ) accounts for effects of specimen density and σ'_c on shear strength behavior. In consolidated undrained triaxial tests, the void ratio after consolidation remains constant during shear and p' increases. An undrained specimen can be assumed at steady state when there is no additional change in $\Delta\sigma_d$ and u_e with increasing ε_a. Effective principle stresses (σ'_1 and σ'_3) at this point were used to determine p'. The steady state line for CU tests was defined by a logarithmic regression through the relationship between e and p'.

The steady state void ratio (e_{SS}) is estimated based on the logarithmic regression using p' at the beginning of shear.

Determining ψ can be difficult for soils containing fine-grained particles as these particles affect specimen density and change the location of the SSL. Rahman et al. (2014) proposed a modified state parameter (ψ*) based on e^* that accounts for the effect of fines on ψ. Equations for determining e^* are in Section 2.7 and application of these equations assumes f_c is below a threshold fined content (f_{thres}) that defines the transition from a coarse-grained skeleton to a fine-grained matrix (this condition can also be defined as $R > R_{opt}$). Although mixtures of WR&T prepared in this study occasionally had $R < R_{opt}$, f_c typically was low enough (1-2 % greater than f_{thres}) that minimal error was introduced in the analysis.

A summary of e^* and ψ* for CU tests on co-mixed WR&T, e_r and ψ for CD and CU tests on waste rock alone, and e_t and ψ for CU tests on tailings alone is in Table 4.4. The initial void ratios (e^*, e_r, and e_t) are representative of specimen properties at initiation of shearing. The void ratios at steady state were determined based on best-fit SSLs for each set of failure points for a given material and p' computed at initiation of shearing. Thus, ψ and ψ* compiled in Table 4.4 represent the vertical distance between the initial void ratio and best-fit SSL. Negative ψ (i.e., e_i below the SSL) coincide with materials that express a tendency to dilate during shear, whereas positive ψ (i.e., e_i above the SSL) are associated with materials that contract during shear (Been and Jefferies 1985).

The relationships between ψ and σ'_c for all tests and between ψ and normalized mixture ratio (R/R_{opt}) for WR&T mixtures are shown in Fig 4.7. The most negative values of ψ occur at lower σ'_c and become more positive with increasing σ'_c (Fig. 4.7a). This trend suggests that the tendency to dilate is stronger at lower σ'_c which agrees with observations from plots of u_e versus ε_a (Fig. 4.1-4.5). In tests performed on WR&T mixtures, the more negative values of ψ are associated with $R/R_{opt} < 1$ suggesting an increase in dilation with increasing tailings content. The fine-garnet and copper mixtures which displayed the strongest dilative tendencies (Fig. 4.2

and 4.4) all plot below R/R_{opt} = 1 and left of ψ = 0 (Fig. 4.7b). The state parameter for the soda ash mixtures remained less negative compared to the fine-garnet and copper mixtures despite having a lower R/R_{opt}. Soda ash mixtures were not as strongly dilative as the fine-garnet and copper mixtures (Fig. 4.2-4.5); thus, ψ for soda ash mixtures is less negative than for fine-garnet and copper mixtures (Fig. 4.7b).

The relationship between e_r and p' for waste rock is shown in Fig. 4.8. Parameters used to define the SSLs for all materials are summarized in Table 4.5 and included in individual plots in Figs. 4.8-4.10. The same steady state line was used for both CD and CU tests on waste rock and developed using a logarithmic regression through e_r determined at the end of shear from CD tests. The location of the initial state relative to the SSL for CD tests agrees with the observed shear behavior (Fig. 4.8). The initial states for σ'_c = 5, 10, and 20 kPa plot below the SSL and displayed dilative behavior during shear. The test at σ'_c = 40 kPa was initially on the SSL and displayed contractive behavior. All CU tests on waste rock are initially below the SSL regardless of shear behavior; however, the steady state e_r-p' points from all tests fall along the SSL (Fig. 4.8). Waste rock tested at σ'_c = 40 had the least negative ψ which agrees with the observed decrease in dilative tendencies as σ'_c increased (Table 4.5 and Fig. 4.1).

Relationships between e_t and p' for each fine-garnet, copper, and soda ash tailings and between e^* and p' for coarse-garnet tailings are shown in Fig. 4.9. The SSLs regressed through e_t-p' points defining steady state conditions were all statistically significant with coefficients of determination ≥ 0.41 (Table 4.5). The slope of the SSLs (λ in Fig. 4.9) increase with increasing f_c, which agrees with trends reported by Been and Jefferies (1985). Fine-garnet, coarse-garnet, and copper tailings all displayed dilative tendencies during undrained shear (Figs. 4.2a, 4.3a, and 4.4a), which agree with location of the initial specimen condition relative to the SSL (Fig. 4.9) and negative ψ computed for each material (Table 4.4). The most negative ψ corresponded to coarse-garnet tests at σ'_c = 20 kPa as this material exhibited the strongest tendency to dilate (Fig. 4.3a). Fine-garnet tailings had more negative ψ compared to copper tailings for all σ'_c and also displayed stronger dilation during shear (Fig. 4.2a and 4.4a). Soda ash tailings displayed purely contractive tendencies during undrained shear (Fig. 4.5a) that agrees with location of initial specimen conditions relative to the SSL (Fig. 4.9d) and positive ψ for all tests (Table 4.4).

Relationships between e^* and p' for each WR&T mixture are shown in Fig. 4.10. Although scatter exists in e^*-p' points for the mixtures used to define SSLs, all initial conditions plot below the best-fit SSLs and agree with a tendency to dilate observed in all mixtures. Mixtures prepared at $R < R_{opt}$ have more negative ψ^* relative to mixtures at R ≈ R_{opt} (Fig. 4.7b). The fine-garnet and copper mixtures consistently were prepared at $R < R_{opt}$ (Table 4.1) and had the lowest R/R_{opt} (Fig. 4.7) that coincides with the highest tailings content. These mixtures also had the most negative ψ^* (Table 4.4 and Fig. 4.7b).

Soda ash mixtures also were consistently prepared at $R < R_{opt}$, but had a higher R/R_{opt} compared to fine-garnet and copper mixtures (Fig. 4.7). The equivalent state parameter for soda ash mixtures was similar to ψ for CU tests on waste rock (Table 4.4), which supports similarity observed in shear behavior between the two materials (Fig. 4.1b and Fig. 4.5b). Coarse-garnet mixtures were prepared at $R \approx R_{opt}$ and ψ^* becomes less negative as σ'_c increased (Table 4.4 and Fig. 4.7a) due to suppressed dilatancy with increased σ'_c. At σ'_c = 40 kPa, ψ^* is negative even though the coarse-garnet mixture expressed negligible volume change ($u_e \approx 0$); however, the initial e^* nearly falls on the SSL (Fig. 4.10b) and agrees with observations reported by Been and Jefferies (1985).

Steady state behavior of co-mixed WR&T also was analyzed in terms of e_r and e_t for each mixture to determine whether violating the assumption that $f_c < f_{thres}$ introduced error in e^* and ψ^*. The SSLs developed for each individual material (i.e., waste rock or tailings alone) were used to predict shear behavior based on initial e_r or e_t of the mixture. Initial e_r-p' points for all WR&T mixtures are presented in Fig. 4.11 with the SSL for waste rock. Anticipated shear behavior based on position of initial e_r relative to the SSL does not agree with observed shear behavior of the mixtures, suggesting that e_r is unable to capture the actual behavior for WR&T mixtures. The initial e_r for fine-garnet mixtures at σ'_c = 10 and 20 kPa plot above the SSL and imply contractive behavior; however, these mixtures displayed dilative tendencies during shear (Fig. 4.2b). Additionally, the initial e_r for the coarse-garnet mixture at σ'_c = 40 kPa implies dilative behavior (i.e., e_r below the SSL), whereas the mixture actually expressed negligible volume change (Fig. 4.3b). Compared to e_r, e^* consistently captured actual observed shear behavior of co-mixed WR&T (Fig. 4.10) and supports the use of e^* and ψ^* when evaluating shear behavior of mixtures.

Initial e_t-p' points for all WR&T mixtures are presented in Fig. 4.12 with the SSL for each tailings. Similar to the analysis using e_r, shear behavior predicted using initial e_t for each mixture does not agree with observed shear behavior, demonstrating that e_t is not suitable for characterizing shear behavior of WR&T mixtures. Initial e_t for copper mixtures all plot above the SSL (Fig. 4.12c), which suggests contractive behavior even though the mixture dilated during each test (Fig. 4.4b). The evaluation of shear behavior of mixtures as a function of e_r and e_t were inaccurate compared to the original analysis using e^*. The inability of e_r and e_t to capture shear behavior when used to determine ψ validates the application of e^* to co-mixed WR&T even when $R < R_{opt}$.

4.3 Discussion

4.3.1 Fines or Tailings Composition Effects

Previous studies that investigated the shear behavior of waste rock mixed with tailings indicate that the gravel dominates shear strength and behavior of the mixture (Leduc et al. 2004; Khalili et al. 2010; Wijewickreme et al. 2010). However, only a single tailings source was evaluated in these studies. Results discussed in Section 4.1 demonstrate that tailings composition affects shear behavior of WR&T mixtures. A comparison of shear behavior of all mixtures at σ'_c = 40 kPa is shown in Fig. 4.13. All fine-garnet and copper mixture specimens were prepared at $R < R_{opt}$ (Table 4.1) and expressed the strongest tendency to dilate of all materials at σ'_c = 40 kPa (Fig. 4.13a). Fine-garnet and copper tailings contained an abundance of silt, which appears to have a dominant effect on shear behavior of the mixture, contrary to the results reported by Khalili et al. (2010). However, soda ash tailings had similar PSD and Atterberg limits to tailings tested by Khalili et al. (2010), and in both cases shear behavior was dominated by the waste rock skeleton of the mixture (Fig. 4.1a, 4.5a, and 4.13). Similar to the soda ash mixtures, shear behavior of coarse-garnet mixtures was comparable to the waste rock alone (4.1a and 4.3a). At σ'_c = 40 kPa, the amount of contraction (i.e., positive u_e) in the coarse-garnet mixtures was similar to waste rock alone (Fig. 4.13a).

Tailings composition has less influence on shear strength than on shear behavior of WR&T mixtures. Waste rock mixed with sandy (coarse-garnet) or silty (fine-garnet and copper) tailings had comparable ϕ' as waste rock alone (Table 4.3), whereas waste rock mixed with clayey tailings (soda ash) had slightly lower ϕ'. Despite the soda ash tailings having the highest average ϕ' among the tailings (41°), this mixture resulted in the lowest average ϕ' (38°) due to lubrication of the waste rock particle contacts via soda ash tailings.

4.3.2 Mixture Effects

4.3.1.1 Waste Rock and Tailings Mixtures

Soils composed of sand and silt provide a useful analog for fine-garnet and copper tailings mixed with waste rock. Extensive testing has been conducted to evaluate the shear behavior of silty sands at varying fines contents and σ'_c (e.g., Thevanayagam 1998; Salgado et al. 2000; Carraro et al. 2009; Rahman and Lo 2014). These studies have shown that an increase in f_c corresponds to an increase in dilatancy during shear for sands mixed with nonplastic silts, which agrees with the observed increase in dilatancy with decreasing R/R_{opt} for fine-garnet and copper mixtures (Fig. 4.7b and 4.13a).

Thevanaygam (1998) suggested using different void ratios that depend on the structure of silty sands to characterize shear strength behavior. At low f_c when fine-grained particles are contained within the void space of coarse particles, the void ratio of the coarse-particle skeleton (e_r for WR&T mixtures) should be used to characterize shear behavior. At high f_c when coarse-grained particles float in a fine-grained matrix, the void ratio of the fine-grained material (e_t in WR&T mixtures) should be used to characterize shear behavior. However, if e_r is close to the maximum void ratio, soil particles can be arranged in a metastable structure and the shear behavior may be difficult to explain using e_r and/or e_t. Fine-grained particles can exist between the contacts of coarse-grained particles in a metastable structure and support the coarse particles via participating in transfer of normal forces. Thus, neither e_r or e_t may accurately capture the soil structure and shear behavior. Carraro et al. (2009) also noted that these void ratios (e_r and e_t) are not able to differentiate between silts and clays, which can have considerably different effects on the shear behavior of soil mixtures (e.g., fine-garnet and copper tailings mixtures versus soda ash mixtures).

Co-mixed WR&T prepared in this study more than likely had metastable soil structures, as triaxial specimens were prepared with a target $e_r = e_{r,max}$. Additionally, mixtures frequently were prepared at $R < R_{opt}$, which further increases e_r (Table 4.1) and may have changed the soil structure into a tailings matrix with floating waste rock particles. Fine-garnet and copper mixtures had the lowest R relative to R_{opt} and highest e_r of all mixtures (Table 4.1). Shear behavior for these mixtures was dominated by the tailings (Fig. 4.2 and 4.4). Soda ash mixtures also were prepared at $R < R_{opt}$, but had a lower e_r more comparable to waste rock alone (Table 4.1). Higher compressibility of soda ash tailings and lower tailings content contributed to more contact between waste rock particles (i.e., lower e_r) in soda ash mixtures than in fine-garnet and copper mixtures. Similarity of e_r for waste rock alone and soda ash mixtures agrees with the similar behavior observed for both materials (Fig. 4.1 and 4.5).

Thevanayagam et al. (2002) investigated the effect of silt on undrained shear behavior of silty sand. In test specimens where silt was contained within a metastable sand skeleton, silt provided a cushioning effect that prevented the loose sand skeleton from collapsing. This cushioning effect increased strength of the soil mixture compared to clean sand due to an increase in dilation and deviator stress ($\Delta\sigma_d$). The observations made by Thevanayagam et al. (2002) agree with the trends observed in waste rock mixed with fine-garnet and copper tailings that displayed the largest $\Delta\sigma_d$ of any material (Fig. 4.13b).

4.3.1.2 Coarse-Garnet Tailings as a Mixture

Coarse-garnet tailings contained approximately 10 % fines and behaved as a mixture similar to co-mixed WR&T with fine-garnet tailings. The coarse-garnet tailings alone were strongly dilative at σ'_c = 40 kPa, similar to the fine-garnet tailings mixed with waste rock (Fig. 4.13a). Sand particles in the coarse-garnet tailings can be viewed analogous to the waste rock particles and fines analogous to the fine-garnet tailings. As the coarse-garnet specimen consolidated and subsequently sheared, sand particles contracted and applied stress to the fine-grained fraction retained in the void space. The shear response of coarse-garnet tailings alone was strongly dilative, similar to the fine-garnet and waste rock mixture.

The optimum mixture ratio for the coarse garnet as a mixture of sand and fines was calculated to be 10.2 following procedures outlined in Section 2.4. The maximum void ratio of the clean coarse-garnet sand (i.e., particles ≥ 0.075 mm) was 0.89 following procedures in ASTM D 4254. The mixture ratio for the coarse-garnet tailings at the original f_c (10.1 %) was 8.90. Considering that R is less than R_{opt}, the particle structure of the coarse-garnet tailings likely was a metastable structure with some sand particles floating in a silt matrix (see Fig. 2.3). The fine-grained fraction of the coarse-garnet tailings, which predominantly was silt, controlled shear behavior of the soil and sand particles provide a secondary reinforcing effect.

The strong dilative tendencies displayed by the coarse-garnet tailings (Fig. 4.3a and 4.3b) agree with behavior observed on similar soils by Thevanayagam et al. (2002), Rahman et al. (2014), and Carraro et al. (2009). Carraro et al. (2009) attributed the increased dilatancy of silty sands to interlocking between angular silt and sand particles that created a “jamming” effect during shear. Surfaces of the sand grains in coarse-garnet tailings likely were not perfectly smooth and provided increased interlocking potential with the angular silt particles that could lead to additional dilation during shear. This effect may be exaggerated with the coarse-garnet tailings particles, which were very angular as a result of ore extraction processes.

4.3.3 Salinity Effects

High salinity of the pore fluid in soda ash tailings is a possible explanation for the high ϕ' of the tailings alone. Previous studies have reported an increase in shear strength with increasing pore fluid salinity for hard rock mine tailings and natural clays such as bentonite (e.g., Rodriguez 2006; Siddiqua et al. 2014). The presence of salt in the pore fluid decreases the diffuse double layer on the clay particles that induces particle flocculation. Tiwari et al. (2005) report that soils with as little as 10 % clay content can flocculate and that these clay flocs can behave similarly to a silt or sand particle and increase shear strength. Soda ash tailings contained 18.0 % clay (Table 3.1) and clay particle flocculation is believed to be the main contribution to an increase in shear strength.

The effect of salinity is exaggerated when clay minerals are composed of montmorillonite or illite (Sides and Barden 1971). Clay minerals in the soda ash tailings were identified as mixed layered illite and smectite based on XRD and XRF results (Table 3.2), which further support the hypothesis that salinity contributed to an elevated ϕ' in soda ash tailings. Newson et al. (2006) conducted CU triaxial compression tests on bauxite residue that had similar Atterberg limits, particle size distribution, and pore fluid chemistry to the soda ash tailings. Results from triaxial tests on the bauxite residue demonstrated a higher than average ϕ' of 42°, supporting the results obtained for the soda ash tailings.

Table 4.1. Summary of test parameters and results for each material. Failure criterion of reaching the K_f line was used to determine the effective friction angle and test parameters at failure.

Material	Test Type	Target σ_c' (kPa)	σ_c' (kPa)	σ_{1f}'[a] (kPa)	σ_{3f}'[a] (kPa)	ϕ' (°)	ε_{af} (%)	Initial[b]		Final[c]		B	R	R_{opt}
								e_r	e_t	e_r	e_t			
Waste Rock	CD	5	5.7	51.6	8.7	45.4	1.1	0.69	-	0.72	-	0.97	-	-
		5	6.1	58.5	11.8	41.6	4.0	0.68	-	0.71	-	0.96	-	
		10	10.8	84.5	18.2	40.2	6.8	0.72	-	0.72	-	0.98	-	
		20	20.7	127.6	27.6	40.1	5.9	0.72	-	0.72	-	0.95	-	
		40	40.0	222.5	48.4	40.0	8.4	0.72	-	0.67	-	0.96	-	
	CU	5	6.3	56.8	14.5	36.4	10.5	0.75	-	0.68	-	0.99	-	
		10	12.6	64.0	15.2	38.1	2.7	0.82	-	0.76	-	0.98	-	
		20	22.8	102.2	27.0	35.6	7.1	1.06	-	0.72	-	0.97	-	
		40	42.5	96.0	23.6	37.3	4.0	0.89	-	0.71	-	1.00	-	
Fine-Grained Garnet	CU	5	4.3	19.4	4.9	36.6	10.0	-	1.13	-	0.76	0.99	-	-
		10	9.8	25.2	7.2	33.9	11.3	-	1.16	-	0.72	0.98	-	
		20	20.0	78.8	19.6	37.0	11.8	-	1.09	-	0.70	0.98	-	
		40	40.0	96.4	24.6	36.3	10.8	-	1.06	-	0.65	0.97	-	
Coarse-Grained Garnet	CU	5	4.7	42.4	8.7	41.2	6.2	-	0.83	-	0.67	0.98	-	-
		10	10.0	45.1	10.6	38.3	6.3	-	0.81	-	0.70	0.98	-	
		20	20.0	584.8	121.8	40.9	5.7	-	0.80	-	0.61	0.99	-	
		20	20.2	437.7	96.4	39.7	4.4	-	0.79	-	0.60	0.99	-	
		40	39.9	300.4	68.1	39.1	5.9	-	0.79	-	0.64	0.96	-	
Copper	CU	5	5.1	13.6	3.6	35.9	11.2	-	2.60	-	0.69	0.99	-	-
		10	9.9	19.6	5.6	34.0	5.3	-	1.62	-	0.66	0.99	-	
		20	19.9	29.8	8.0	35.3	5.7	-	1.34	-	0.64	0.95	-	
		40	39.9	98.5	25.4	36.1	8.9	-	1.33	-	0.62	0.98	-	

Note: σ_c' = effective confining stress; σ_{1f}' = major effective principle stress at failure; σ_{3f}' = minor effective principle stress at failure; ϕ' = effective friction angle; ε_{af} = axial strain at failure; e_r = waste rock void ratio; e_t = tailings void ratio; B = Skempton's pore pressure parameter; R = mixture ratio; R_{opt} = optimum mixture ratio; CD = consolidated drained triaxial test; CU = consolidated undrained triaxial test.

[a]Corrected for additional stresses due to membrane.

[b]Void ratio at the beginning of shear for CD tests and as-placed conditions for CU tests.

[c]Void ratio at the end of the shearing for CD tests and during shear for CU tests.

Table 4.1 (Continued.) Summary of test parameters and results for each material. Failure criterion of reaching the K_f line was used to determine the effective friction angle and test parameters at failure.

Material	Test Type	Target σ_c' (kPa)	σ_c' (kPa)	$\sigma_{1f}'^{a}$ (kPa)	$\sigma_{3f}'^{a}$ (kPa)	ϕ' (°)	ε_{af} (%)	Initial[b] e_r	Initial[b] e_t	Final[c] e_r	Final[c] e_t	B	R	R_{opt}
Soda Ash	CU	5	5.0	11.7	2.5	40.6	3.3	-	3.55	-	1.50	1.00	-	-
		10	12.0	20.5	6.1	32.8	6.6	-	3.55	-	1.33	0.98	-	
		10	12.3	18.5	5.8	31.6	7.5	-	3.55	-	1.32	0.99	-	
		10	10.0	18.9	2.5	50.3	15.1	-	3.55	-	1.31	0.97	-	
		20	19.8	24.0	4.2	44.5	15.4	-	3.55	-	1.24	1.00	-	
		40	39.1	59.3	9.9	45.5	12.6	-	3.55	-	1.11	0.98	-	
Fine-Garnet Mixture	CU	5	6.8	80.2	17.5	39.9	6.0	0.70	1.15	0.75	1.31	0.96	2.53	2.45
		10	13.4	100.1	21.2	40.6	2.5	1.04	1.15	0.91	0.90	0.95	1.69	
		20	22.7	112.9	23.9	40.6	2.8	1.02	1.15	0.91	0.91	0.95	1.72	
		40	44.0	229.7	49.2	40.3	2.4	0.75	1.15	0.71	1.03	0.96	2.33	
Coarse-Garnet Mixture	CU	5	8.3	91.7	18.6	41.5	3.8	0.69	0.82	0.63	0.66	0.98	2.19	2.12
		10	12.9	120.1	28.8	37.8	21.8	0.69	0.78	0.61	0.58	0.97	2.16	
		20	23.1	97.3	24.0	37.1	5.7	0.66	0.77	0.62	0.67	0.97	2.26	
		40	40.6	146.0	31.4	40.3	3.8	0.71	0.80	0.63	0.61	0.95	2.16	
Copper Mixture	CU	5	8.0	79.5	17.9	39.2	3.3	0.90	1.36	0.83	1.18	0.99	2.43	3.04
		10	12.8	139.6	28.8	41.1	4.0	0.80	1.34	0.75	1.21	0.97	2.71	
		20	23.7	204.0	45.0	39.7	4.7	0.81	1.34	0.76	1.18	1.00	2.67	
		40	43.3	255.2	58.4	38.9	5.7	0.87	1.32	0.77	1.06	0.95	2.46	
Soda Ash Mixture	CU	5	8.4	79.3	19.3	37.5	6.5	0.94	3.55	0.78	2.78	0.96	4.78	5.75
		10	12.1	131.5	32.7	37.0	9.7	0.87	3.55	0.64	2.35	0.95	5.16	
		20	22.8	89.7	22.3	37.0	4.1	0.94	3.53	0.81	2.92	0.96	4.74	
		40	43.4	138.6	33.7	37.5	7.7	0.99	3.53	0.78	2.58	0.95	4.50	

Note: σ_c' = effective confining stress; σ_{1f}' = major effective principle stress at failure; σ_{3f}' = minor effective principle stress at failure; ϕ' = effective friction angle; ε_{af} = axial strain at failure; e_r = waste rock void ratio; e_t = tailings void ratio; B = Skempton's pore pressure parameter; R = mixture ratio; R_{opt} = optimum mixture ratio; CD = consolidated drained triaxial test; CU = consolidated undrained triaxial test.

[a]Corrected for additional stresses due to membrane.

[b]Void ratio at the beginning of shear for CD tests and as-placed conditions for CU tests.

[c]Void ratio at the end of the shearing for CD tests and during shear for CU tests.

Table 4.2. Effective friction angles (in degrees) for the six failure criteria defined by Brandon et al. (2006) from consolidated undrained triaxial tests performed on copper tailings at effective confining stress of 5, 10, 20, and 40 kPa.

Failure Criterion	σ'_c				Average	Standard Deviation
	5 kPa	10 kPa	20 kPa	40 kPa		
$\Delta\sigma_{d,max}$	33.4	32.3	33.8	33.6	33.3	0.6
$(\sigma_1'/\sigma_3')_{max}$	44.8	38.5	36.0	36.7	39.0	3.5
$u_{e,max}$	33.9	24.9	34.8	32.6	31.5	3.9
$A = 0$	35.8	33.9	NA	35.1	35.0	0.8
K_f Line	35.9	34.0	35.3	36.1	35.3	0.8
ε_{af} = 15%	37.1	33.7	35.1	35.5	35.3	1.2

Note: σ'_c = effective confining stress; $\Delta\sigma_{d,max}$ maximum deviator stress; $(\sigma_1'/\sigma_3')_{max}$ = maximum principle stress ratio; $u_{e,max}$ = maximum excess pore pressure; A = Skempton's pore pressure parameter; K_f = failure line in p'-q space; ε_{af} = axial strain at failure; NA = not applicable.

Table 4.3. Average effective friction angles for all materials tested. The standard deviation of each failure criterion is given in parentheses.

Material	Test Type	ϕ' (°)			Practical Estimate
		$\Delta\sigma_{d,max}$	K_f Line	ε_{af} = 15%	
Waste Rock	CD	41.4 (1.3)	41.5 (2.3)	41.9 (1.9)	41
	CU	37.0 (1.4)	36.9 (0.9)	37.7 (1.0)	37
Fine-Garnet Tailings	CU	35.0 (1.0)	36.0 (1.2)	35.4 (1.2)	35
Coarse-Garnet Tailings	CU	37.7 (1.7)	39.8 (1.1)	38.2 (1.2)	38
Copper Tailings	CU	33.3 (0.6)	35.3 (0.8)	35.3 (1.2)	34
Soda Ash Tailings	CU	40.6 (6.6)	45.2 (6.8)	39.4 (5.0)	41
Fine-Garnet Mixture	CU	39.9 (1.4)	40.4 (0.3)	39.9 (0.9)	40
Coarse-Garnet Mixture	CU	39.1 (1.6)	39.2 (1.8)	38.8 (1.6)	39
Copper Mixture	CU	38.8 (0.4)	39.7 (0.9)	38.7 (0.3)	39
Soda Ash Mixture	CU	38.6 (1.0)	37.3 (0.2)	38.6 (1.0)	38

Note: ϕ' = effective friction angle; $\Delta\sigma_{d,max}$ = maximum deviator stress; K_f = failure line in p'-q space; ε_{af} = axial strain at failure; CD = consolidated drained; CU = consolidated undrained.

Table 4.4. Void ratio (initial and steady state) and state parameters for waste rock alone and mixed with tailings. The equivalent granular void ratios and state parameter are shown for coarse-garnet tailings and waste rock and tailings mixtures.

Material	Target σ_c' (kPa)	σ_c' (kPa)	e^{*a}	$e^*_{SS}{}^a$	Ψ*
Waste Rock CD	5	5.65	0.69	0.75	-0.05
	10	10.77	0.72	0.72	0.00
	20	20.66	0.72	0.72	0.00
	40	9.97	0.72	0.67	0.06
Waste Rock CU	5	6.30	0.75	0.87	-0.12
	10	11.91	0.76	0.82	-0.06
	20	22.82	0.72	0.79	-0.07
	40	42.50	0.71	0.75	-0.04
Fine Garnet Tailings f_c = 63.3 %	5	4.28	0.76	0.82	-0.06
	10	9.84	0.72	0.78	-0.06
	20	20.00	0.70	0.75	-0.05
	40	40.01	0.65	0.71	-0.06
Coarse Garnet Tailings[b] f_c = 10.1 %	5	4.70	0.77	0.84	-0.07
	10	10.04	0.80	0.83	-0.02
	20	20.04	0.71	0.81	-0.10
	20	20.22	0.70	0.81	-0.11
	40	39.93	0.74	0.79	-0.05
Copper Tailings f_c = 45.3 %	5	5.05	0.69	0.71	-0.02
	10	9.93	0.66	0.69	-0.03
	20	19.92	0.64	0.67	-0.03
	40	39.91	0.62	0.64	-0.02
Soda Ash Tailings f_c = 73.5 %	5	4.95	1.50	1.38	0.12
	10	12.01	1.33	1.24	0.09
	10	12.29	1.32	1.23	0.08
	10	10.03	1.31	1.27	0.04
	20	19.78	1.24	1.16	0.08
	40	39.13	1.11	1.04	0.07

Note: σ_c' = effective confining stress; e^* = initial equivalent granular void ratio; e^*_{SS} = equivalent granular void ratio at steady state; Ψ* = equivalent granular state parameter; f_c = fines content.
[a]The equivalent granular void ratio for waste rock and tailings alone is the void ratio of the waste rock or tailings.

Table 4.4. (Continued). Void ratio (initial and steady state) and state parameters for waste rock alone and mixed with tailings. The equivalent granular void ratios and state parameter are shown for coarse-garnet tailings waste rock and tailings mixtures.

Material	Target σ_c' (kPa)	σ_c' (kPa)	e^{*a}	$e^*_{SS}{}^{a}$	Ψ^*
Fine Garnet Mixtures	5	6.78	0.70	0.82	-0.12
	10	13.39	0.74	0.80	-0.06
	20	22.71	0.74	0.78	-0.04
	40	43.97	0.65	0.76	-0.11
Coarse Garnet Mixtures	5	8.31	0.72	0.98	-0.26
	10	12.94	0.84	0.94	-0.10
	20	23.14	0.81	0.90	-0.09
	40	43.27	0.80	0.85	-0.04
Copper Mixtures	5	7.96	0.69	1.19	-0.51
	10	12.75	0.60	1.11	-0.51
	20	23.66	0.59	1.00	-0.41
	40	43.27	0.59	0.88	-0.30
Soda Ash Mixtures	5	8.38	0.66	0.79	-0.13
	10	12.13	0.55	0.76	-0.22
	20	22.76	0.69	0.71	-0.02
	40	43.38	0.65	0.67	-0.02

Note: σ_c' = effective confining stress; e^* = initial equivalent granular void ratio; e^*_{SS} = equivalent granular void ratio at steady state; Ψ^* = equivalent granular state parameter; f_c = fines content.
[a]The equivalent granular void ratio for waste rock and tailings alone is the void ratio of the waste rock or tailings.

Table 4.5. Fitting parameters used to define the steady state line for waste rock alone, tailings alone, and waste rock mixed with tailings.

Material	$e_{\lambda,SS}$	λ	R^2
Waste Rock CD	0.99	0.065	0.99
Fine-Garnet Tailings	0.89	0.049	0.92
Coarse-Garnet Tailings	0.88	0.024	0.41
Copper Tailings	0.77	0.033	0.96
Soda Ash Tailings	1.65	0.165	0.97
Fine-Garnet Mixtures	0.90	0.038	0.30
Coarse-Garnet Mixtures	1.18	0.089	0.22
Copper Mixtures	1.62	0.195	0.73
Soda Ash Mixtures	0.94	0.071	0.09

Note: $e_{\lambda,SS}$ = fitting constant to determine the location of the steady state line (SSL); λ = slope of the SSL; R^2 = coefficient of determination.

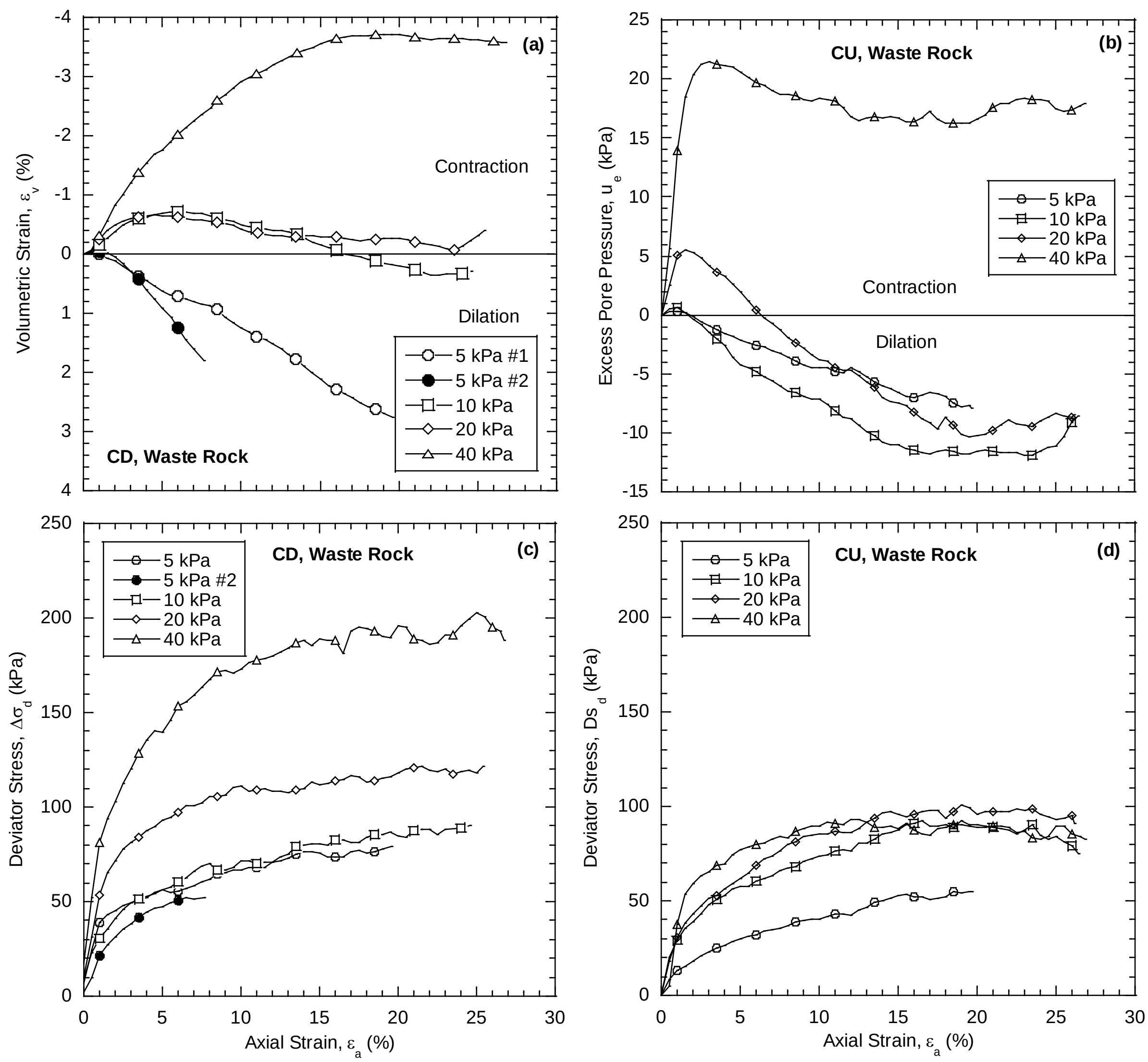

Fig. 4.1. Relationships of (a) volumetric strain, (b) excess pore pressure, (c) deviator stress from CD tests, and (d) deviator stress from CU tests versus axial strain for experiments conducted on the synthetic waste rock at effective confining pressures of 5, 10, 20, and 40 kPa.

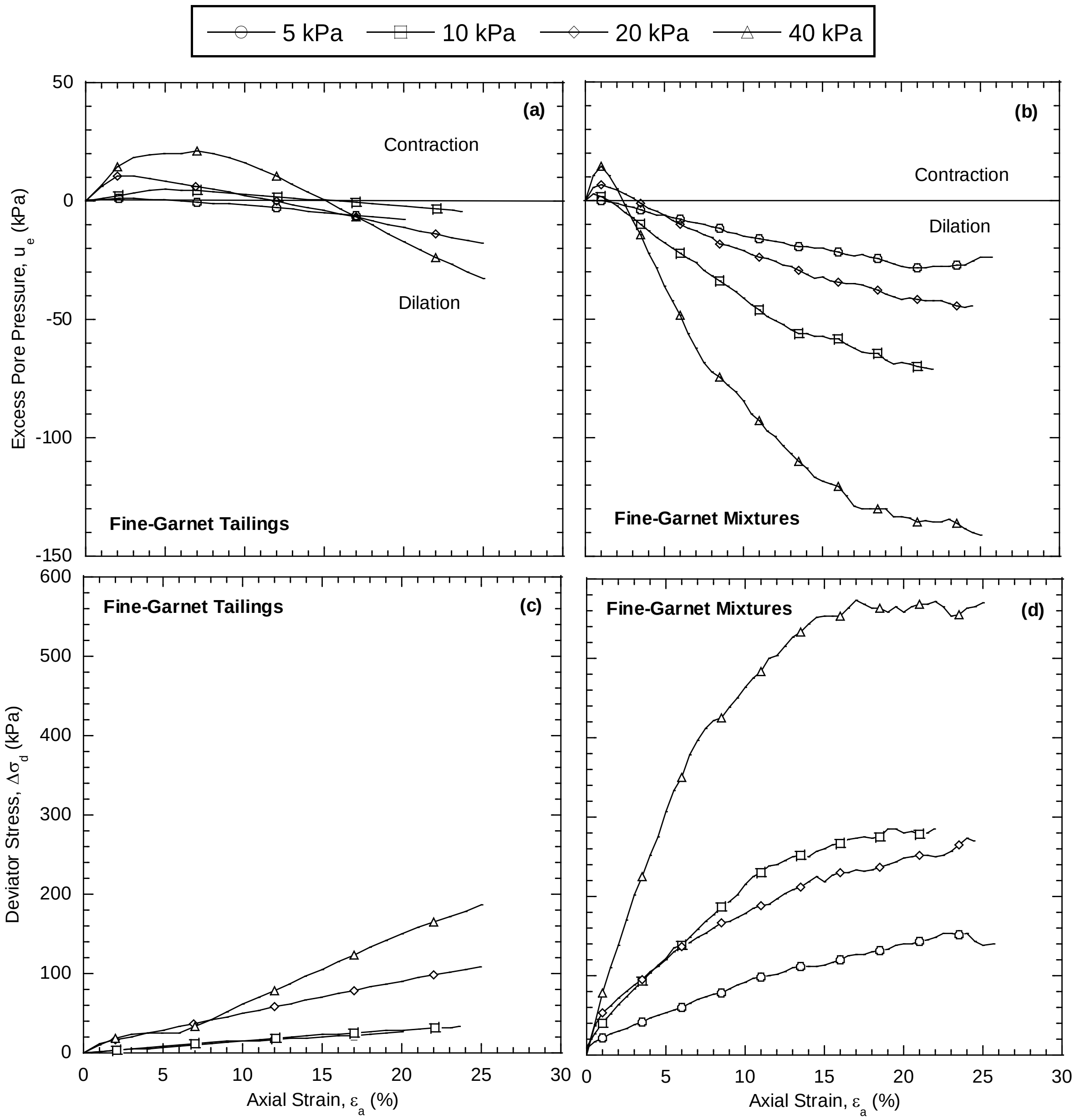

Fig. 4.2. Relationships of (a) fine-garnet tailings excess pore pressure, (b) fine-garnet mixtures excess pore pressure, (c) fine-garnet tailings deviator stress, and (d) fine-garnet mixtures deviator stress versus axial strain for consolidated-undrained triaxial compression tests.

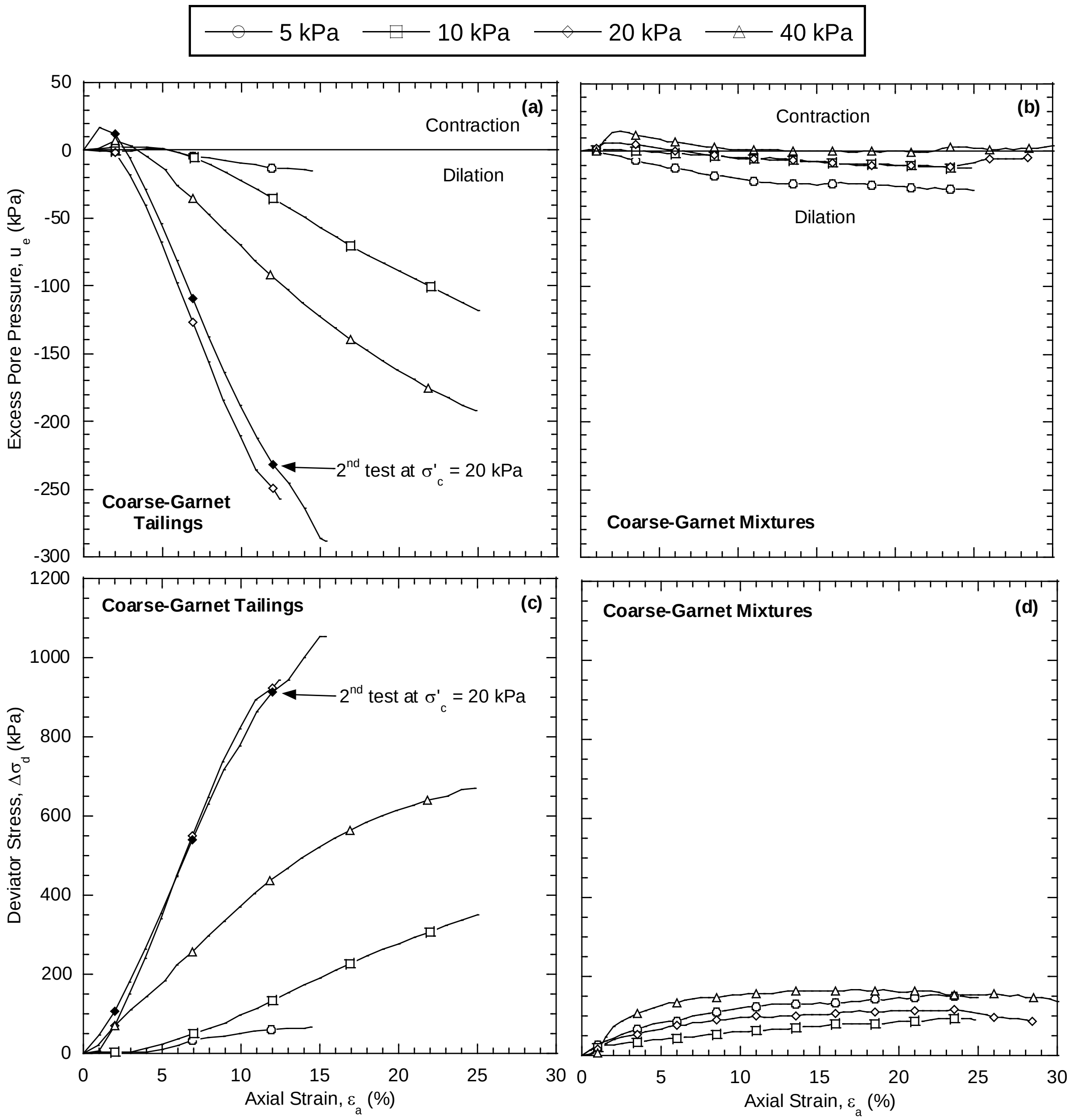

Fig. 4.3. Relationships of (a) coarse-garnet tailings excess pore pressure, (b) coarse-garnet mixtures excess pore pressure, (c) coarse-garnet tailings deviator stress, and (d) coarse-garnet mixtures deviator stress versus axial strain for consolidated-undrained triaxial compression tests.

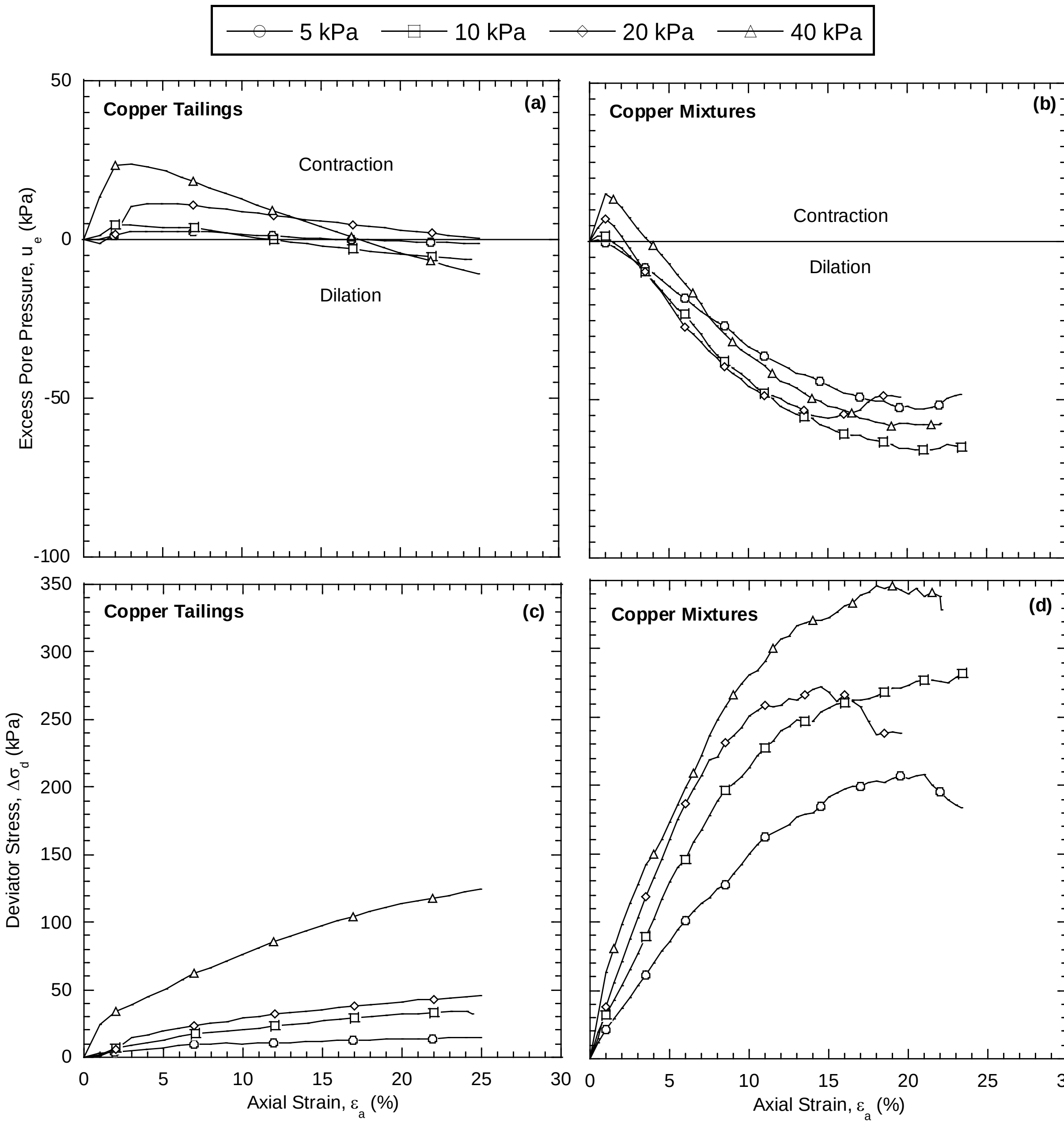

Fig. 4.4. Relationships of (a) copper tailings excess pore pressure, (b) copper mixtures excess pore pressure, (c) copper tailings deviator stress, and (d) copper mixtures deviator stress versus axial strain for consolidated-undrained triaxial compression tests.

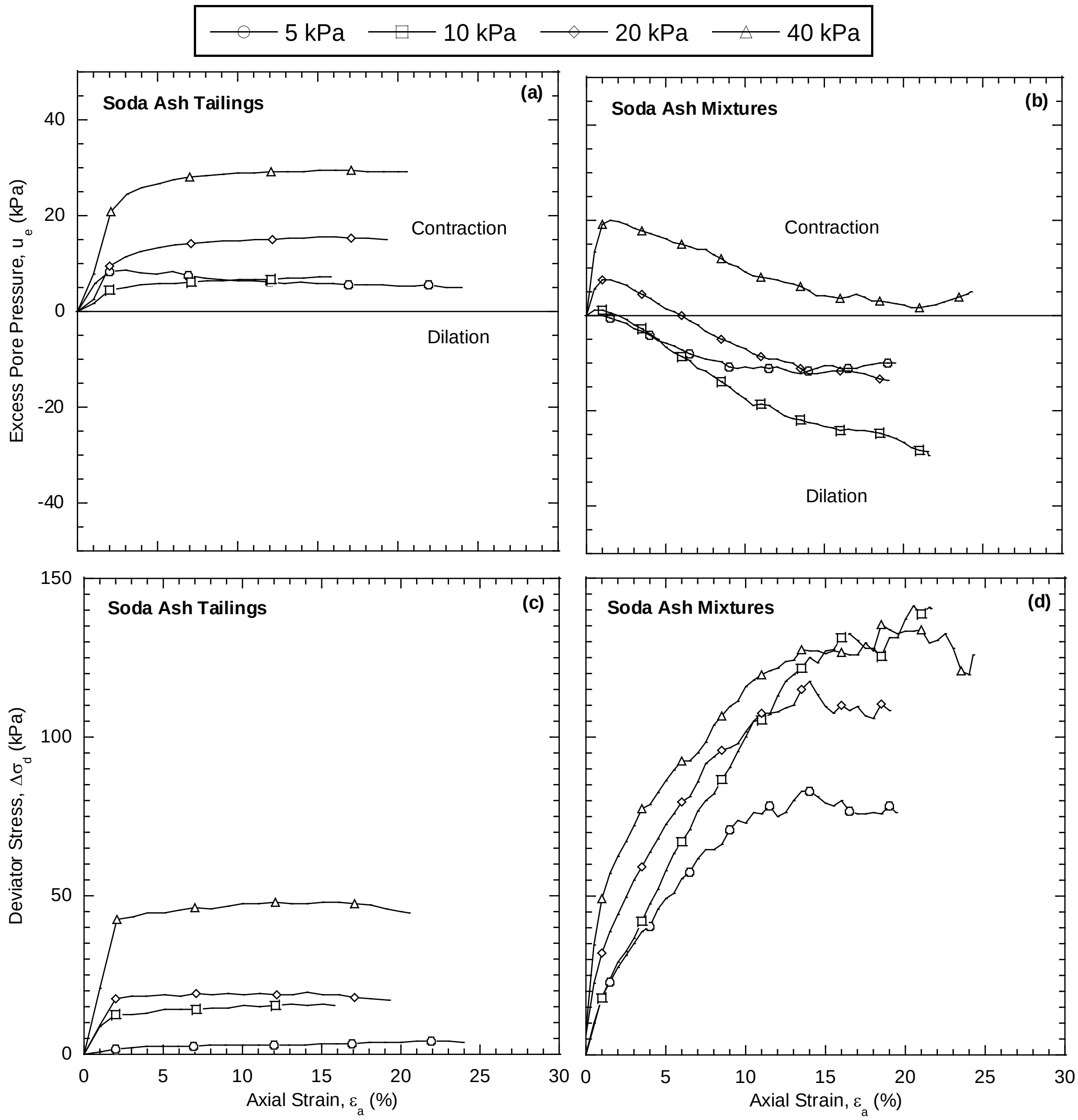

Fig. 4.5. Relationships of (a) soda ash tailings excess pore pressure, (b) soda ash mixtures excess pore pressure, (c) soda ash tailings deviator stress, and (d) soda ash mixtures deviator stress versus axial strain for consolidated-undrained triaxial compression tests. Only the third test conducted at an effective confining stress of 10 kPa is shown.

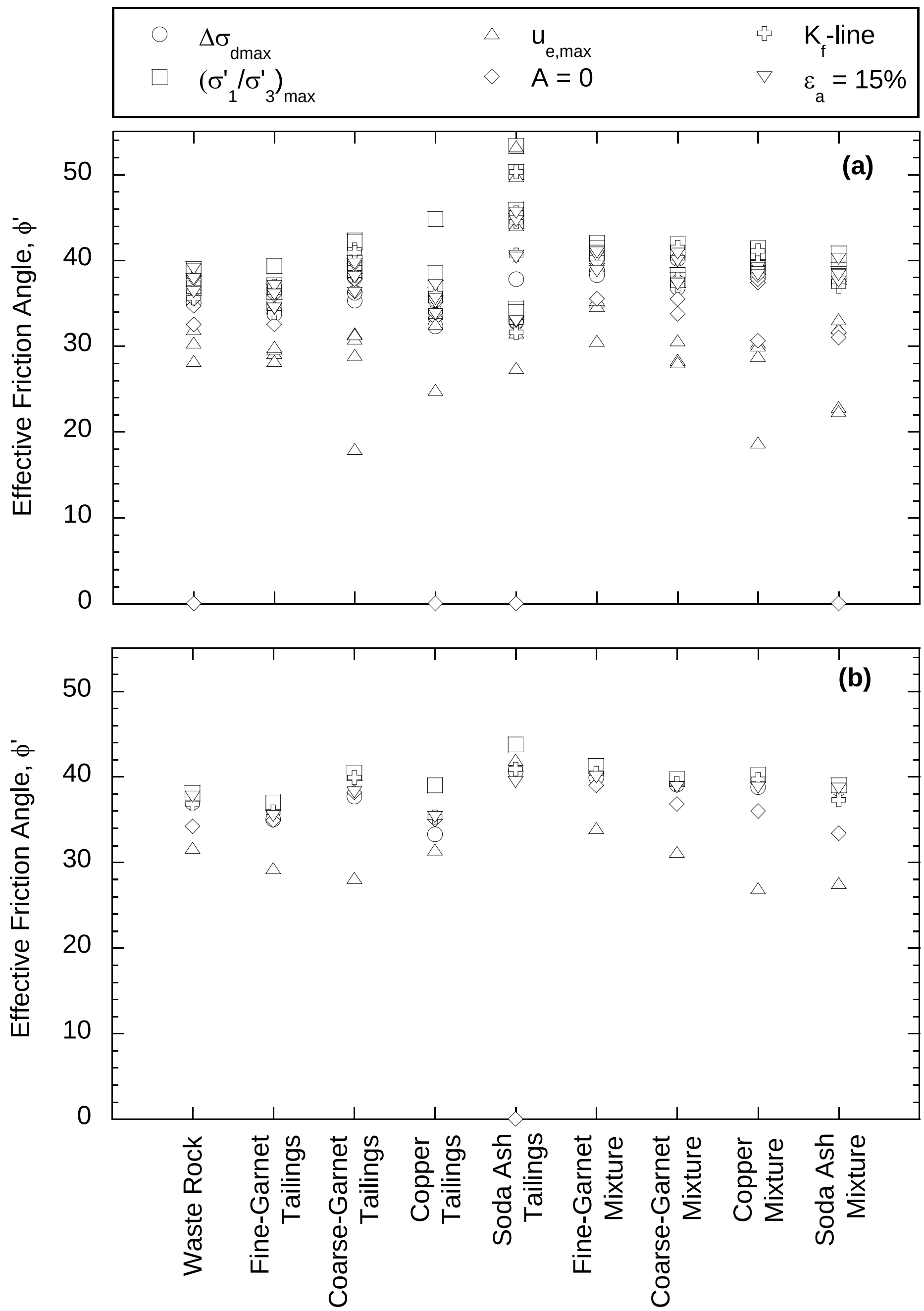

Fig. 4.6. Effective peak friction angles from (a) each test for each material and (b) arithmetic averaged values defined using the six failure criteria proposed by Brandon et al. (2006): (1) maximum deviator stress, $\Delta\sigma_{d,max}$; (2) maximum principle stress ratio, $(\sigma'_1/\sigma'_3)_{max}$; (3) maximum excess pore pressure, $u_{e,max}$; (4) Skempton's pore pressure parameter (A) equal to zero; (5) reach the failure (K_f) line in p'-q space; and (6) limiting axial strain (ε_a = 15%). The failure criterion of A = 0 could not be applied to waste rock tested at an effective confining stress (σ'_c) of 40 kPa, copper tailings tested at σ'_c = 20 kPa, any of the tests conducted on soda ash tailings, and the soda ash mixture tested at σ'_c = 20 kPa. The friction angle for these tests was assigned a value of zero.

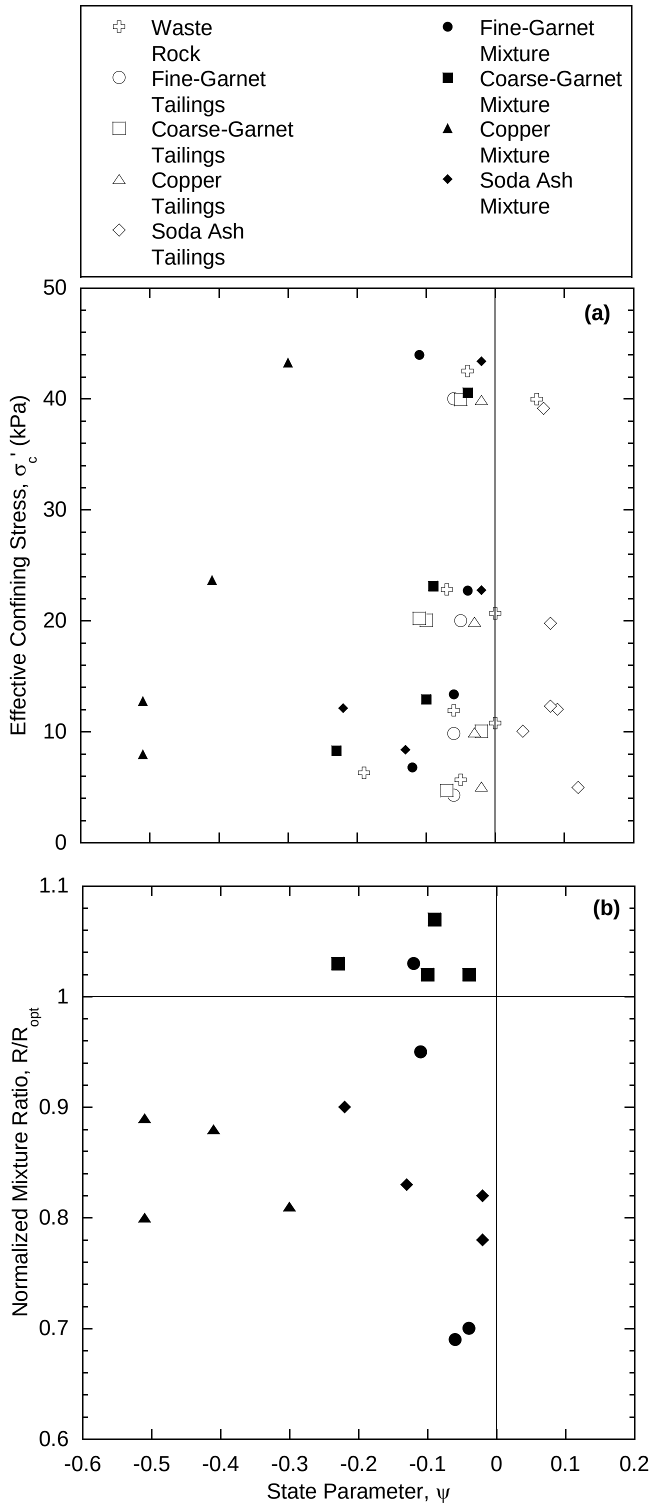

Fig. 4.7. Relationships of (a) effective confining stress from each test for each material and (b) normalized mixture ratio (R/R_{opt}) from each test for each WR&T mixture versus the state parameter.

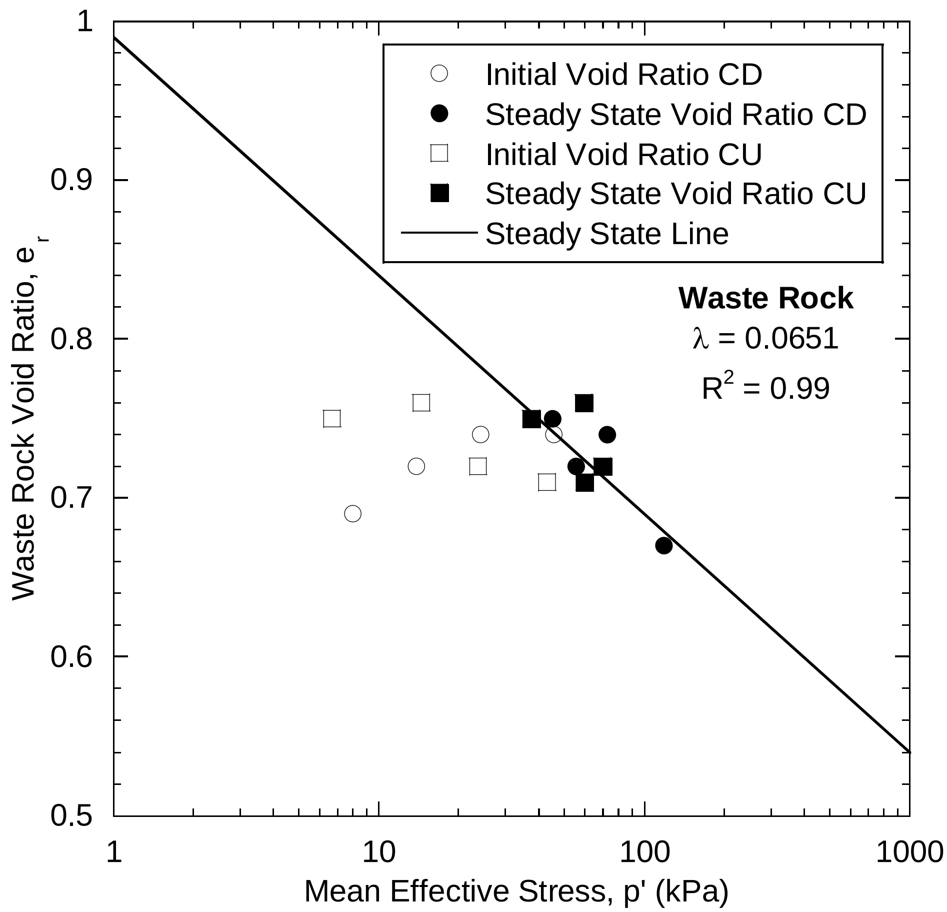

Fig. 4.8. Relationship of void ratio with mean effective stress for consolidated drained and undrained triaxial tests on waste rock alone. The initial and steady states are shown with the steady state line determined from consolidated drained triaxial experiments conducted on waste rock. The waste rock void ratio for the CU test at σ'_c = 5 kPa was determined using specimen dimensions prior to application of cell pressure. All other void ratios were determined based on specimen water content which was measured after shearing occurred.

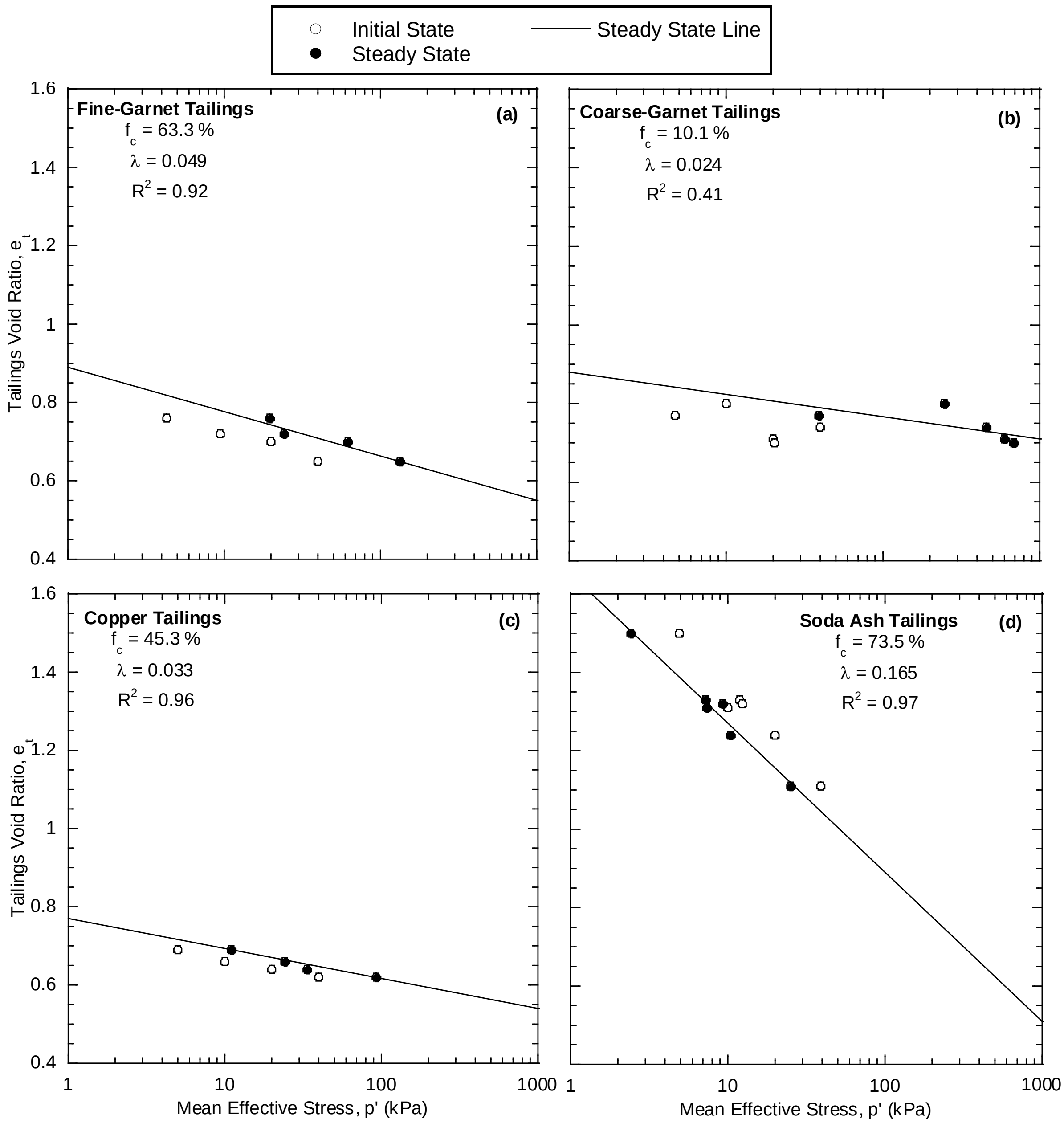

Fig. 4.9. Relationship of tailings void ratio with mean effective stress for consolidated undrained triaxial tests on (a) fine-garnet, (b) coarse-garnet, (c) copper, and (d) soda ash tailings. The initial and steady states are shown with the steady state line for each tailings. Coarse-garnet tailings were considered a mixture and analyzed using the equivalent granular void ratio.

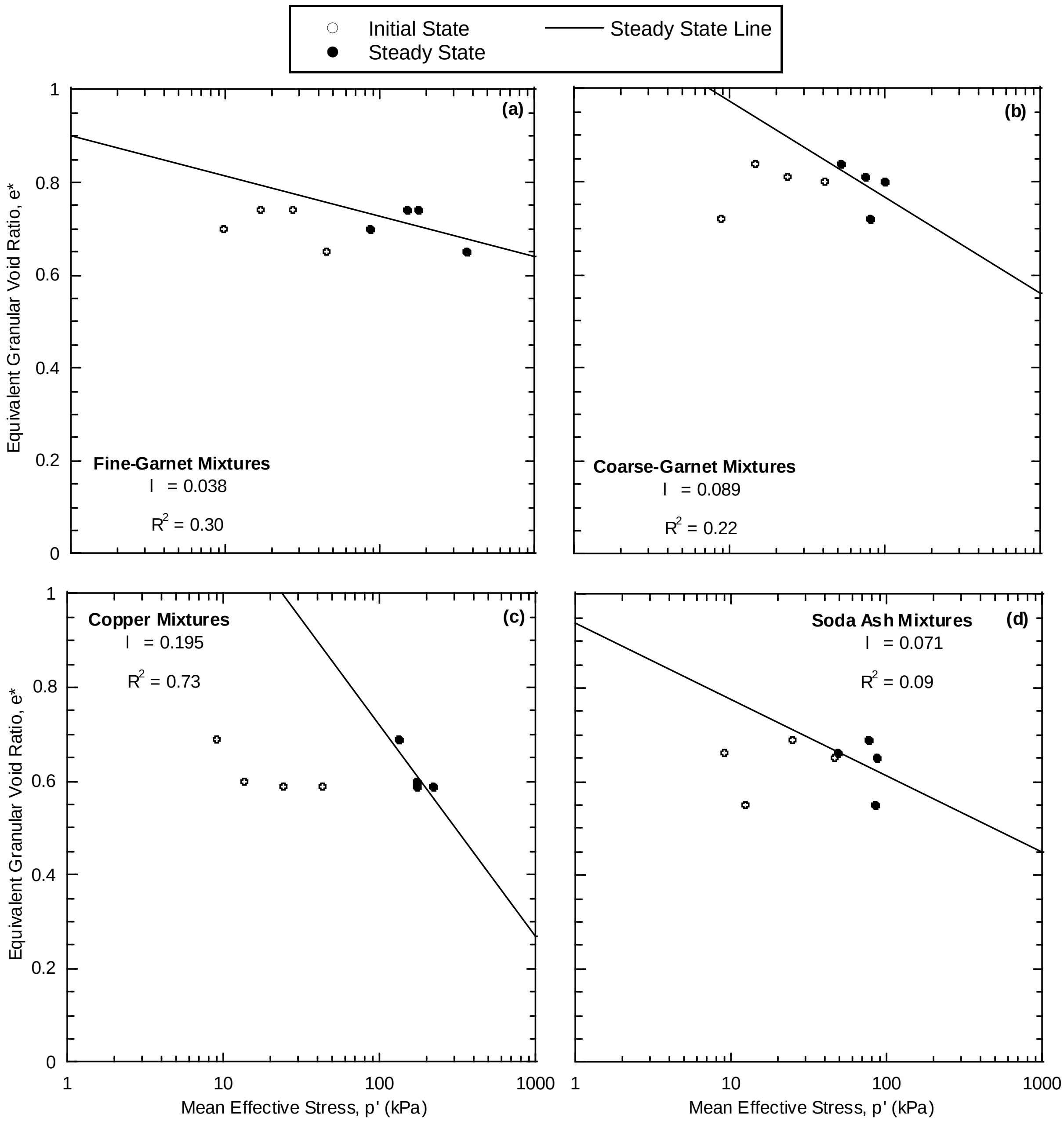

Fig. 4.10. Relationship of equivalent granular void ratio with mean effective stress for consolidated undrained triaxial tests on waste rock mixed with (a) fine-garnet, (b) coarse-garnet, (c) copper, and (d) soda ash tailings. The initial and steady states are shown with the steady state line for each waste mixture.

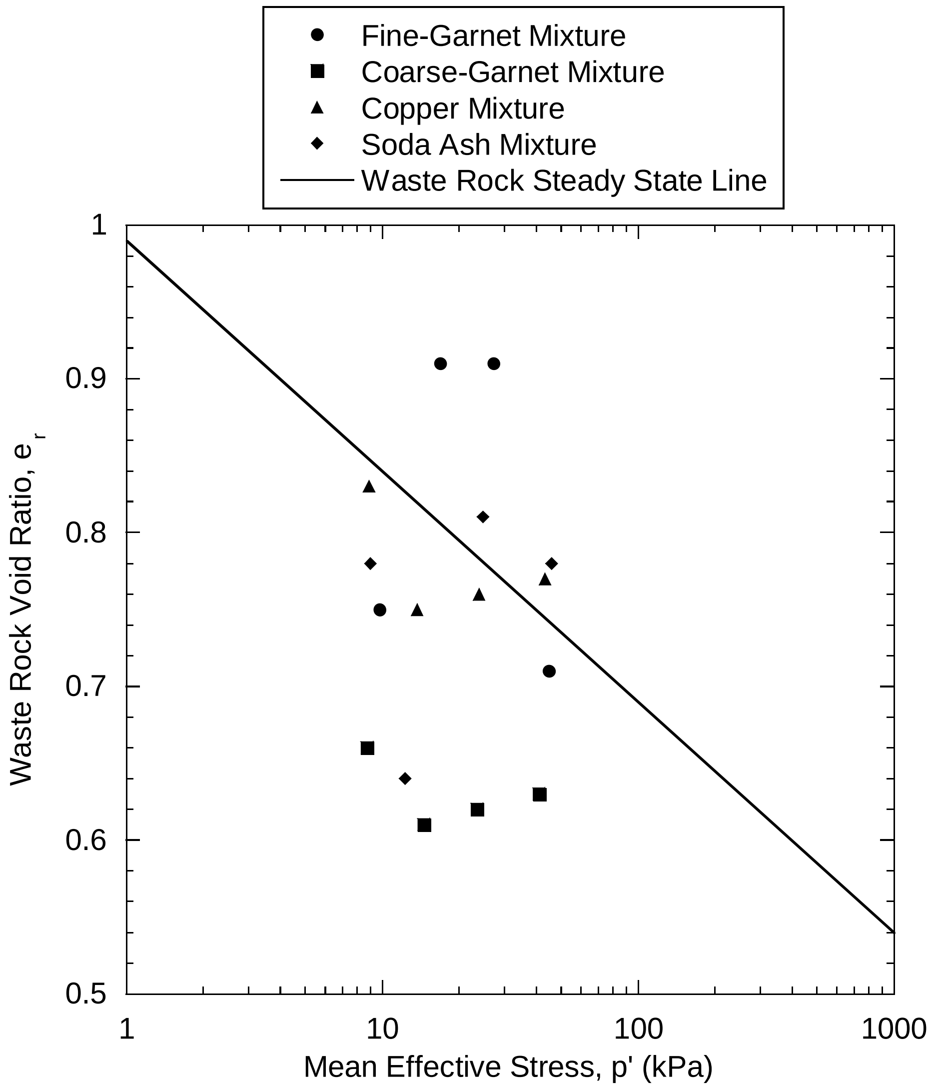

Fig. 4.11. Relationship of waste rock void ratio with mean effective stress for consolidated undrained triaxial tests on waste rock mixed with fine-garnet, coarse-garnet, copper, and soda ash tailings. The steady state for each mixture is shown with the steady state line for waste rock.

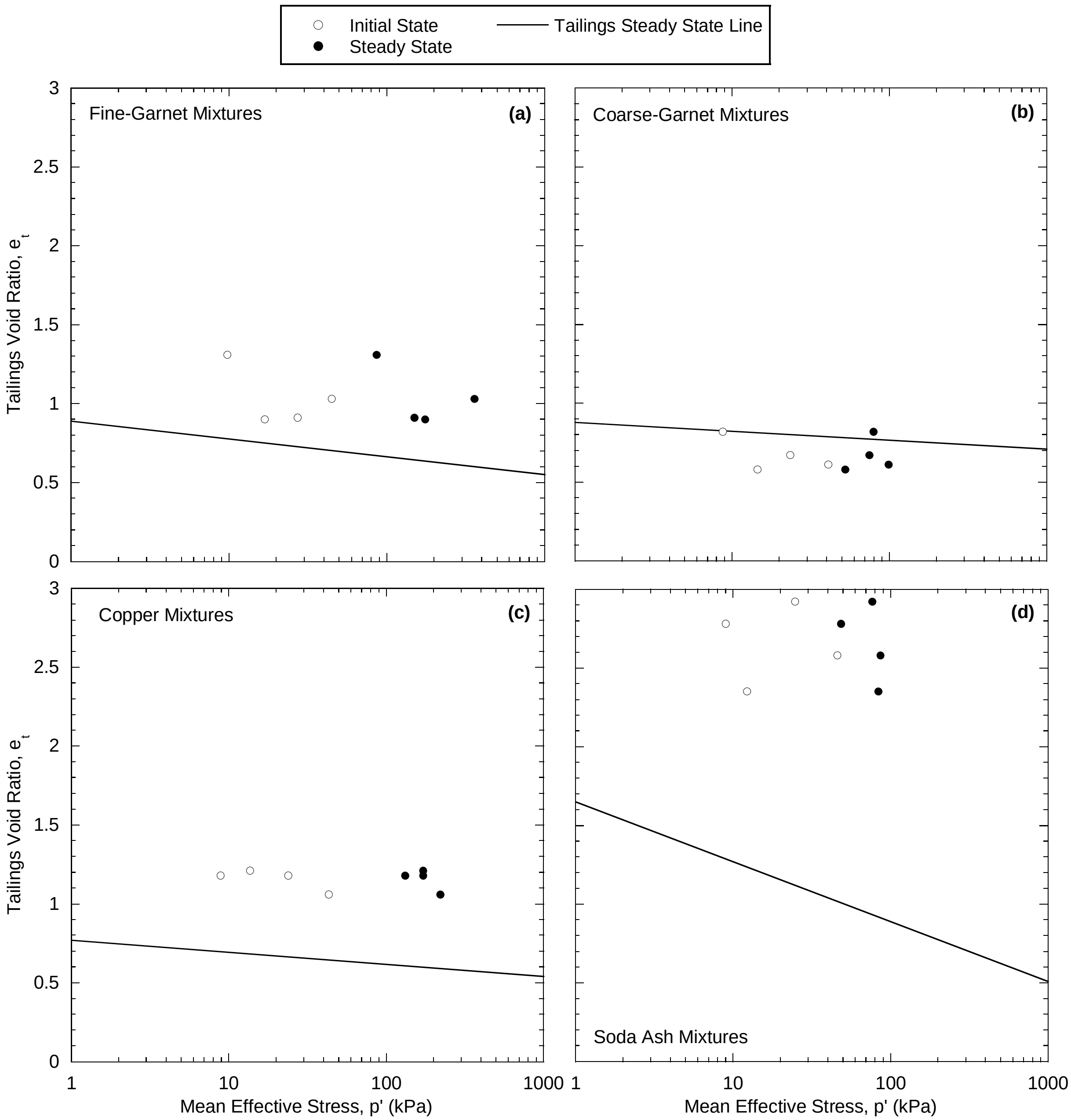

Fig. 4.12. Relationship of tailings void ratio with mean effective stress for consolidated undrained triaxial tests on waste rock mixed with (a) fine-garnet, (b) coarse-garnet, (c) copper, and (d) soda ash tailings. The initial and steady states are shown with the steady state line for tailings.

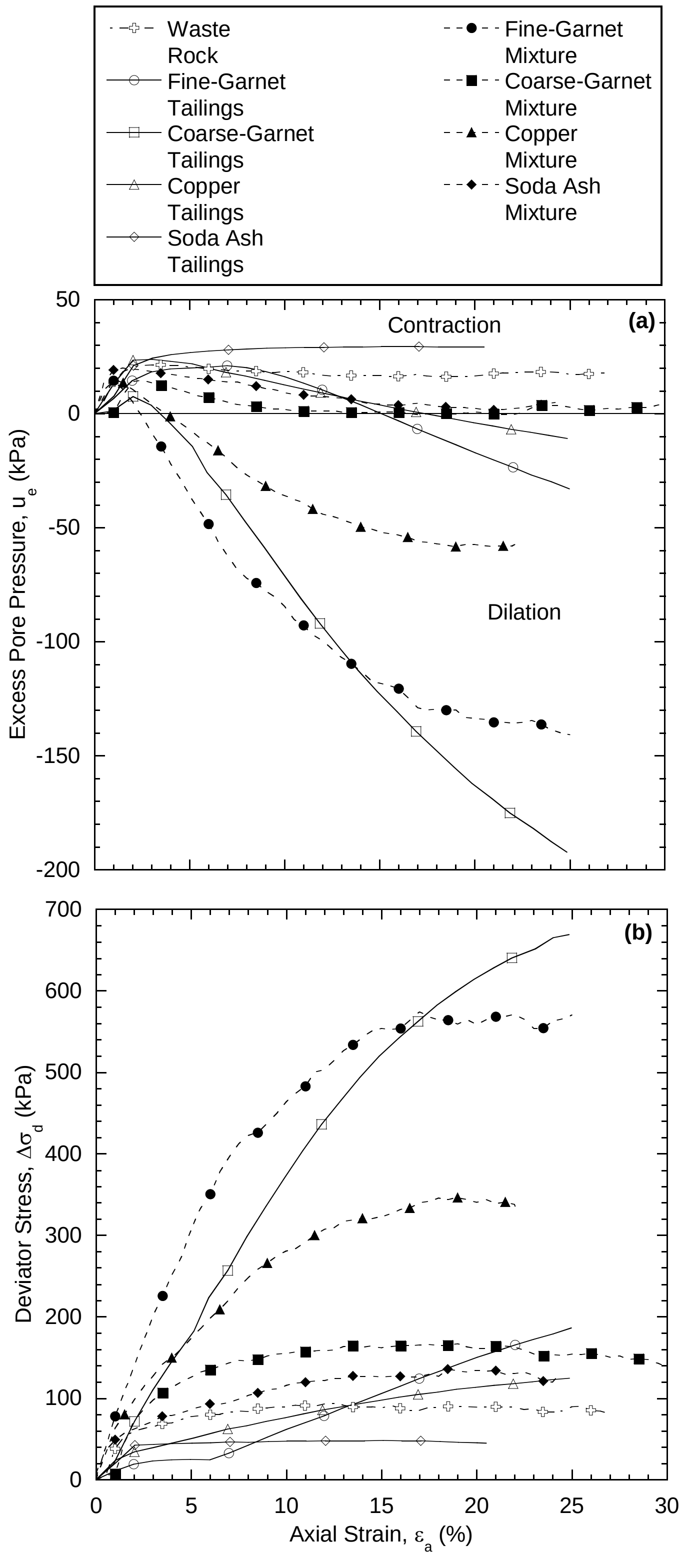

Fig. 4.13. Comparison of shear behavior for each material at an effective confining stress of 40 kPa. Excess pore pressure (a) and deviator stress (b) versus axial strain is shown for undrained triaxial compression tests conducted on each material.

CHAPTER 5: SUMMARY, CONCLUSIONS, AND FUTURE WORK

5.1 Summary and Conclusions

The effect of tailings composition on shear behavior of co-mixed waste rock and tailings (WR&T) was evaluated with a series of drained and undrained triaxial compression tests. Mine waste mixtures were created from a synthetic waste rock and four different types of tailings: (1) fine-grained garnet, (2) coarse-grained garnet, (3) copper, and (4) soda ash. Waste rock and WR&T mixtures were tested in a large scale triaxial apparatus to accommodate particles up to 25 mm in diameter, whereas tailings were evaluated in a traditional sized apparatus (specimen diameter = 38 mm). Shear strength behavior of mine waste mixtures was compared to behavior of individual materials. The following are observations and conclusions drawn from this study.

- Shear strength of co-mixed WR&T was similar to waste rock used in the mixture, regardless of tailings composition. The average effective stress friction angle (ϕ') for the waste rock was 41°, whereas ϕ' of the tailings ranged from 34° (copper) to 41° (soda ash). The mixtures had slightly lower ϕ' ranging from 40° (fine-garnet mixtures) to 38° (soda ash mixtures).
- Saline pore fluid in the soda ash tailings contributed to a high ϕ' (41°) for a normally-consolidated clay prepared from a slurry. Dissolved salts in the pore fluid likely caused clay particles to flocculate that increased ϕ'. The 18 % clay content in the soda ash tailings may have provided a lubricating effect on the waste rock particles to decrease ϕ' compared to other WR&T mixtures.
- Shear behavior of WR&T mixtures was a function of mixture ratio (*R*) and tailings composition. Tailings controlled shear behavior when *R* was less than the optimum mixture ratio (R_{opt}) and tailings were composed of silt. Shear behavior was controlled by waste rock when $R \geq R_{opt}$ and tailings were composed of sand or clay. Waste rock

became increasingly contractive as σ'_c increased. In WR&T mixtures, contraction of waste rock particles transferred normal and shear stress to tailings within the waste rock void space.

- Fine-garnet, copper, and soda ash mixtures were prepared at an actual $R < R_{opt}$, which corresponds to a soil structure where waste rock particles "float" in a tailings matrix. Shear behavior of this mixture structure was a function of tailings composition. Fine-garnet and copper mixtures expressed strong dilative tendencies, which were exaggerated relative to the dilative tendencies of the pure tailings specimens due to particle interlocking between silt and waste rock. Soda ash mixtures displayed contractive behavior, similar to soda ash tailings and waste rock alone.
- Coarse-garnet mixtures were prepared at $R > R_{opt}$ and displayed similar shear behavior to waste rock alone. Coarse-garnet tailings alone expressed strong dilative tendencies at all σ'_c. The higher R indicated more contact between waste rock particles, which limited participation of tailings in transferring normal and shear stresses.
- Shear behavior of tailings alone was accurately captured by the state parameter (ψ). The strong dilative tendencies expressed by coarse-garnet tailings tested at σ'_c = 20 kPa coincided with the most negative ψ. Soda ash tailings, which displayed purely contractive behavior, had positive ψ for all tests.
- The equivalent granular state parameter (ψ^*) was applicable to co-mixed WR&T and accurately captured observed shear behavior. State parameter analyses agreed with trends of increasing dilation with decreasing σ'_c and $R < R_{opt}$ observed when comparing shear behavior of all materials.
- The equivalent granular void ratio (e^*) was able to characterize the soil structure of co-mixed WR&T and explain observed shear behavior. Use of the waste rock or tailings

void ratio instead of *e** inaccurately predicted shear behavior and demonstrated that *e** is applicable for describing shear strength behavior of co-mixed WR&T.

5.2 Future Work

The present research considered only the shear behavior of homogeneous mixtures of waste rock and tailings prepared at an optimum mixture ratio. Further research can be conducted to investigate the effect of mixture ratio and mixing methods. Identifying mixing methods that are applicable to the field scale would be beneficial to determine the feasibility of co-mixed WR&T as water-balance covers. Research focusing on the unsaturated shear behavior of WR&T mixtures is also required to determine the feasibility of waste mixtures in water-balance covers. Additionally, actual waste rock mixed with different tailings sources can be studied to investigate the chemical effects on the shear strength behavior of mine waste mixtures.

REFERENCES

Albright, W.H., Benson, C.H., and Waugh, W.J. (2010). *Water Balance Covers for Waste Containment, Principles and Practice*, American Society of Civil Engineers, ASCE Press, Reston, VA.

Aubertin, M., Bussière, B., and Chapuis, R.P. (1996). Hydraulic conductivity of homogenized tailings from hard rock mine, *Canadian Geotechnical Journal*, 33(3), 470-482.

Been, K. and Jefferies, M.G. (1985). A state parameter for sands, *Géotechnique*, 35(2), 99-112.

Blight, G. (2010*). Geotechnical Engineering for Mine Waste Storage Facilities*, CRC Press, Taylor & Francis Group, London, UK.

Bolton, M.D. (1986). The strength and dilatancy of sands, *Géotechnique*, 36(1), 65-78.

Brandon, T.L., Rose, A.T., and Duncan, J.M. (2006). Drained and undrained strength interpretation for low-plasticity silts, *Journal of Geotechnical and Geoenvironmental Engineering*, 132(2), 250-257.

Bussière, B. (2007). Colloquium 2004: Hydrogeotechnical properties of hard rock tailings from metal mines and emerging geoenvironmental disposal approaches, *Canadian Geotechnical Journal*, 44(9), 1019-1052.

Carraro, J.A.H., and Prezzi, M. (2008). A new slurry-based method of preparation of specimens of sand containing fines, *Geotechnical Testing Journal*, 31(1), 1-11.

Carraro, J.A.H., Prezzi, M., and Salgado, R. (2009). Shear strength and stiffness of sands containing plastic or nonplastic fines, *Journal of Geotechnical and Geoenvironmental Engineering*, 135(9), 1167-1178.

Chu, J. and Leong, W.K., (2002). Effect of fines on instability behavior of loose sand, *Géotechnique*, 52(10), 751-755.

Daliri, F., Kim, H., Simms, P., and Sivathayalan, S. (2014). Impact of desiccation on monotonic and cyclic shear strength of thickened gold tailings, *Journal of Geotechnical and Geoenvironmental Engineering*, 140, 13p.

Eger, P., Lapakko, K., and Chamberlain, P.G. (1984). Mixed disposal of waste rock and tailings to reduce trace metal release from waste rock, *Proc. Symposium on Surface Mining, Hydrology, Sedimentology, and Reclamation, Lexington, KY*, 49-56.

Fines, P., Wilson, G.W., Landriault, D., Langetine, L., and Hulett, L. (2003). Co-mixing of tailings, waste rock and slag to produce barrier cover systems, *Proc. 6th Intl Conf. on Acid Rock Drainage, Cairns, QLD*, 1019-1022.

Gorakhki, M.R. and Bareither, C. A. (2014). Salinity effects on the geotechnical characterization of mine tailings, *Proc. Tailings and Waste 2014, Colorado State University, Fort Collins, CO*, 10pp.

Holtz, W.G. and Ellis, W. (1961). Triaxial shear characteristics of clayey gravel soils, *Proc. 5th International Conference on Soil Mechanics and Foundation Engineering*, 1, 143-149.

Khalili, A. and Wijewickreme, D. (2008). New slurry displacement method for reconstitution of highly gap-graded specimens for laboratory element testing, *Geotechnical Testing Journal*, 31(5), 424-432.

Khalili, A., Wijewickreme, D., and Wilson, W. (2010). Mechanical response of highly gap-graded mixtures of waste rock and tailings. Part I: Monotonic shear response, *Canadian Geotechnical Journal*, 47(5), 552-565.

Kuerbis, R. and Vaid, Y.P. (1988). Sand sample preparation- the slurry deposition method, *Soils and Foundations*, 28(4), 107-118.

Lambe, T.W. and Whitman, R.V. (1969). Soil Mechanics. John Wiley & Sons, Inc.: New York.

Leduc, M., Backens, M., and Smith, M.E. (2004). Tailings co-disposal at the Esquel gold mine Patagonia, Argentina, *Proc. SME Annual Meeting, Denver, Colorado,* 5 pp.

Lee, K.L. and Seed, H.B. (1967). Drained strength characteristics of sands, *Journal of the Soil Mechanics and Foundations Division*, 93(6), 117-141.

Li, A., Andruchow, B., Wislesky, I., and Olson, O. (2011). Field testing of co-disposal techniques for acid generating tailings and waste rock at Cerro de Maimón, *Proc. Tailings and Mine Waste 2011, Univ. of British Colombia,* 13 pp.

Marachi, N.D., Chan, C.K., and Seed, H.B. (1972). Evaluation of properties of rockfill materials, *Journal of Soil Mechanics and Foundation Engineering,* 98(SM1), 95-114.

Matyas, E.L., Welch, D.E., and Reades, D.W. (1984). Geotechnical parameters and behaviour of uranium tailings, *Canadian Geotechnical Journal*, 21(3), 489-504.

Morris, P.H. and Williams, D.J. (1997). Results of field trials of co-disposal of coarse and fine coal waste, *Transactions of the Institution of Mining and Metallurgy*, 106, A38-A41.

Newson, T., Dyer, T., Adam, C., and Sharp, S. (2006). Effect of structure on the geotechnical properties of bauxite residue, *Journal of Geotechnical and Geoenvironmental Engineering*, 132(2), 143-151.

Penman, A.D.M. (1953). Shear characteristics of a saturated silt, measured in triaxial compression, *Géotechnique*, 3(8), 312-328.

Qiu, Y. and Sego, D.C. (2001). Lab properties of mine tailings, *Canadian Geotechnical Journal*, 38(1), 183-190.

Rahman, M.M., Lo, S.R., and Gnanendran, C.T. (2008). On equivalent granular void ratio and steady state behaviour of loose sand with fines, *Canadian Geotechnical Journal*, 45(10), 1439-1455.

Rahman, M.M., Lo, S.R., and Gnanendran, C.T. (2009). Reply to the discussion by Wanatowski and Chu on “On equivalent granular void ratio and steady state behaviour of loose sand with fines”, *Canadian Geotechnical Journal*, 46(4), 483-486.

Rahman, M.M., Baki, M.A.L., and Lo, S.R. (2014). Prediction of undrained monotonic and cyclic liquefaction behavior of sand with fines based on the equivalent granular state parameter, *International Journal of Geomechanics*, 14(2), 254-266.

Rahman, M.M. and Lo, S.R. (2014). Undrained behavior of sand-fines mixtures and their state parameter, *Journal of Geotechnical and Geoenvironmental Engineering*, 140(7), 12p.

Rodriguez, R. (2006). Hydrogeotechnical characterization of a metallurgical waste, *Canadian Geotechnical Journal*, 43, 1042-1060.

Rowe, P.W. (1962). The stress-dilatancy relation for static equilibrium of an assembly of particles in contact, *Proc. Royal Society*, London, 256 A, 500-527.

Rowe, P.W., Barden, L., and Lee, I.K. (1964). Energy components during the triaxial cell and direct shear tests, *Géotechnique*, 14(3), 247-261.

Salgado, R., Bandini, P., and Karim, A. (2000). Shear strength and stiffness of silty sand, *Journal of Geotechnical and Geoenvironmental Engineering*, 126(5), 451-462.

Schofield, A.N. and Wroth, C.P. (1968). Critical State Soil Mechanics. McGraw-Hill: London.

Seed, H.B. and Lee, K.L. (1967). Undrained strength characteristics of cohesionless soils, *Journal of the Soil Mechanics and Foundations Division*, 93(6), 330-360.

Siddiqua, S., Siemens, G., Blatz, J., Man, A., and Lim, B.F. (2014). Influence of pore fluid chemistry on the mechanical properties of clay-based materials, *Geotechnical and Geological Engineering*, 32, 14p.

Sides, G. and Barden, L. (1971). The microstructure of dispersed and flocculated samples of kaolinite, illite, and montmorillonite, *Canadian Geotechnical Journal*, 8, 391-399.

Stoeber, J.N., Fox, Z.P., Abshire, M.S., and Overton, D.D. (2012). Evaluating the shear strength of mine waste rock, *Proc. Tailings and Mine Waste 2012*, *Colorado State University, Fort Collins, CO*, 265-280.

Thevanayagam, S. (1998). Effect of fine and confining stress on undrained shear strength of silty sands, *Journal of Geotechnical and Geoenvironmental Engineering*, 124(6), 479-491.

Thevanayagam, S., Shenthan, T., Mohan, S., and Liang, J. (2002). Undrained fragility of clean sands, silty sands, and sandy silts, *Journal of Geotechnical and Geoenvironmental Engineering*, 128(10), 849-859.

Tiwari, B., Tuladhar, G.R., and Marui, H. (2005). Variation in residual shear strength of the soil with the salinity of pore fluid, *Journal of Geotechnical and Geoenvironmental Engineering*, 131(12), 1445-1456.

Wang, S., Luna, R., and Stephenson, R.W. (2011). A slurry consolidation approach to reconstitute low-plasticity silt specimens for laboratory triaxial testing, *Geotechnical Testing Journal*, 34(4), 1-9.

Wang, S. and Luna, R. (2012). Monotonic behavior of Mississippi River Valley silt in triaxial compression, *Journal of Geotechnical and Geoenvironmental Engineering*, 138(4), 516-525.

Wickland, B.E., and Wilson, G.W. (2005). Self-weight consolidation of mixtures of mine waste rock and tailings, *Canadian Geotechnical Journal*, 42(2), 327-339.

Wickland, B.E., Wilson, G.W., Wijewickreme, D., and Klein B. (2006). Design and evaluation of mixtures of mine waste rock and tailings, *Canadian Geotechnical Journal*, 43, 928-945.

Wickland, B.E., Wilson, G.W. and Wijewickreme, D. (2010). Hydraulic conductivity and consolidation response of mixtures of mine waste rock and tailings, *Canadian Geotechnical Journal*, 47(4), 472-485.

Wijewickreme, D., Khalili, A., and Wilson, G. W. (2010). Mechanical response of highly gap-graded mixtures of waste rock and tailings. Part II: Undrained cyclic and post-cyclic shear response, *Canadian Geotechnical Journal*, 47(5), 566-582.

Williams, D. J. and Kuganathan, V. (1993). Geotechnical properties relevant to co-disposal of coal washery wastes, *Geotechnical Management of Waste and Contamination*, 485-493.

Williams, D.,J., Wilson, G.W., and Panidis, C. (2003). Waste rock and tailings mixtures as a possible seal for potentially acid forming waste rock, *Proc. 6th Intl Conf. on Acid Rock Drainage, Cairns, QLD*, 427-435.

Wilson, G. W., Newman, L.L., and Ferguson, K.D. (2000). The co-disposal of waste rock and tailings, *Proc. 5th Intl Conf. on Acid Rock Drainage, Denver, CO*, 789-796.

Wilson, G.W., Plewes, H.D., Williams, D., and Roberston, J. (2003). Concepts for co-mixing of tailings and waste rock, *Proc. 6th Intl Conf. on Acid Rock Drainage, Cairns, QLD*, 437-443.

Wilson, G. W., Wickland, B., Palkovits, F., and Longo, S. (2009). The implementation of paste rock systems for preventing acid rock drainage from waste rock and tailings impoundments, *Proc. 8th Intl Conf. on Acid Rock Drainage, Skelleftea, Sweden*, 13p.

APPENDIX A: MEMBRANE CORRECTION PROCEDURE FOR TRIAXIAL COMPRESSION TESTS

A.1 Introduction

Rubber membranes used on the exterior of triaxial test specimens can enhance the measured strength of specimens via resistance against the applied axial load and increasing the confining stress (Henkel and Gilbert 1952; Kuerbis and Vaid 1990). Triaxial testing on mine waste rock or other coarse, angular particles requires multiple membranes or thick membranes to avoid membrane puncture (Khalili et al. 2010). Henkel and Gilbert (1952) provide a graphical solution to correct for membrane-induced stresses based on the membrane elastic modulus (E) and specimen strain. They also provide an analytical approach to correct for membrane-induced stress based on compression shell and hoop tension theories.

The analytical method in Henkel and Gilbert (1952) was modified by La Rochelle et al. (1988) to create a set of membrane correction equations based on E, specimen strain, and specimen failure behavior. Kuerbis and Vaid (1990) also developed an analytical membrane correction procedure based on membrane properties (i.e., E, thickness) and specimen strain. These methods were evaluated with triaxial tests conducted on rigid dummies (La Rochelle et al. 1988) or deaired water (Kuerbis and Vaid 1990) encased in a rubber membrane. However, these methods have not been compared and the method proposed by Kuerbis and Vaid (1990) was not evaluated with triaxial tests conducted on soil specimens.

The methods proposed by La Rochelle et al. (1988) and Kuerbis and Vaid (1990) were evaluated to identify an applicable membrane correction procedure for triaxial tests conducted on waste rock and co-mixed mine waste specimens. Triaxial testing was conducted on Ottawa sand such that shear strength behavior and properties could be compared to literature. Additionally, a membrane modulus apparatus was developed based on recommendations in Head (1986) and the effect of membrane use on E was evaluated.

A.2 Determination of Membrane Modulus of Elasticity

The elastic modulus of a membrane (E) used in triaxial compression tests is required to correct for membrane effects on principle stresses. Two membranes were evaluated: a thin, 0.6-mm-thick, membrane and a thick, 5-mm-thick, membrane. The thick membrane was necessary in triaxial strength testing when evaluating coarse, angular materials (i.e., waste rock) to prevent membrane puncture. Variability between membranes was evaluated by conducting tests on three different membranes. The effect of membrane use on E was evaluated for the thin membrane via testing before and after triaxial compression testing.

A schematic of the membrane modulus testing apparatus developed based on recommendations in Head (1986) is shown in Fig. A.1. The elastic modulus was determined by suspending dead weights from a 25-mm-wide membrane strip and measuring vertical elongation (Δl) (Head 1986). Vertical elongation was determined by measuring the change in length between two horizontal reference marks on the membrane. The elastic modulus was calculated using Eq. A.1:

$$E = \frac{T / w}{\Delta l / l_o} \tag{A.1}$$

where T is tensile force exerted by the hanging weights, w is width of the membrane strip, and l_o is initial length between the horizontal reference marks. Dividing E obtained from Eq. A.1 by the membrane thickness yields E in units of stress.

Specimen dimensions and average E for the thin and thick membranes are summarized in Table A.1. Relationships of stress versus strain for the thin and thick membranes are shown in Fig. A.2. La Rochelle et al. (1988) tested a 0.7-mm-thick membrane and reported E = 0.72 kN/m, which is comparable to values determined for the thin membrane. As seen from the stress-strain curves in Fig. A.2, there is a linear relationship between stress and strain for each membrane. A linear regression was applied to data from all three tests for a given membrane and the slope of the regression line represents E. Continued use of a membrane caused a decrease in E. The new thin membrane had an E of 0.54 kN/m, which decreased to 0.50 kN/m following completion of 20 triaxial compression tests.

A.3 Membrane Correction Procedures

A.3.1 La Rochelle et al. (1988)

A flow chart for the La Rochelle et al. (1988) membrane correction procedure is presented in Fig. A.3. Implementation of this procedure requires initial specimen and membrane characteristics as well as observation of membrane behavior during shearing to guide application of appropriate equations. The first step in the procedure is to correct the confining stress (σ_c) for additional lateral stress (p_{om}) applied on the specimen by the membrane:

$$p_{om} = 2E\frac{d_o - d_{im}}{d_o \cdot d_{im}} \tag{A.2}$$

where E is in kN/m, d_o is initial diameter of the specimen, and d_{im} is initial inner diameter of the membrane. The actual initial confining stress applied to the specimen prior to shear is the sum of σ_c and p_{om}. During shear, the specimen cross-sectional area and stress corrections are conducted depending on the mode of specimen failure, which is either bulging or failure along a defined shear plane (Fig. A3).

A.3.1.1 Bulging Failure

A triaxial compression specimen can be assumed to deform as a right cylinder during bulging failure. The specimen height decreases during axial deformation and the diameter increases. The corrected cross-sectional area (A_c) is computed as,

$$A_c = A_o\frac{1+\varepsilon_v}{1-\varepsilon_a} \tag{A.3}$$

where A_o is initial specimen cross-sectional area, ε_a is axial strain, and ε_v is volumetric strain. Axial and volumetric strains can be calculated using Eqs. A.4 and A.5, respectively:

$$\varepsilon_a = \frac{\Delta h}{h_o} \tag{A.4}$$

$$\varepsilon_v = \frac{\Delta V}{V_o} \tag{A.5}$$

where Δh is change in specimen height, h_o is initial specimen height, ΔV is change in specimen volume, and V_o is initial specimen volume. Measurements of Δh and ΔV are made during testing.

The membrane correction procedure for bulging failure depends on whether or not the membrane buckles, i.e. the membrane folds over itself or wrinkles in the membrane develop. If no buckling occurs, the membrane continues to increase σ_c via p_{om} applied during shearing and also increases the major principle stress (σ_1) due to resistance to axial deformation. The resistance to axial deformation in the σ_1-direction (σ_{1m}) is determined using Eq. A.6 and then subtracted from the measured σ_1.

$$\sigma_{1m} = \frac{\pi \cdot d_o \cdot E \cdot \varepsilon_a}{A_c} \tag{A.6}$$

If buckling of the membrane occurs, the stress that resists axial resistance is relieved, but the membrane will apply a hoop stress to the specimen that further increases the minor principle stress (σ_3). The increase in confining stress (σ_{3m}) is calculated using Eq. A.7. The minor principle stress is then determined by adding σ_{3m} and p_{om} to σ_c.

$$\sigma_{3m} = 0.75 \frac{E\sqrt{\varepsilon_a}}{d_o} \tag{A.7}$$

A.3.1.2 Shear Plane Failure

The membrane correction for shear plane failure only occurs once a shear plane has formed. Therefore, the bulging failure correction (i.e., Eqs. A.6 and A.7) applies to the triaxial specimen until a defined shear plane forms. After shear plane formation, the cross-sectional area changes due to continued bulging and movement along the shear plane. Final dimensions of the specimen, shown schematically in Fig. A.4, are required to determine the shear plane area and stress correction. Measurements of total change in height (Δh_t), final specimen diameter (d_a), and length the shear plane extends beyond the specimen (Δd) are recorded at the end of the test. The final area of the shear plane (A_{ce}) is assumed to be an ellipse with the major axis the same as d_a and the minor axis (d_b) calculated with Eq. A.8.

$$d_b = d_a - 2\Delta d \tag{A.8}$$

Using d_a and d_b, A_{ce} can be determined using Eq. A.9.

$$A_{ce} = \frac{1}{4} \cdot \pi \cdot d_a \cdot d_b \tag{A.9}$$

The corrected area after shear plane formation and during specimen deformation is calculated as follows:

$$A_c = A_f + \left(A_{ce} + A_f\right) \cdot \left(\frac{\varepsilon_a - \varepsilon_{af}}{\varepsilon_{ae} - \varepsilon_{af}}\right) \tag{A.10}$$

where A_f is cross-sectional area at formation of the shear plane (i.e., cross-sectional area at peak stress determined with Eq. A.3), ε_{af} is axial strain at shear plane formation, and ε_{ae} is axial strain at the end of the test. As the specimen deforms along the shear plane, the membrane applies a resisting force that artificially increases the deviator stress ($\Delta\sigma_d$). The corrected deviator stress ($\Delta\sigma_{dcorr}$) can computed as,

$$\Delta\sigma_{d,corr} = \Delta\sigma_d - \frac{1.5 \cdot \pi \cdot d_o}{A_c} \sqrt{E \cdot f \cdot d_o \cdot \delta} \tag{A.11}$$

where f is friction between the membrane and test specimen, and δ is strain from movement along the shear plane. Strain along the shear plane is calculated using Eq. A.12:

$$\delta = \delta_e \frac{\varepsilon_a - \varepsilon_{af}}{\varepsilon_{ae} - \varepsilon_{af}} \tag{A.12}$$

where δ_e is δ at the end of the test ($\delta_e = \Delta h_l/h_o$). La Rochelle et al. (1988) report that f is related to the critical state friction angle (ϕ'_{cs}) via $f = \sigma_3' \tan(\phi'_{cs})$. Thus, an initial guess of ϕ'_{cs} is required for this membrane correction procedure and an iterative process will yield the actual ϕ'_{cs}.

A.3.2 Kuerbis and Vaid (1990)

The membrane correction outlined by Kuerbis and Vaid (1990) only requires membrane properties and strain within the specimen. Observations of specimen failure and specimen dimensions at the end of testing are not needed, which simplifies the correction procedure. The following equations are used to correct σ_1 (Eq. A.13) and σ_3 (Eq. A.14):

$$\sigma_{1corr} = \sigma_1 - \frac{4 \cdot E \cdot t\left(2 + \varepsilon_v + \varepsilon_a\right)\left(3\varepsilon_a + \varepsilon_v\right)}{3d_o\left(2 - \varepsilon_v + \varepsilon_a\right)} \tag{A.13}$$

$$\sigma_{3corr} = \sigma_3 - \frac{4 \cdot E \cdot t\left(2 + \varepsilon_v + \varepsilon_a\right) \cdot \varepsilon_v}{3d_o\left(2 - \varepsilon_v + \varepsilon_a\right)} \tag{A.14}$$

where t is initial thickness of the membrane and E is in kPa. Eqs. A.13 and A.14 are applied to all collected triaxial data from a given experiment.

A.3.3 Membrane Correction Evaluation

Consolidated drained (CD) triaxial compression tests were conducted on Ottawa sand and a synthetic mine waste rock using two membranes: (1) thin = a 0.6-mm-thick latex membrane and (2) thick = a 5-mm-thick rubber membrane. Tests on Ottawa sand were completed using the thin membrane alone and both the thin and thick membranes together to evaluate the effect of the thick membrane on measured triaxial data. Accuracy of the membrane correction procedures proposed by La Rochelle et al. (1988) and Kuerbis and Vaid (1990) was evaluated via comparison of shear testing results on Ottawa sand, waste rock, and literature.

All triaxial compression specimens were prepared in a 300-mm-tall by 150-mm-thick split mold lined with the desired membrane(s). Ottawa sand was compacted in six layers of equal thickness via hand tamping to a target dry density equal to 95 % of maximum dry density determined with standard compaction effort (ASTM D 698). Waste rock was prepared in a loose state by displacing deaired water following a modified procedure developed by Khalili and Wijewickreme (2008). All CD triaxial tests were conducted with a confining pressure (σ'_c) of 150 kPa on Ottawa sand and 40 kPa on waste rock following procedures in ASTM D 7181. Membrane correction procedures described previously for La Rochelle et al. (1988) and Kuerbis and Vaid (1990) were applied for each membrane in the two-membrane tests, i.e., once for the thin membrane and once for the thick membrane.

Relationships between deviator stress ($\Delta\sigma_d$) and axial strain (ε_a) are presented in Fig. A.5 for Ottawa sand for the single and dual membrane experiments and in Fig. A.6 for waste rock for dual membrane experiments. Data are shown as uncorrected and corrected using both La Rochelle et al. (1988) and Kuerbis and Vaid (1990) membrane correction procedures. The uncorrected $\Delta\sigma_d$ decreased to a constant stress after failure for tests conducted on Ottawa sand with a single membrane (Fig. A.5a). However, $\Delta\sigma_d$ continued to increase after failure in the dual membrane tests (Fig. A.5b). Deviator stress corrected using the La Rochelle et al. (1988) showed similar behavior in both experiments, characterized by a more pronounced decrease following peak stress and modest decreasing trend between $\Delta\sigma_d$ and ε_a for ε_a > 10 %. Data corrected using the method outlined by Kuerbis and Vaid (1990) show similar trends as the uncorrected data. Corrected and uncorrected $\Delta\sigma_d$ for waste rock increased with increasing ε_a for ε_a < 15 % and remained constant for ε_a > 15 % (Fig. A.6). Deviator stress corrected using the La Rochelle et al. (1988) method was identical to the uncorrected $\Delta\sigma_d$ but the Kuerbis and Vaid (1990) method reduced $\Delta\sigma_d$ compared to the La Rochelle et al. (1988) method.

Peak (ϕ'_p) and critical state (ϕ'_{cs}) friction angles from single and dual membrane experiments on Ottawa sand and the dual membrane experiment on waste rock are summarized in Table A.2. Uncorrected and corrected ϕ'_p for single and dual membrane tests are within ± 2° of ϕ'_p for comparable materials reported in Lambe and Whitman (1969), Bareither et al. (2008), and Salgado et al. (2000). Values of ϕ'_{cs} for Ottawa sand corrected using the La Rochelle et al. (1988) method are equal to or lower than ϕ' for quartz and do not agree with literature. The peak friction angle for waste rock (40.9°) corrected using the La Rochelle et al. (1988) method is similar to ϕ'_p (41.7°) for a waste rock with similar particle size distribution (Khalili et al. 2010). Uncorrected ϕ'_p (43.3°) and corrected (42.7°) using the Kuerbis and Vaid (1990) method are 1-2° higher than the value reported by Khalili et al. (2010).

Each Ottawa sand specimen failed along a shear plane that extended beyond the specimen edge and into the membrane. As the specimen approached critical state, additional movement along the shear plane occurred, which further increased the resistive force applied by the membrane. Kuerbis and Vaid (1990) do not account for the additional load induced by the membrane during shear plane failure, which renders $\Delta\sigma_d$ equivalent to the uncorrected value and may overestimate ϕ'. A decrease in $\Delta\sigma_d$ of 30 kPa was computed immediately after formation of the shear failure plane based on data corrected following the La Rochelle et al. (1988) method in the dual membrane test (Fig. A.5). This $\Delta\sigma_d$ correction may overestimate induced stress by the membrane and lead to an underestimate of ϕ'_{cs}. Inaccurate values of ϕ'_{cs} likely are due to error in the final specimen dimensions which were difficult to measure in dual membrane tests, introducing a potential overestimate of d_a. Measurement accuracy of final dimensions was further complicated for all tests since a change in stress state (i.e., removal of cell pressure) was necessary in order to make measurements.

The waste rock specimen displayed bulging failure during shear. For this failure condition, La Rochelle et al. (1988) only apply a correction to σ_3 leaving $\Delta\sigma_d$ unchanged and equivalent to uncorrected data. However, since σ_3 is increased, ϕ'_p corrected using the La Rochelle et al. (1988) is less than the uncorrected ϕ'_p. Not correcting σ_3 for the additional stresses applied by the membrane artificially increased the strength of waste rock thus increasing ϕ'_p. During bulging failure, the Kuerbis and Vaid (1990) method increases σ_3 and decreases σ_1 resulting in a lower $\Delta\sigma_d$ compared to uncorrected $\Delta\sigma_d$ and corrected using the La Rochelle et al. (1988) method. Despite the reduced $\Delta\sigma_d$, ϕ'_p and ϕ'_{cs} corrected using the Kuerbis and Vaid (1990) method were higher than values corrected with the La Rochelle et al. (1988) method. Applying a correction to both σ_1 and σ_3 increased the principle stress ratio at failure ($(\sigma'_1/\sigma'_3)_f = 5.21$) and at critical state ($(\sigma'_1/\sigma'_3)_{cs} = 4.70$) relative to the La Rochelle et al. (1988) method ($(\sigma'_1/\sigma'_3)_f = 4.79$ and ($(\sigma'_1/\sigma'_3)_{cs} = 4.47$) which increases ϕ'_p and ϕ'_{cs}. The membrane correction for σ_1 is larger than the correction for σ_3 and may underestimate the actual σ_1 applied to the specimen causing an overestimation of ϕ' as observed when comparing the values of ϕ' for waste rock with literature values.

REFERENCES

Bareither, C.A., Edil, T.B., Benson, C.H., and Mickelson, D.M. (2008). Geological and physical factors affecting the friction angle of compacted sands, *Journal of Geotechnical and Geoenvironmental Engineering*, 134(10), 1476-1489.

Head, K. H. (1986). Manual of Soil Laboratory Testing Vol. 2, Pentech Press Limited: London.

Henkel, D.J. and Gilbert, G.D. (1952). The effect of the rubber membrane on the measured triaxial compression strength of clay samples, *Géotechnique*, 3(1), 20-29.

Khalili, A. and Wijewickreme, D. (2008). New slurry displacement method for reconstitution of highly gap-graded specimens for laboratory element testing, *Geotechnical Testing Journal*, 31(5), 424-432.

Khalili, A., Wijewickreme, D., and Wilson, W. (2010). Mechanical response of highly gap-graded mixtures of waste rock and tailings. Part I: Monotonic shear response, *Canadian Geotechnical Journal*, 47(5), 552-565.

Kuerbis, R.H. and Vaid, Y.P. (1990). Corrections for membrane strength in the triaxial test, *Geotechnical Testing Journal*, 13(4), 361-369.

La Rochelle, P., Leroueli, S., Trak, B., Blais-Leroux, L., and Tavenas, F. (1988). Observational Approach to Membrane and Area Corrections in Triaxial Tests, *Advanced Triaxial Testing of Soils and Rock,* ASTM, STP 977, 715-731.

Lambe, T.W. and Whitman, R.V. (1969). Soil Mechanics. John Wiley & Sons, Inc.: New York.

Salgado, R., Bandini, P., and Karim, A. (2000). Shear strength and stiffness of silty sand, *Journal of Geotechnical and Geoenvironmental Engineering*, 126(5), 451-462.

Table A.1. Dimensions and average modulus of elasticity (*E*) for the thin and thick membranes.

Membrane	Width (mm)	Thickness (mm)	Diameter (mm)	Area (mm^2)	Elastic Modulus (kN/m)	Elastic Modulus (kPa)
Thin New	25.2	0.60	146.7	15.2	0.54	900
Thin Used	24.6	0.62	145.8	15.5	0.50	805
Thick	25.2	4.71	150.3	118.8	5.1	1090

Table A.2. Comparison of friction angles measured on Ottawa sand for uncorrected data and data corrected following procedures proposed by La Rochelle et al. (1988) and Kuerbis and Vaid (1990).

Method	Ottawa Sand Thin Membrane Only		Ottawa Sand Thick and Thin Membranes		Waste Rock Thick and Thin Membranes	
	ϕ'_p	ϕ'_{cs}	ϕ'_p	ϕ'_{cs}	ϕ'_p	ϕ'_{cs}
La Rochelle et al. (1988)	30.6	26.1	31.7	24.1	40.9	39.4
Kuerbis and Vaid (1990)	32.0	30.6	32.9	31.7	42.7	40.4
Uncorrected	32.1	30.8	33.4	32.3	43.3	44.8

Note: ϕ'_p = peak friction angle; ϕ'_{cs} = critical state friction angle

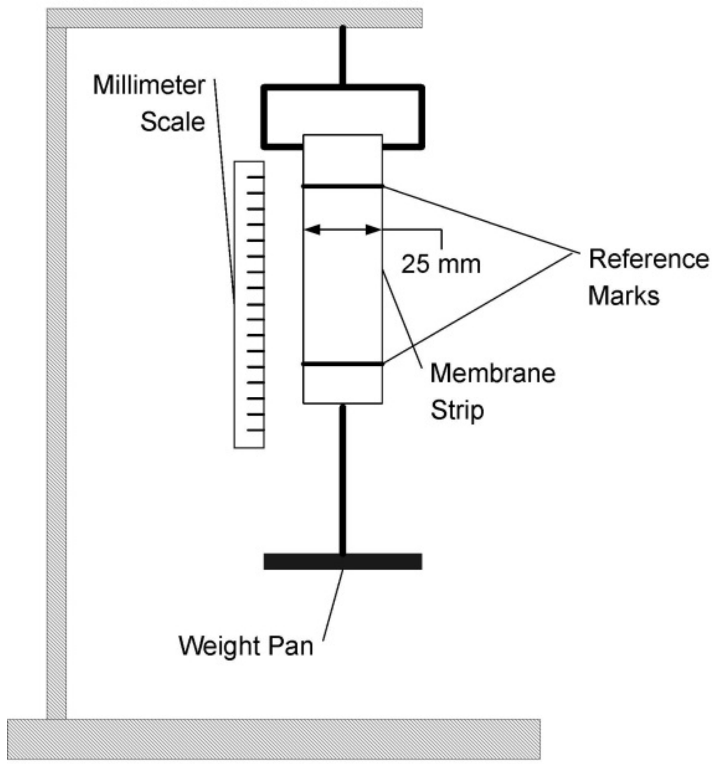

Fig. A.1. Testing apparatus used to determine the elastic modulus of a membrane.

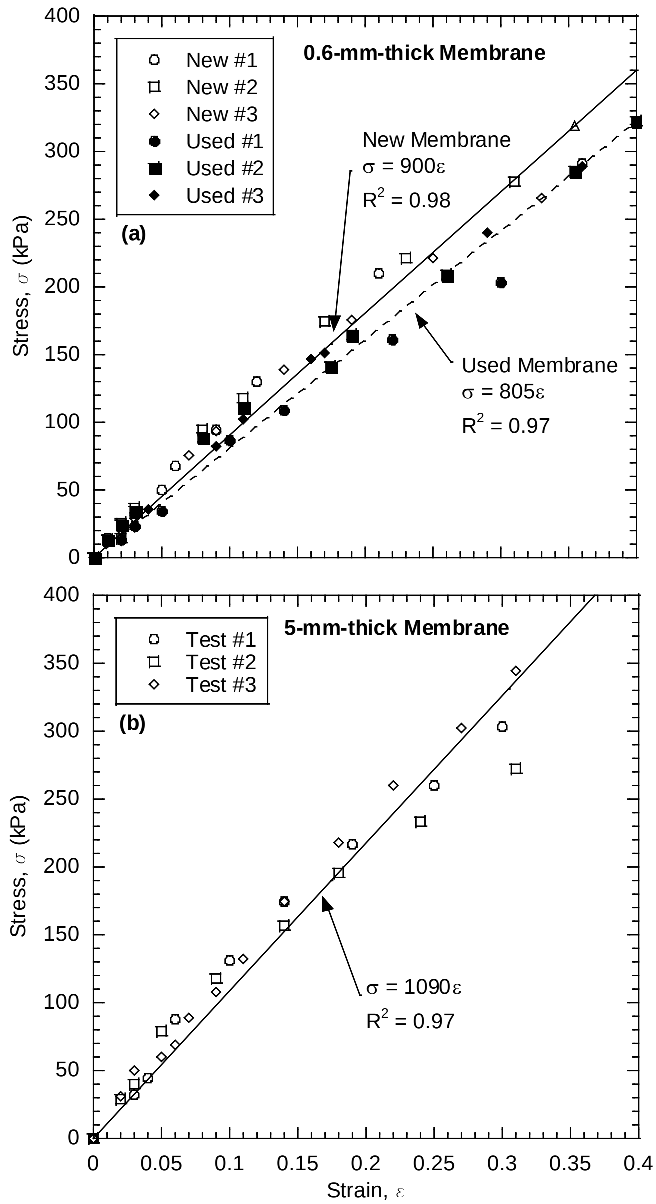

Fig. A.2. Stress-strain relationships for the (a) 0.6-mm-thick membrane and (b) 5-mm-thick membrane. Slopes of linear regressions applied to the data were taken as the elastic modulus for the membrane.

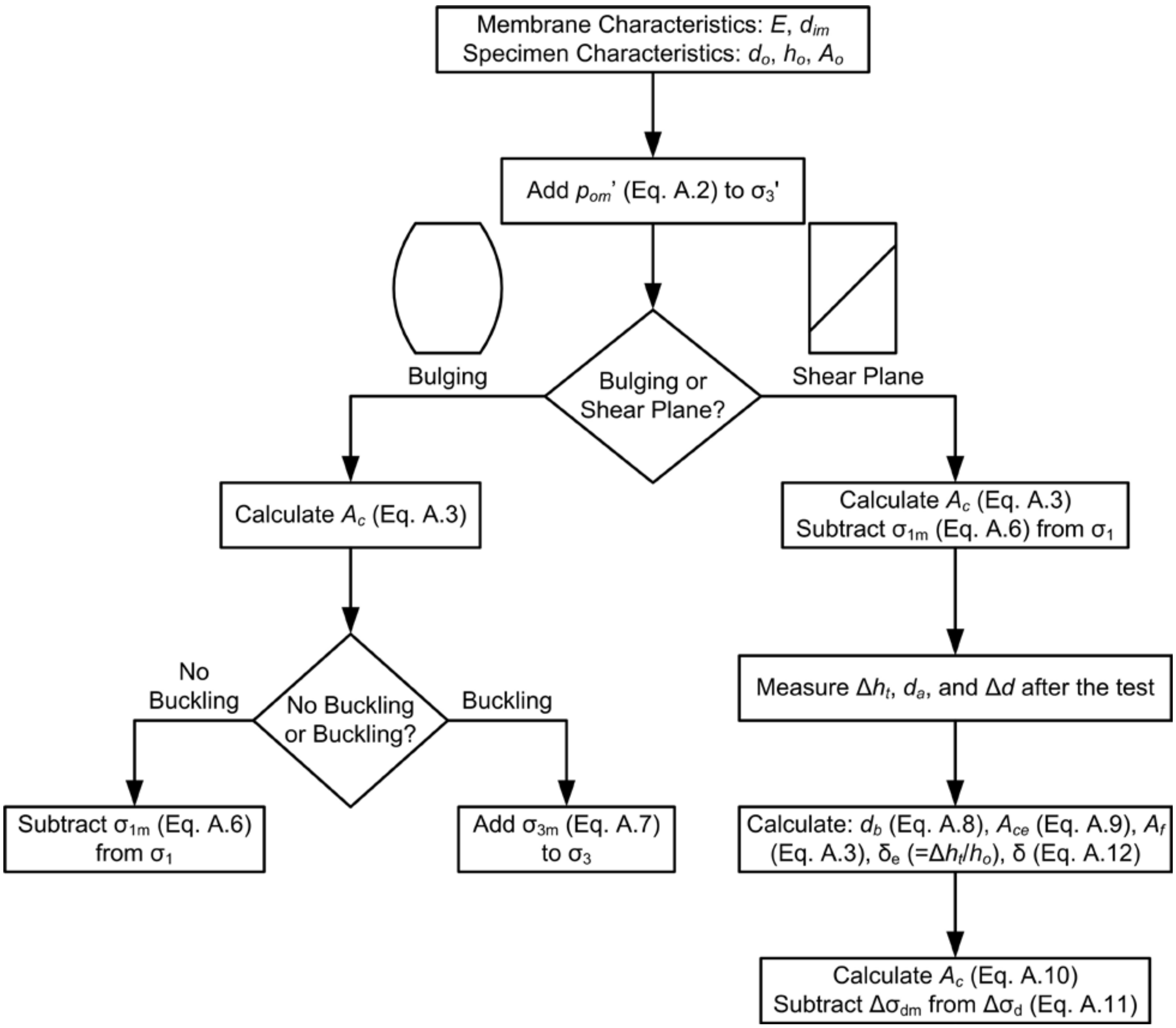

Fig. A.3. Flow chart for the membrane correction procedure described in La Rochelle et al. (1988). Numbers in parentheses refer to equations described in the text.

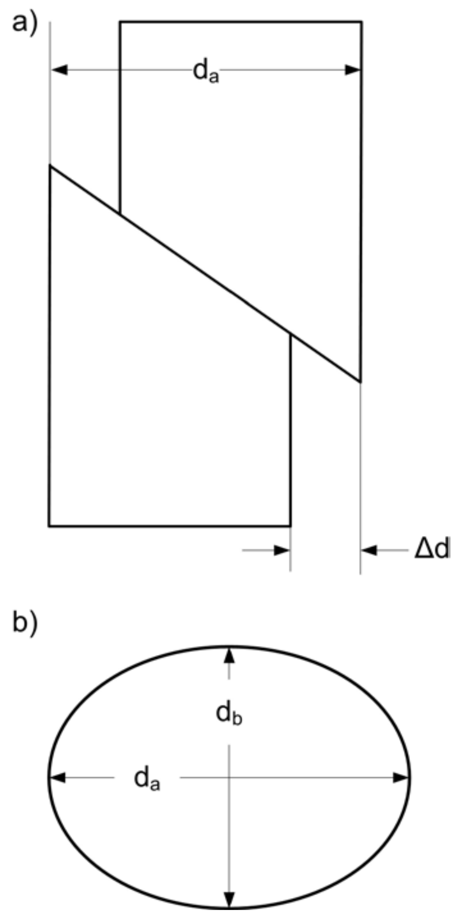

Fig. A.4. Schematic of (a) a specimen failing along a shear plane and (b) plan view of the shear plane. Dimensions annotated on the diagram are used in calculating the shear plane and stress correction. Adapted from La Rochelle et al. (1988).

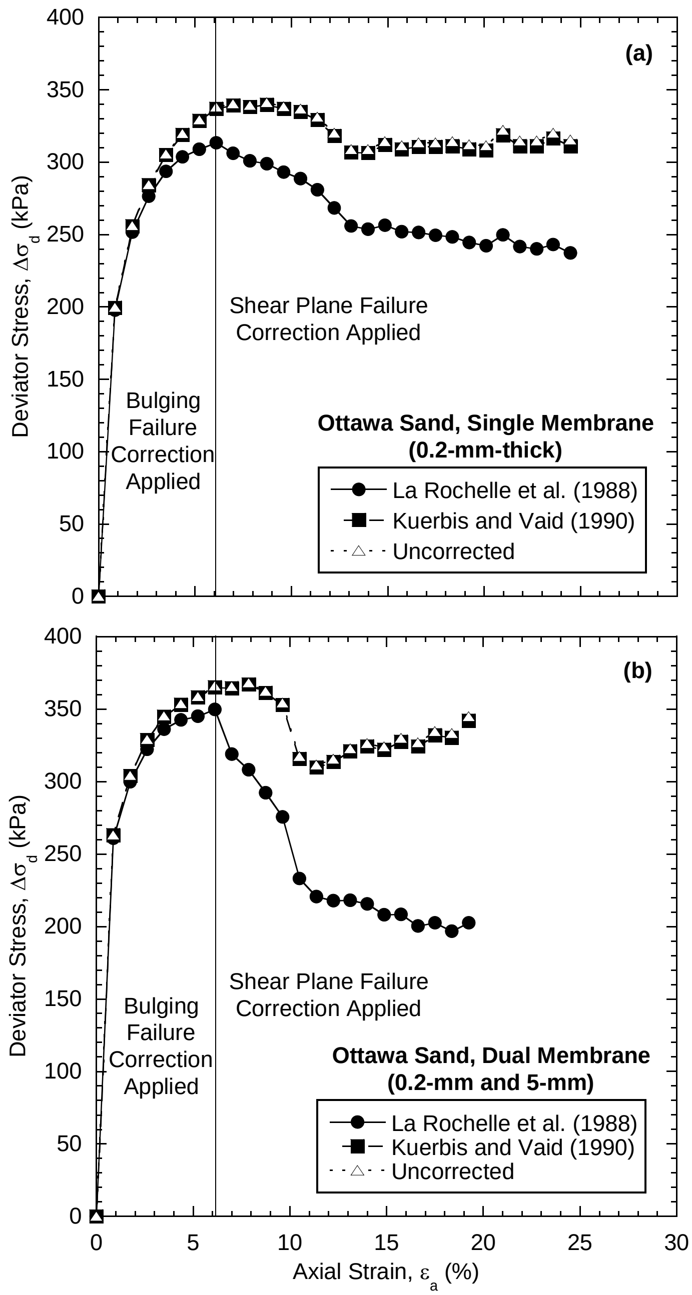

Fig. A.5. Relationship between deviator stress ($\Delta\sigma_d$) and axial strain (ε_a) for (a) single membrane and (b) dual membrane consolidated drained triaxial tests on 150-mm-diameter specimens of Ottawa sand at an effective confining pressure (σ'_c) of 150 kPa.

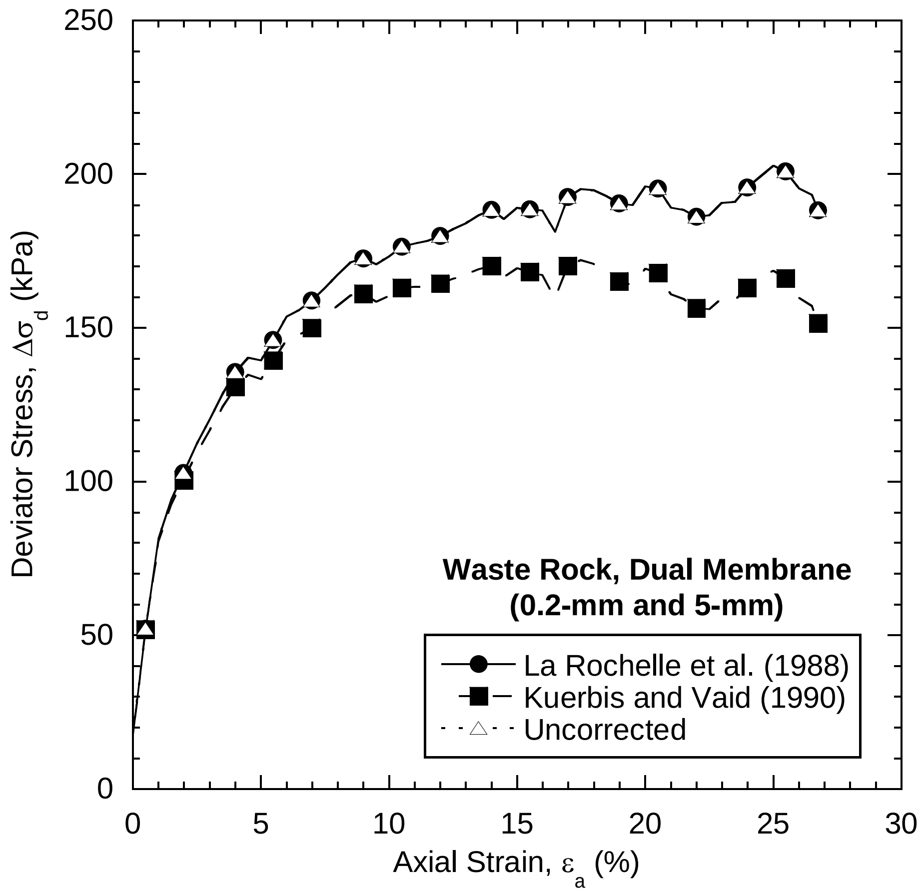

Fig. A.6. Relationship between deviator stress ($\Delta\sigma_d$) and axial strain (ε_a) for dual membrane consolidated drained triaxial tests on 150-mm-diameter specimens of synthetic waste rock at an effective confining pressure (σ'_c) of 40 kPa.

APPENDIX B: SENSOR CALIBRATIONS

The sensors used to measure pressure, axial deformation, and axial loading during triaxial testing were calibrated before conducting tests on waste rock and tailings mixtures. A summary of the calibration factors is presented in Table B.1 for the traditional scale (38-mm specimen diameter) triaxial apparatus and in Table B.2 for the large scale (150-mm specimen diameter) triaxial apparatus. The calibration data is summarized in Fig. B.1 for the pressure transducers, Fig. B.2 for the linear variable displacement transducers (LVDT), and in Fig. B.3 for the load cells.

Table B.1. Calibration factors for the load cell, displacement transducers (LVDT), and pressure transducers connected to the traditional scale (38-mm specimen diameter) triaxial apparatus.

Sensor	Brand	Serial Number	CF	Units	Intercept	Units	Intercept (V)
Load Cell	Artech Industries, Inc.	297852	-616954	$lb/V_s/V_e$	6.1104	lb	0.000095
LVDT	NOVO technik	NR.023262-F.NR.088753/A	-2.0391	$in/V_s/V_e$	1.6324	in	8.0414
Pore Pressure	GeoTac	PS-2448	20085.18	$psi/V_s/V_e$	-0.4369	psi	0.00022
Cell Pressure	ELE International Ltd.	PR-21 SR/80400.147	10060.67	$psi/V_s/V_e$	-2.1445	psi	0.00214

Note: CF = calibration factor, V_s = sensor voltage, V_e = excitation voltage

Table B.2. Calibration factors for the load cell, displacement transducers (LVDT), and pressure transducers connected to the large scale (150-mm specimen diameter) triaxial apparatus.

Sensor	Brand	Serial Number	CF	Units	Intercept	Units
Load Cell	Tovey Engineering	106596A	-6.1722	lb/mV/V	0.4624	lb
LVDT	Macro Sensors	96427	0.8352	in/V	-0.0053	in
Pore Pressure	Omega	N/A	452.0755	kPa/mV/V	1.301024	kPa
Cell Pressure	Omega	N/A	452.0401	kPa/mV/V	-3.98991	kPa

Note: CF = calibration factor, N/A = not available

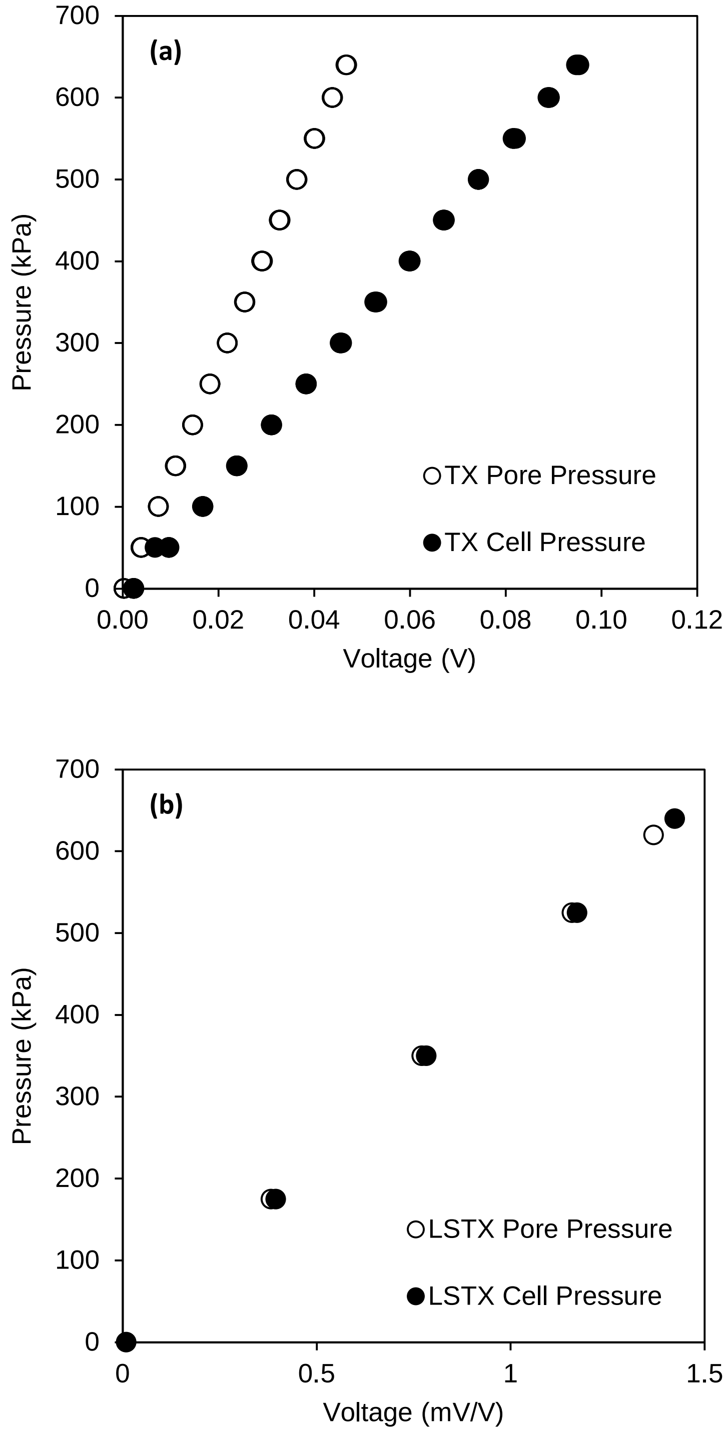

Fig. B.1. Calibration data for the pressure transducers connected to (a) the traditional scale (38-mm specimen diameter) triaxial apparatus and (b) the large scale (150-mm specimen diameter) triaxial apparatus.

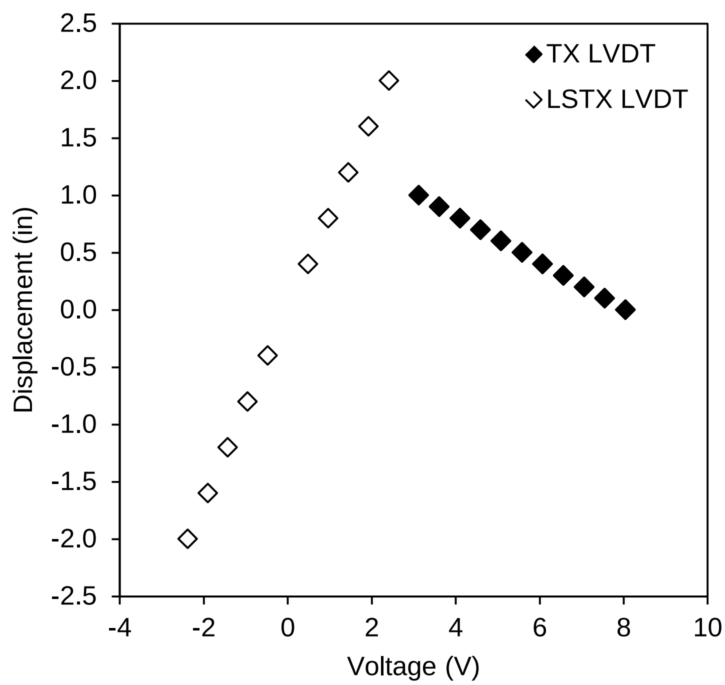

Fig. B.2. Calibration data for the displacement transducers (LVDT) connected to the traditional scale (38-mm specimen diameter) triaxial apparatus (TX) and the large scale (150-mm specimen diameter) triaxial apparatus (LSTX).

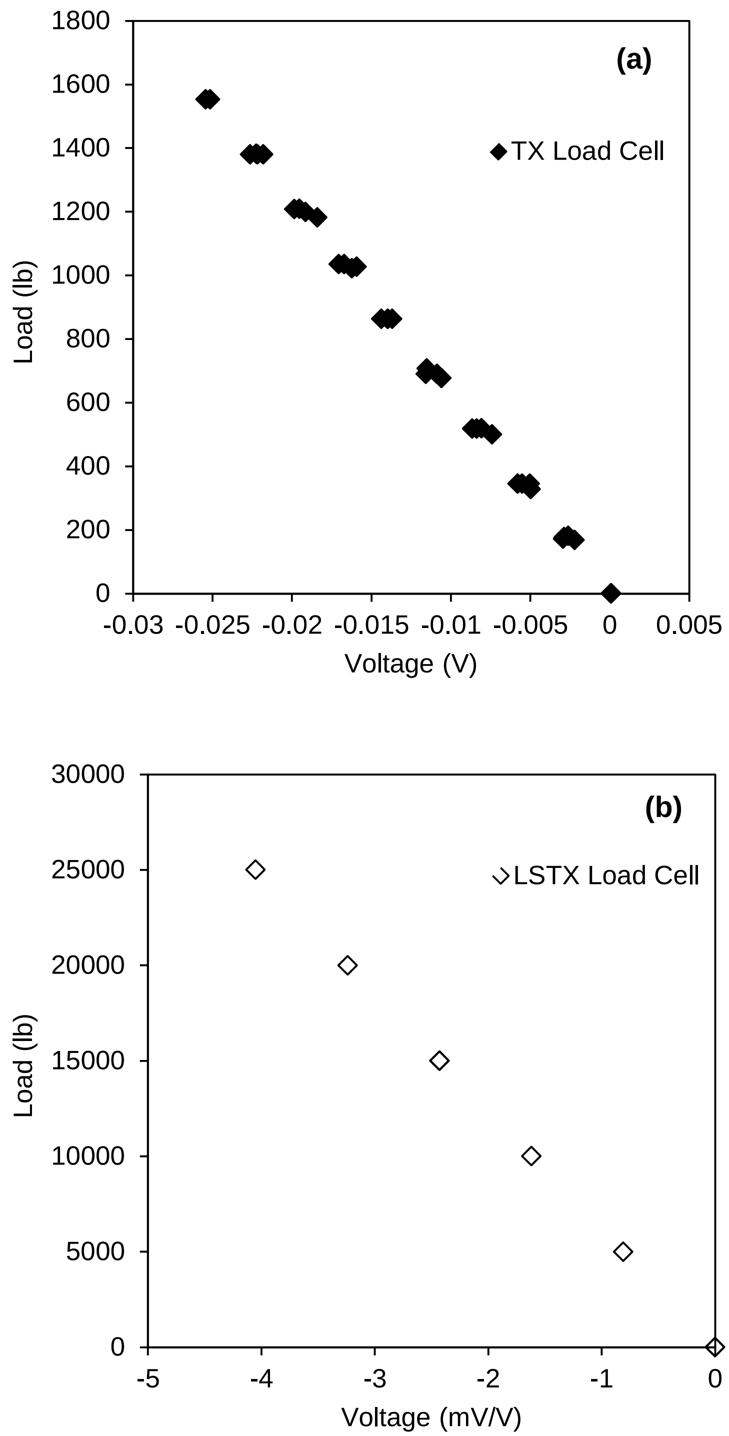

Fig. B.3. Calibration data for the load cells connected to (a) the traditional scale (38-mm specimen diameter) triaxial apparatus and (b) the large scale (150-mm specimen diameter) triaxial apparatus.

APPENDIX C: SCANNING ELECTRON MICROSCOPE IMAGES OF TAILINGS

Scanning electron microscope images of fine-garnet, copper, and soda ash tailings were obtained to observe particle shape and surface characteristics. Images of fine-grained garnet tailings are shown in Fig. C.1 and C.2. Copper tailings are presented in Fig. C.3 and C.4 and soda ash tailings are shown in Fig. C.5 and C.6.

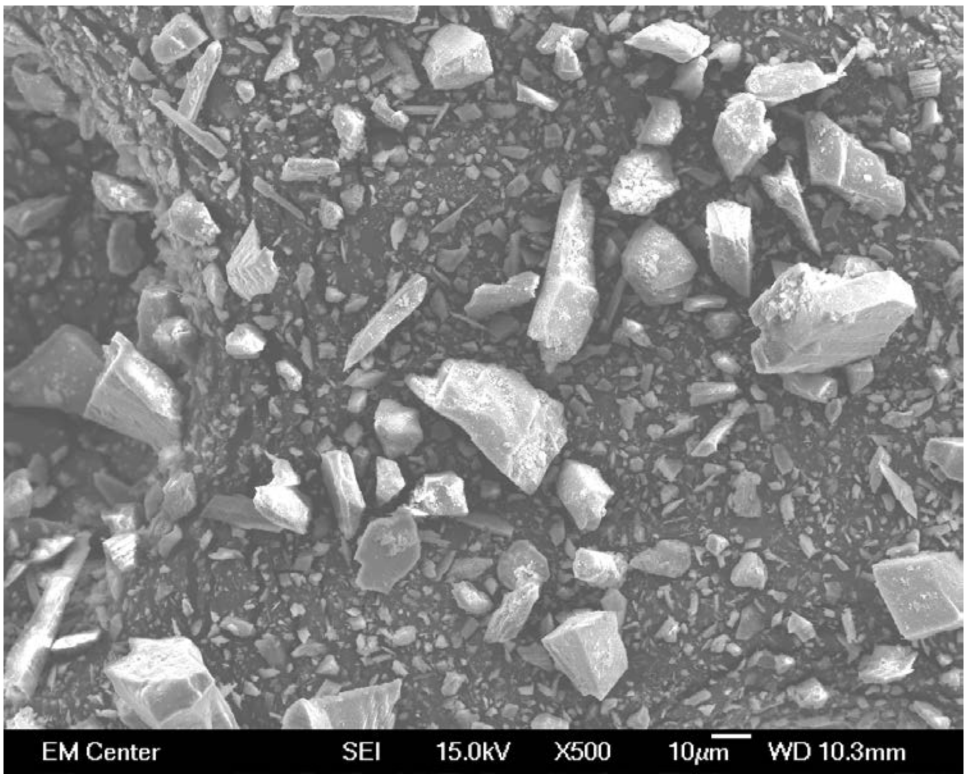

Fig. C.1. Scanning electron microscope image of fine-garnet tailings at 500 times magnification.

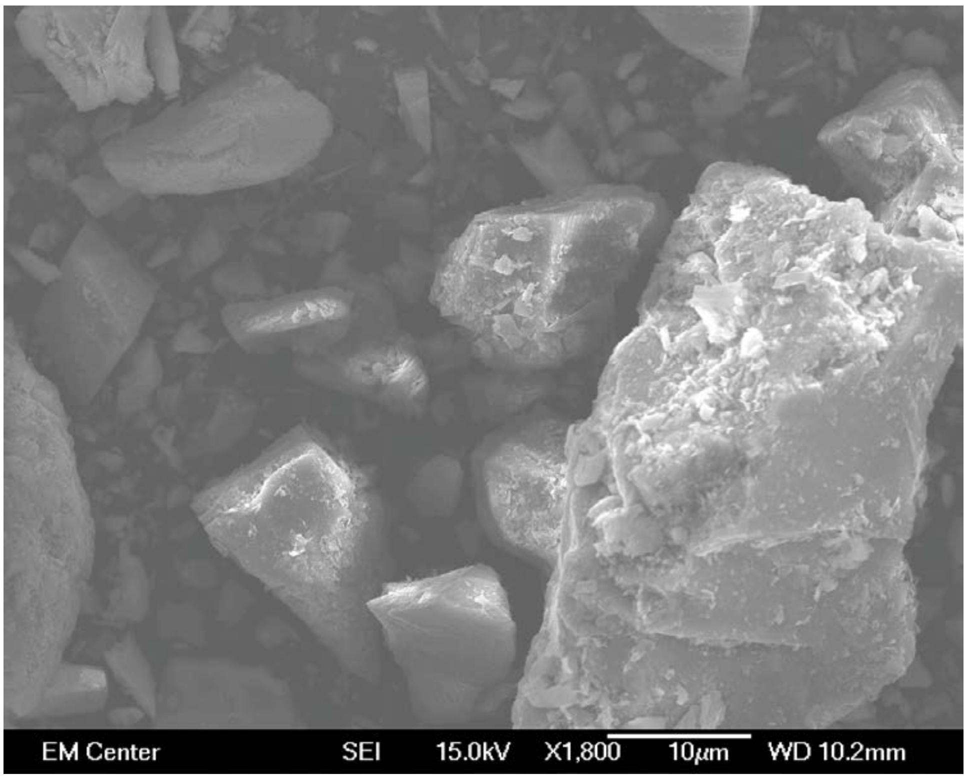

Fig. C.2. Scanning electron microscope image of fine-garnet tailings at 1800 times magnification.

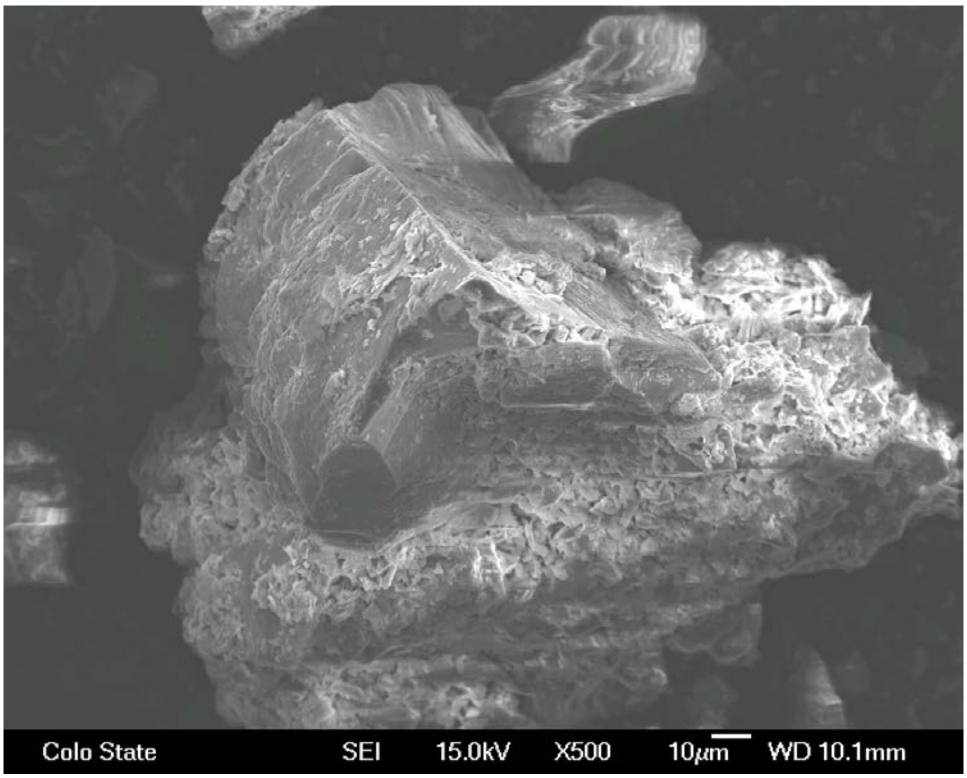

Fig. C.3. Scanning electron microscope image of copper tailings at 500 times magnification.

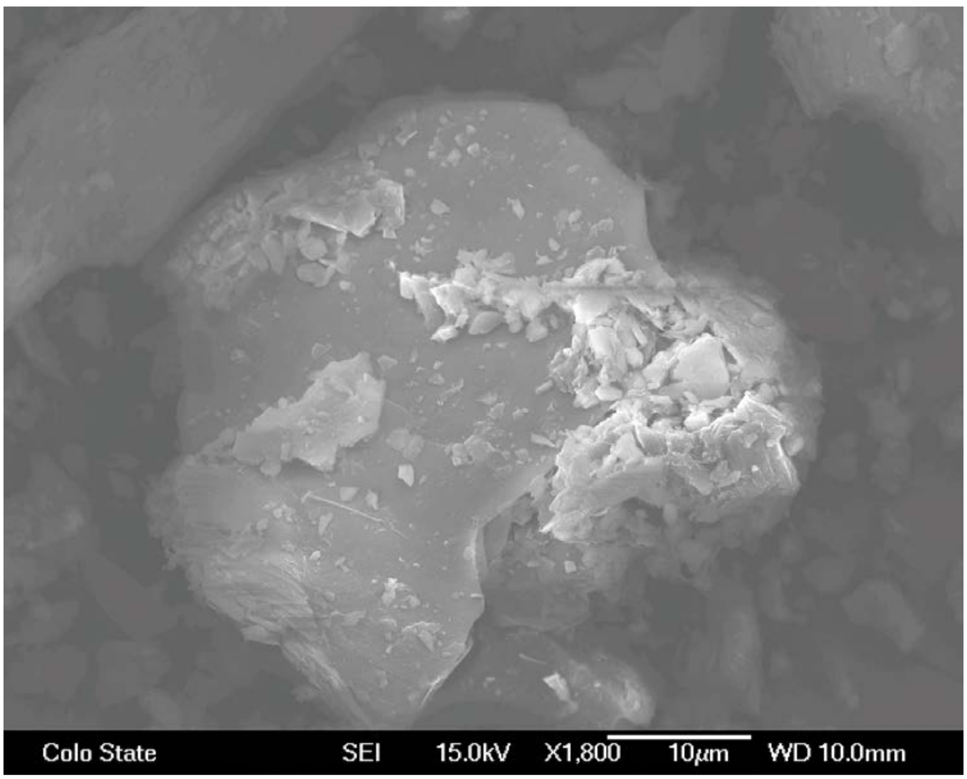

Fig. C.4. Scanning electron microscope image of copper tailings at 1800 times magnification.

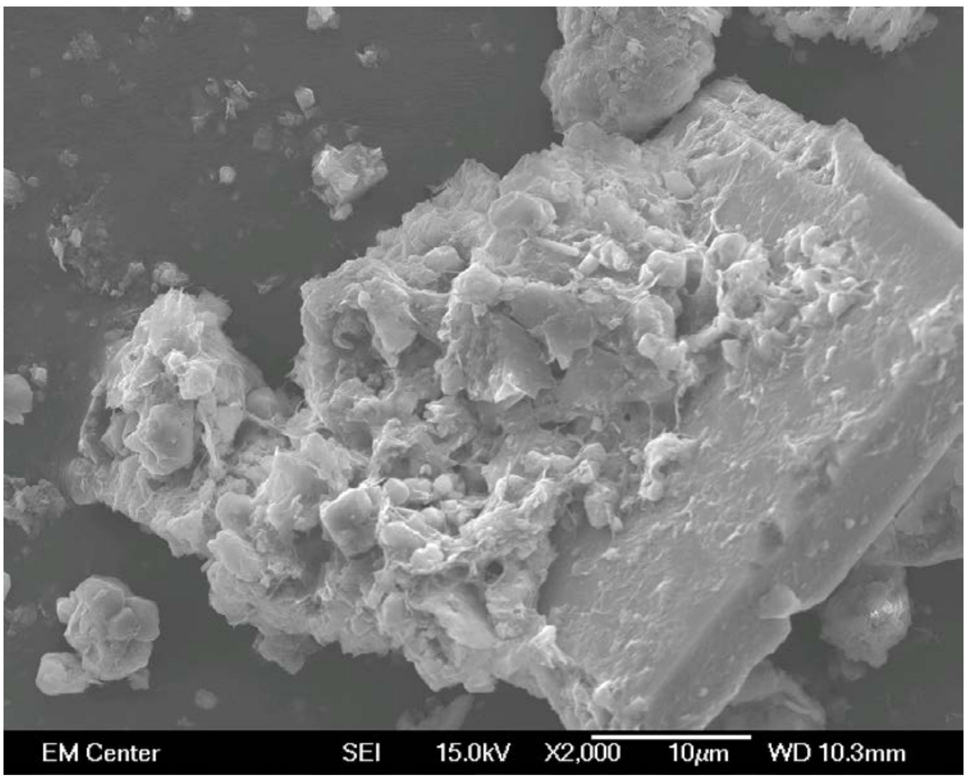

Fig. C.5. Scanning electron microscope image of soda ash tailings at 2000 times magnification.

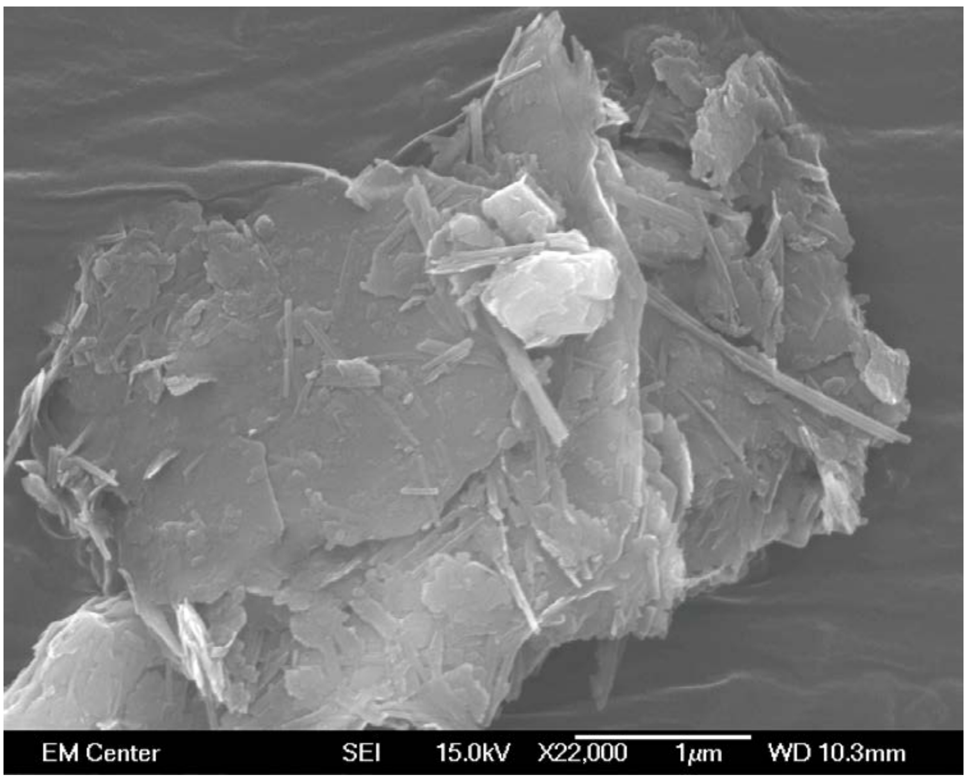

Fig. C.6. Scanning electron microscope image of soda ash tailings at 22,000 times magnification.

APPENDIX D: TAILINGS CONSOLIDATION DATA

Consolidation data were recorded for the fine-grained garnet, copper, and soda ash tailings during triaxial specimen preparation. The consolidation parameters for each tailings are summarized in Table D.1 and agree with values reported by Qiu and Sego (2001) for similar materials. Plots of axial strain versus square root of time for each tailings for the 20 and 40 kPa loadings are presented in Fig. D.1. The data were used to determine an appropriate strain rate during undrained triaxial compression testing according to ASTM D 4767. Details on the consolidation procedure (e.g., load increments, readings times) are discussed in Section 3.3.1. Data were analyzed following the procedure outlined in ASTM D 2435.

REFERENCES

Qiu, Y. and Sego, D. C. (2001). Lab properties of mine tailings, *Canadian Geotechnical Journal* 38(1), 183-190.

Table D.1. Consolidation parameters for fine-garnet, copper, and soda ash tailings. Data from the 20 and 40 kPa loads were used to determine c_v.

Tailings	c_v (m^2/yr)	C_c
Fine-Garnet	215.1	0.02
Copper	277.1	0.10
Soda Ash	141.3	0.33

Note: c_v = coefficient of consolidation; C_c = compression index.

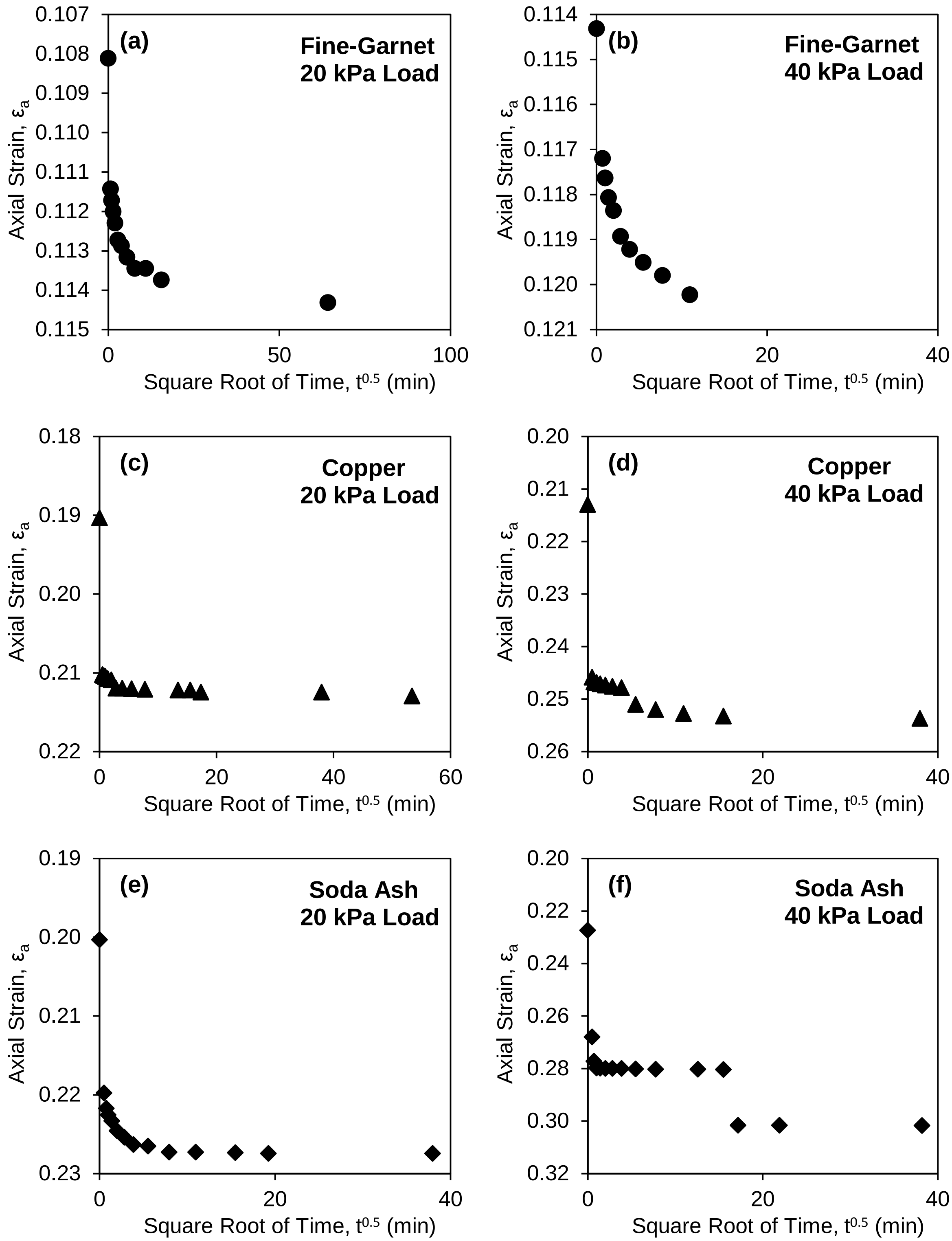

Fig. D.1. Axial strain versus square root of time from consolidation tests for (a) fine-garnet at 20 kPa, (b) fine-garnet at 40 kPa, (c) copper at 20 kPa, (d) copper at 40 kPa, (e) soda ash at 20 kPa, and (f) soda ash at 40 kPa.

APPENDIX E: TRIAXIAL TESTING RESULTS FOR ALL MATERIALS

Summary tables from each triaxial compression test performed on all materials evaluated in this study are presented in this section and include the following: effective confining stress (σ'_c), effective major principle stress at failure (σ'_{1f}), effective minor principle stress at failure (σ'_{3f}), effective peak friction angle (ϕ'_p), axial strain at failure (ε_{af}), Skempton's pore pressure parameter at failure (A_f), critical state effective major principle stress (σ'_{1cs}), critical state effective minor principle stress (σ'_{3cs}), critical state friction angle (ϕ'_{cs}), axial strain at critical state (ε_{ae}), Skempton's pore pressure parameter at critical state (A_e), and the void ratio during shear (e). The void ratio reported for mixtures is the void ratio of the waste rock skeleton (e_r)

Plots of deviator stress, excess pore pressure, and Skempton's pore pressure parameter versus axial strain are shown along with plots of Mohr's circle based on the average ϕ'_p and stress paths that include the peak failure (K_f) line. The summary of results for the consolidated drained triaxial compression tests on waste rock do not contain A_f or A_e, but instead include the initial void ratio (e_o) and the final void ratio (e_f).

Waste Rock Summary: Drained Tests

Target σ_c' (kPa)	σ_c' (kPa)	σ_{1f}' (kPa)	σ_{3f}' (kPa)	ϕ_p'	ε_{af} (%)	σ_{1cs}' (kPa)	σ_{3cs}' (kPa)	ϕ_{cs}'	ε_{ae} (%)	e_o	e_f
5	5.7	51.6	8.7	45.4	1.1	98.7	18.4	43.3	19.6	0.69	0.72
5	6.1	58.5	11.8	41.6	4	58.4	14.0	37.8	7.8	0.68	0.71
10	10.8	84.5	18.2	40.2	6.8	116.0	25.0	40.2	24.6	0.72	0.72
20	20.7	127.6	27.6	40.1	5.9	155.6	34.5	39.6	23.3	0.72	0.72
40	40.0	222.5	48.4	40.0	8.4	246.0	55.0	39.4	26.8	0.72	0.67
			Average	41.5				40.1			

Analysis conducted using a failure criterion of reaching the K_f line in p'-q space

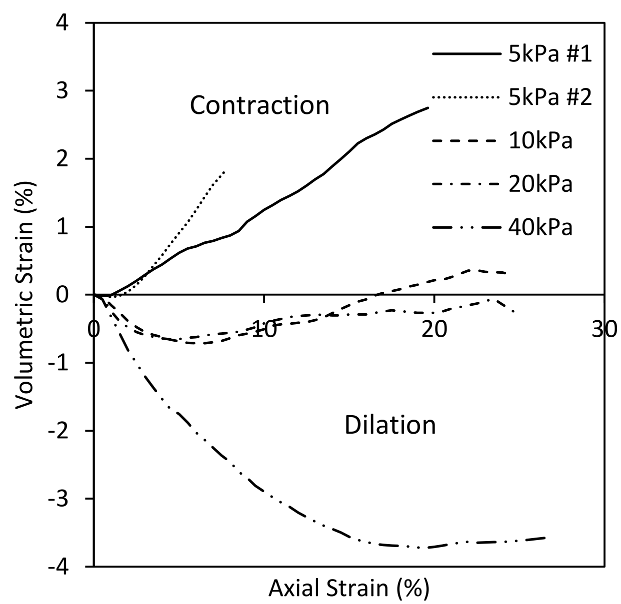

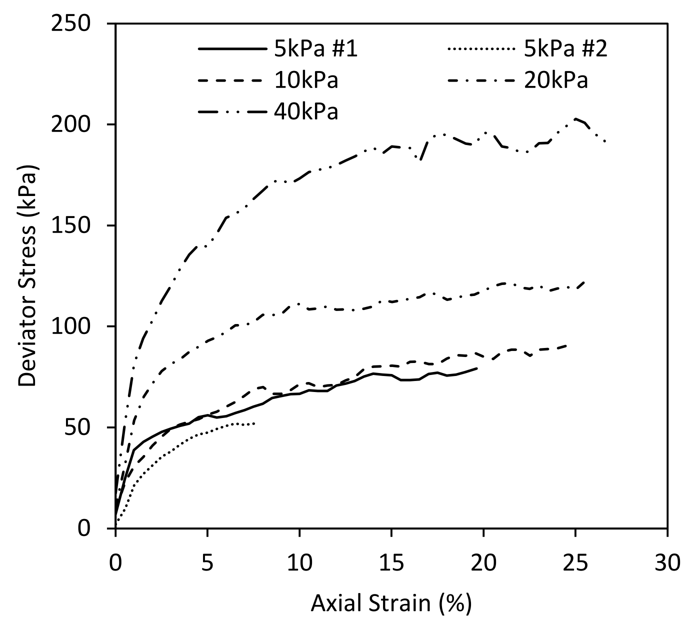

Waste Rock Summary: Drained Tests (Continued)

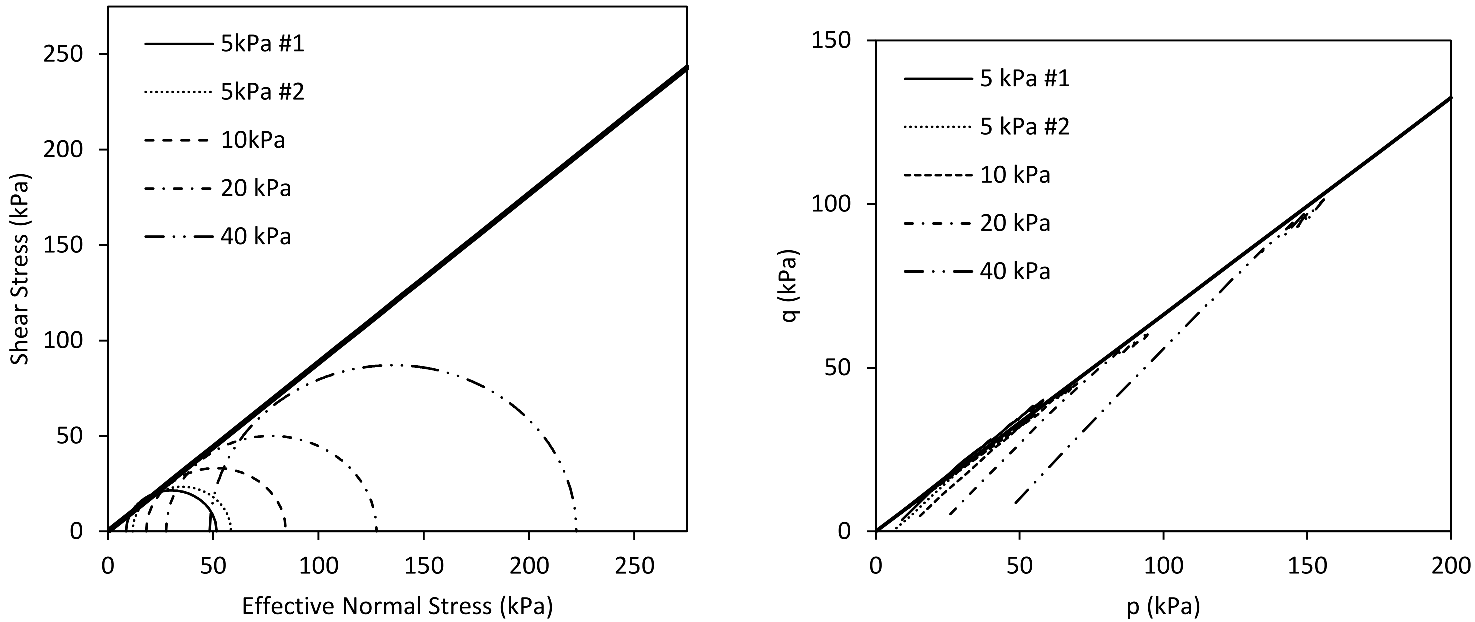

Waste Rock Summary: Undrained Tests

Target σ_c' (kPa)	σ_c' (kPa)	σ_{1f}' (kPa)	σ_{3f}' (kPa)	ϕ_p'	ε_{af} (%)	A_f	σ_{1cs}' (kPa)	σ_{3cs}' (kPa)	ϕ_{cs}'	ε_{ae} (%)	A_e	e_r
5	6.30	56.8	14.5	36.4	10.5	-0.11	71.1	19.1	35.2	19.7	-0.15	0.68
10	12.60	64.0	15.2	38.1	2.7	-0.03	105.5	26.5	36.8	26.4	-0.11	0.76
20	22.82	102.2	27.0	35.6	7.1	-0.02	131.2	37.0	34.1	26.2	-0.09	0.72
40	42.50	96.0	23.6	37.3	4.0	0.29	109.2	30.3	34.5	26.8	0.23	0.71
			Average	36.9					35.2			

Analysis conducted using a failure criterion of reaching the K_f line in p'-q space

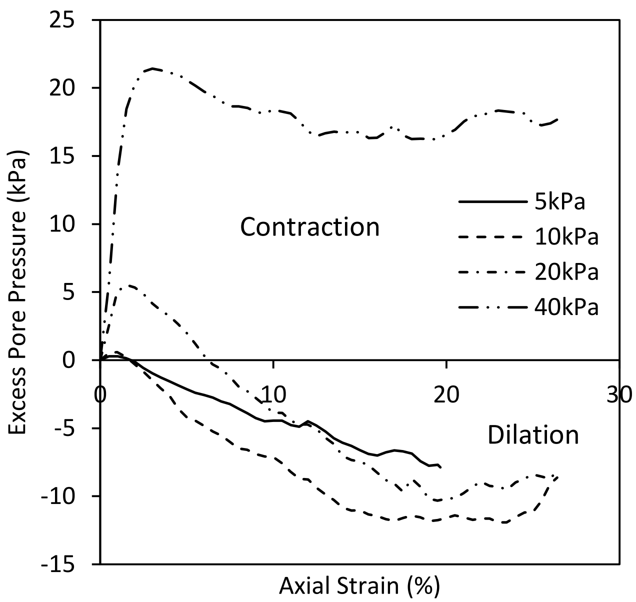

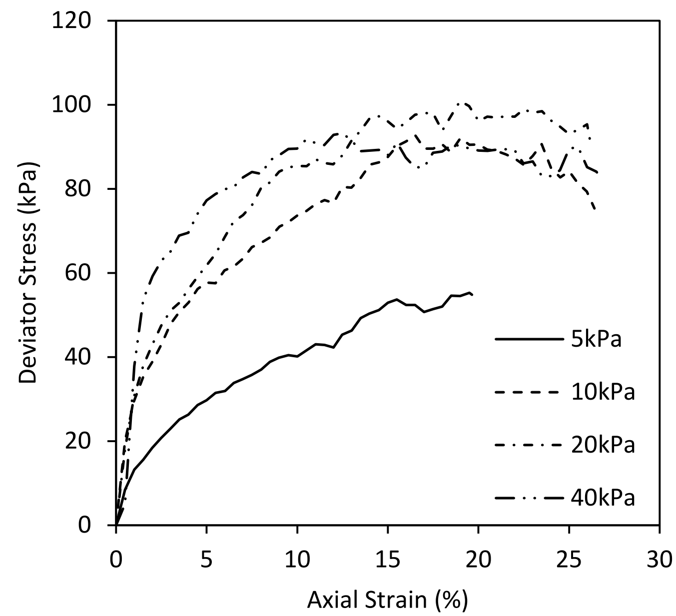

Waste Rock Summary: Undrained Tests (Continued)

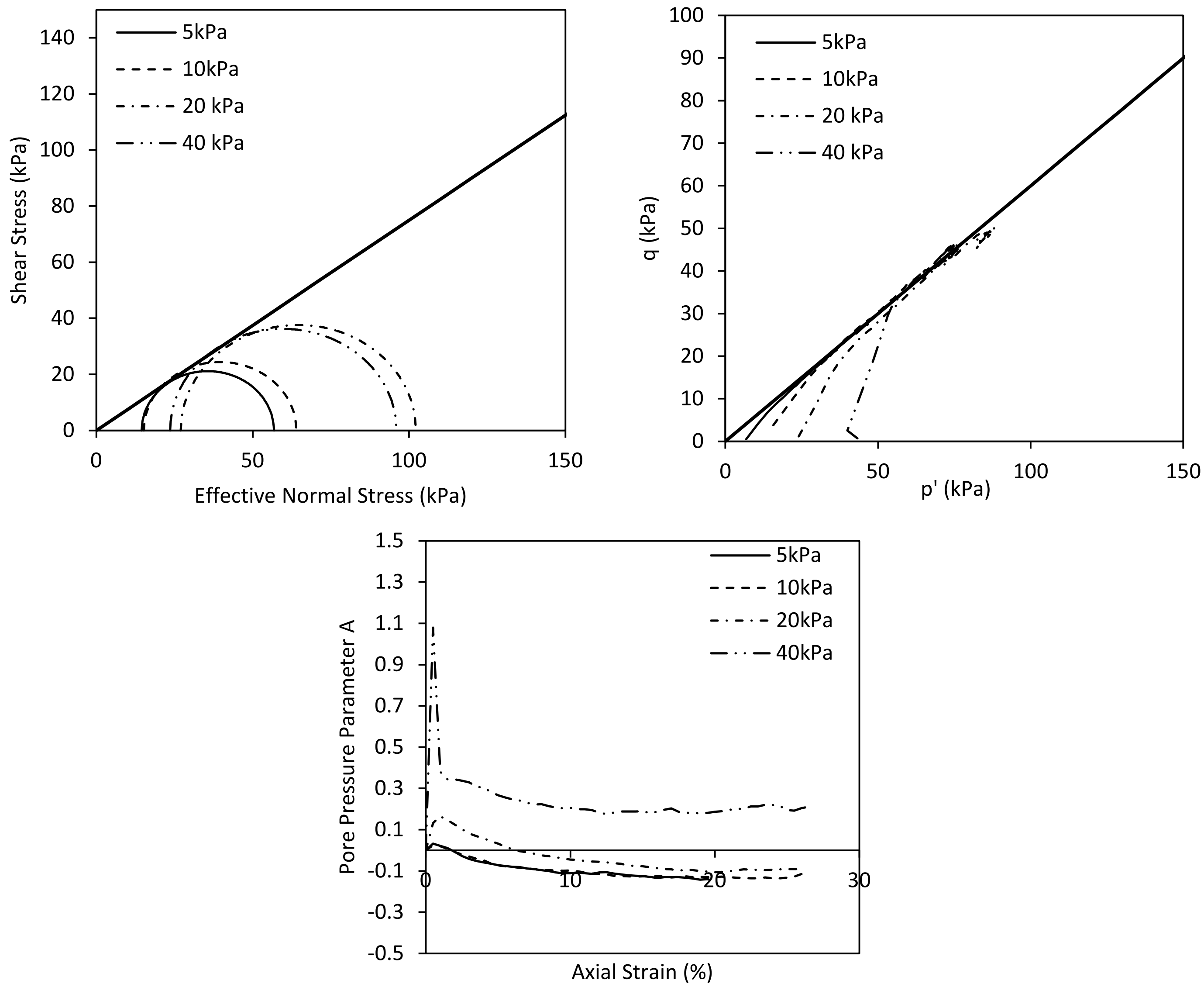

Fine-Garnet Tailings Summary

Target σ_c' (kPa)	σ_c' (kPa)	σ_{1f}' (kPa)	σ_{3f}' (kPa)	ϕ_p'	ε_{af} (%)	A_f	σ_{1cs}' (kPa)	σ_{3cs}' (kPa)	ϕ_{cs}'	ε_{ae} (%)	A_e	e
5	4.28	19.4	4.9	36.6	10.0	-0.13	37.6	10.3	34.7	20.0	-0.29	0.76
10	9.84	25.2	7.2	33.9	11.3	0.11	46.0	13.3	33.5	23.6	-0.13	0.72
20	20.00	78.8	19.6	37.0	11.8	0.00	123.1	30.7	36.9	20.0	-0.13	0.70
40	40.01	96.4	24.6	36.3	10.8	0.18	258.9	70.7	34.8	25.0	-0.18	0.65
			Average	36.0					35.0			

Analysis conducted using a failure criterion of reaching the K_f line in p'-q space

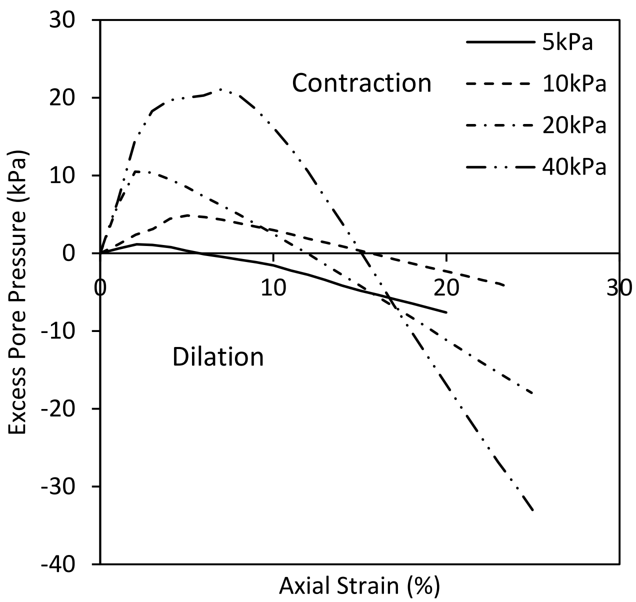

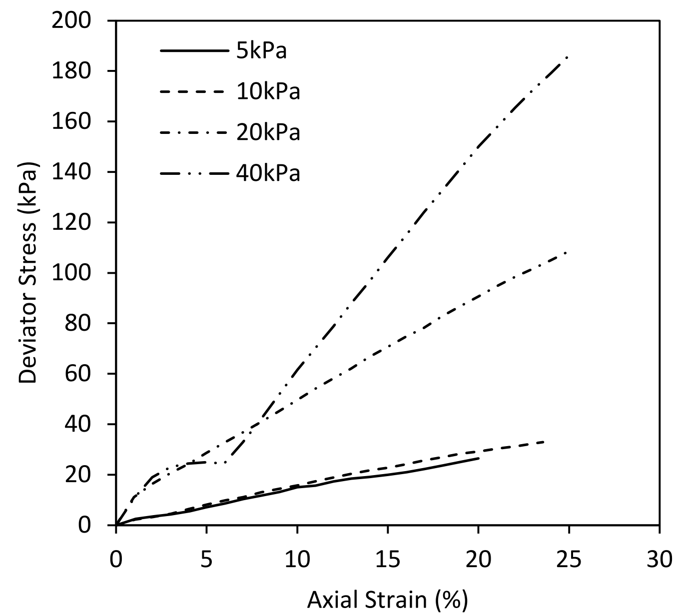

Fine-Garnet Tailings Summary (Continued)

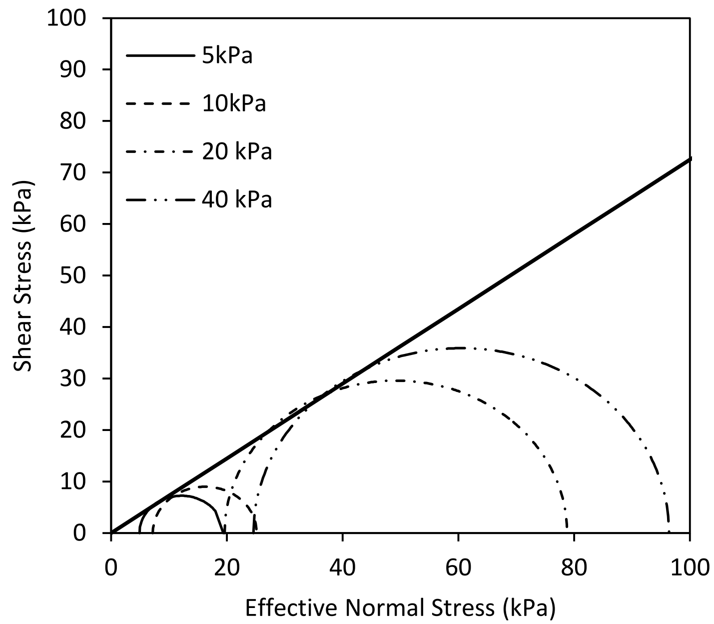

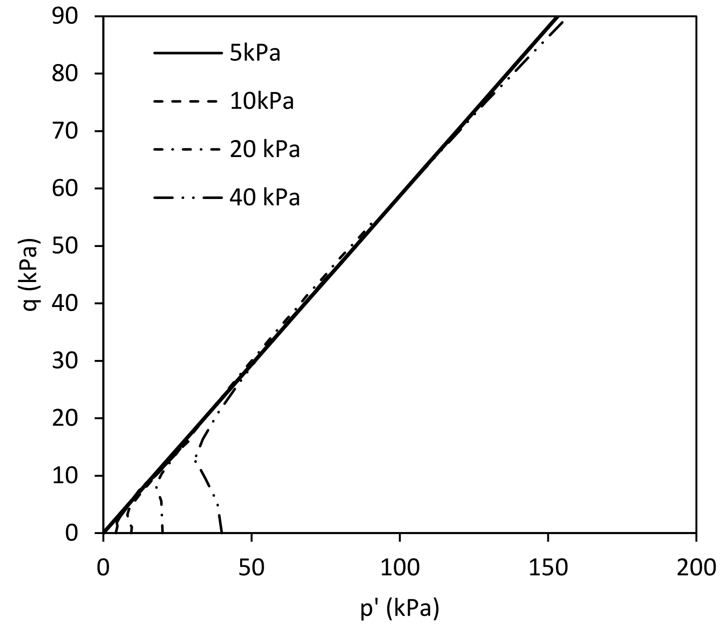

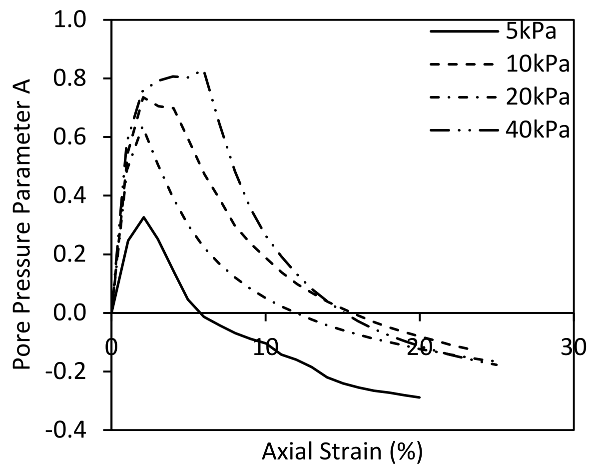

Coarse-Garnet Tailings Summary

Target σ_c' (kPa)	σ_c' (kPa)	σ_{1f}' (kPa)	σ_{3f}' (kPa)	ϕ_p'	ε_{af} (%)	A_f	σ_{1cs}' (kPa)	σ_{3cs}' (kPa)	ϕ_{cs}'	ε_{ae} (%)	A_e	e
5	4.70	42.4	8.7	41.2	6.2	-0.11	81.2	18.5	38.9	14.4	-0.22	0.67
10	10.04	45.1	10.6	38.3	6.3	-0.08	485.7	130.1	35.3	25.0	-0.34	0.70
20 #1	20.04	584.8	121.8	40.9	5.7	-0.22	1238.0	278.4	39.3	12.5	-0.27	0.61
20 #2	20.22	437.7	96.4	39.7	4.4	-0.15	1389.2	334.9	37.7	15.3	-0.27	0.60
40	39.93	300.4	68.1	39.1	5.9	-0.12	906.0	233.0	36.2	24.9	-0.29	0.64
			Average	39.8					37.5			

Analysis conducted using a failure criterion of reaching the K_f line in p'-q space

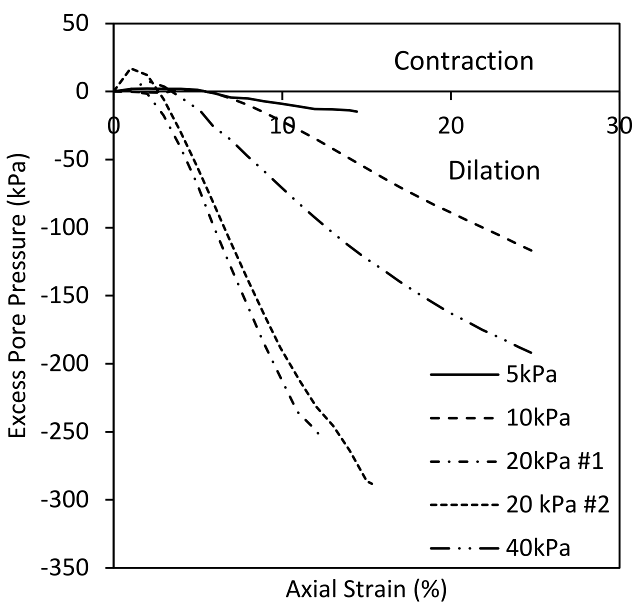

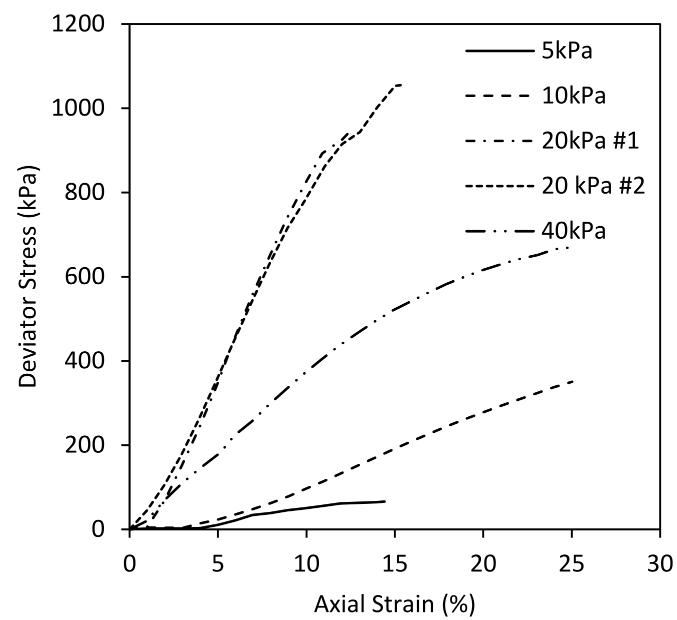

Coarse-Garnet Tailings Summary (Continued)

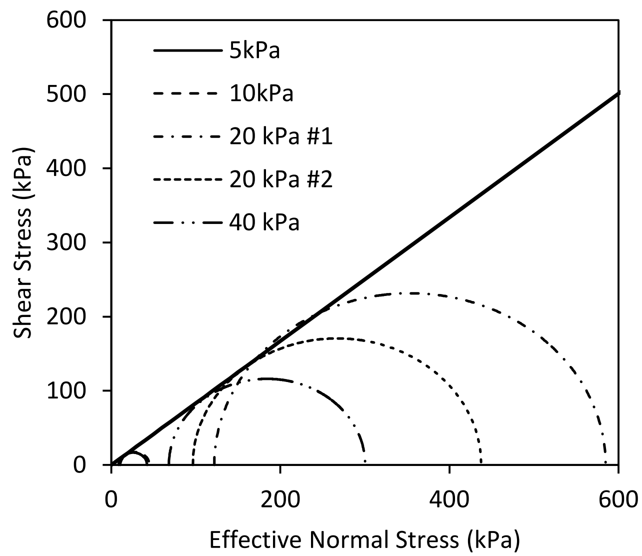

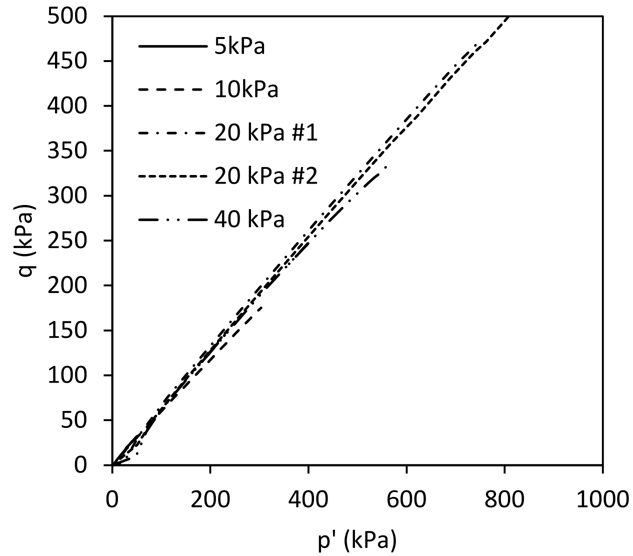

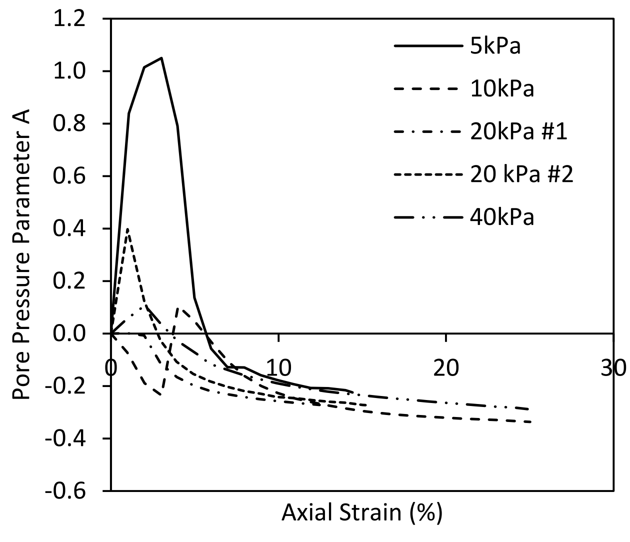

Copper Tailings Summary

Target σ_c' (kPa)	σ_c' (kPa)	σ_{1f}' (kPa)	σ_{3f}' (kPa)	ϕ_p'	ε_{af} (%)	A_f	σ_{1cs}' (kPa)	σ_{3cs}' (kPa)	ϕ_{cs}'	ε_{ae} (%)	A_e	e
5	5.05	13.6	3.6	35.9	11.2	0.11	20.9	6.1	33.4	24.9	-0.09	0.71
10	9.93	19.6	5.6	34.0	5.3	0.28	43.3	14.3	30.2	24.4	-0.19	0.66
20	19.92	29.8	8.0	35.3	5.7	0.52	64.1	18.4	33.7	25.0	0.01	0.64
40	39.91	98.5	25.4	36.1	8.9	0.19	175.5	50.5	33.6	24.9	-0.09	0.62
			Average	35.3					32.7			

Analysis conducted using a failure criterion of reaching the K_f line in p'-q space

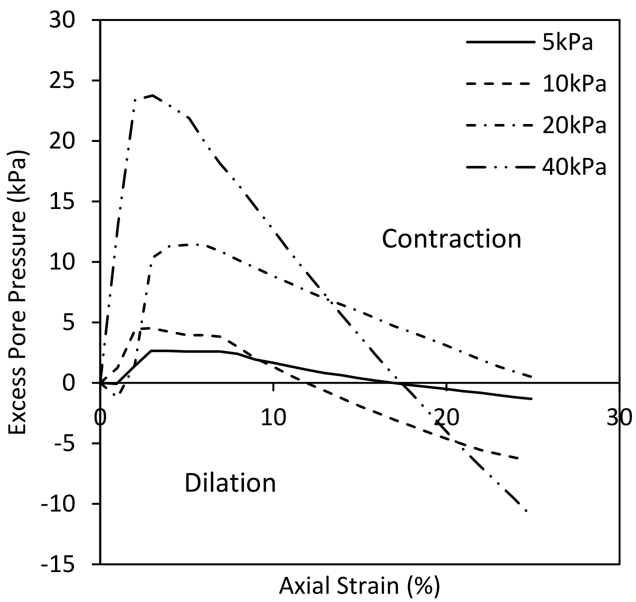

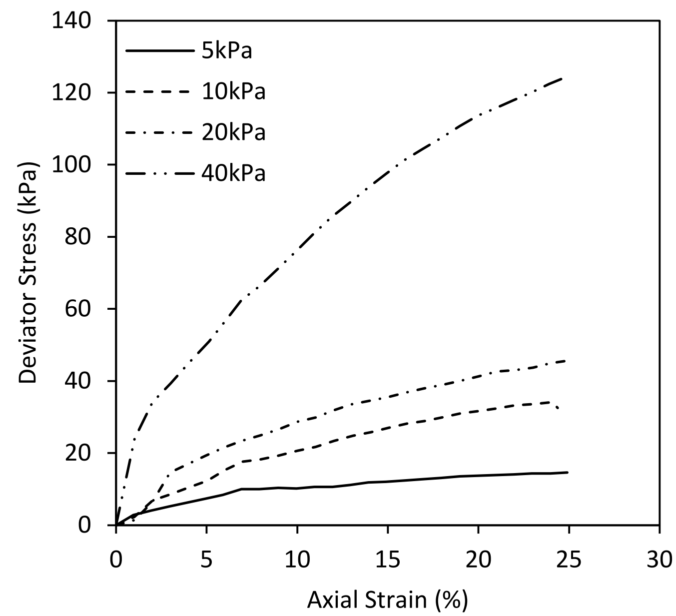

Copper Tailings Summary (Continued)

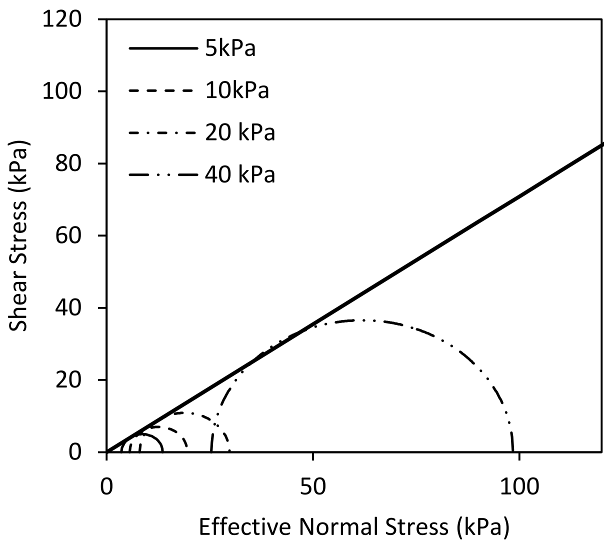

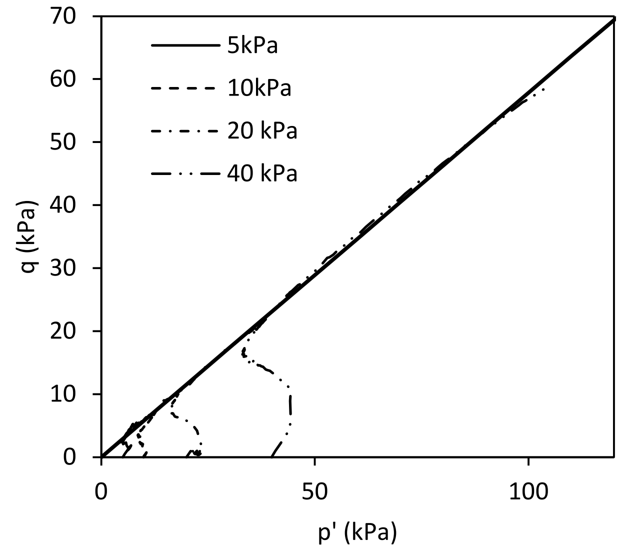

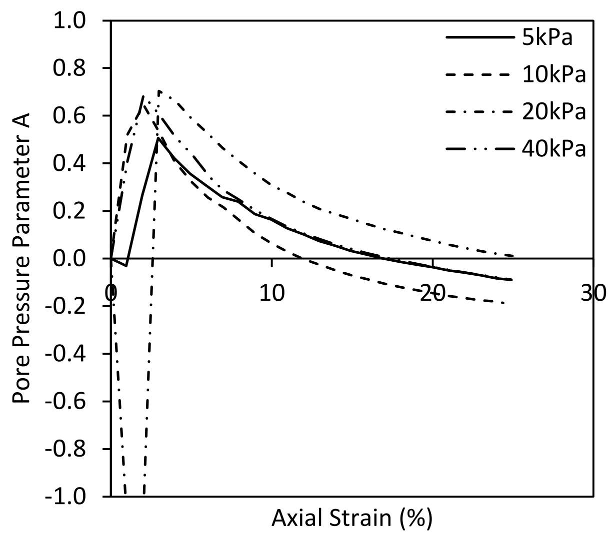

Soda Ash Tailings Summary

Target σ_c' (kPa)	σ_c' (kPa)	σ_{1f}' (kPa)	σ_{3f}' (kPa)	ϕ_p'	ε_{af} (%)	A_f	σ_{1cs}' (kPa)	σ_{3cs}' (kPa)	ϕ_{cs}'	ε_{ae} (%)	A_e	e
5	4.95	11.7	2.5	40.6	3.3	0.26	5.5	0.7	49.9	23.9	0.80	1.50
10 #1	12.01	20.5	6.1	32.8	6.6	0.38	12.2	4.5	27.5	32.3	0.98	1.33
10 #2	12.29	18.5	5.8	31.6	7.54	0.52	15.9	5.2	30.5	19.8	0.67	1.32
10 #3	10.03	18.9	2.5	50.3	15.1	0.44	17.4	2.4	49.4	15.8	0.48	1.31
20	19.78	24.0	4.2	44.5	15.4	0.79	22.0	4.6	40.8	19.3	0.86	1.24
40	39.13	59.3	9.9	45.5	12.6	0.59	54.1	9.7	44.2	20.5	0.66	1.11
			Average	45.2					46.1			

Analysis conducted using a failure criterion of reaching the K_f line in p'-q space

Average excludes the 10 kPa Tests #1-2

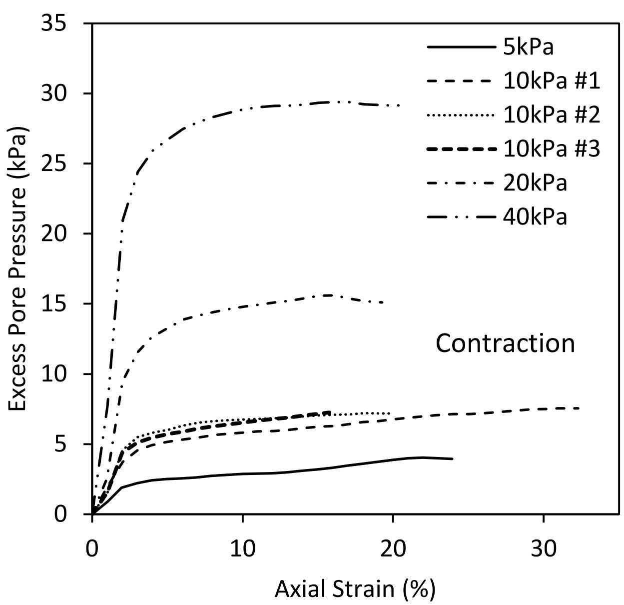

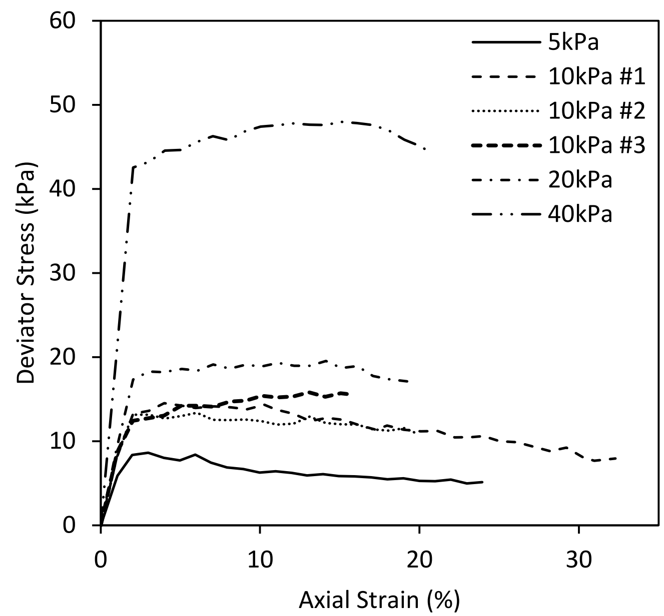

Soda Ash Tailings Summary (Continued)

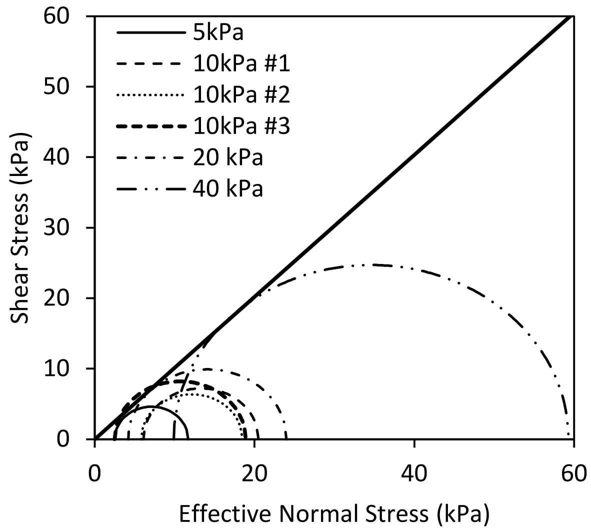

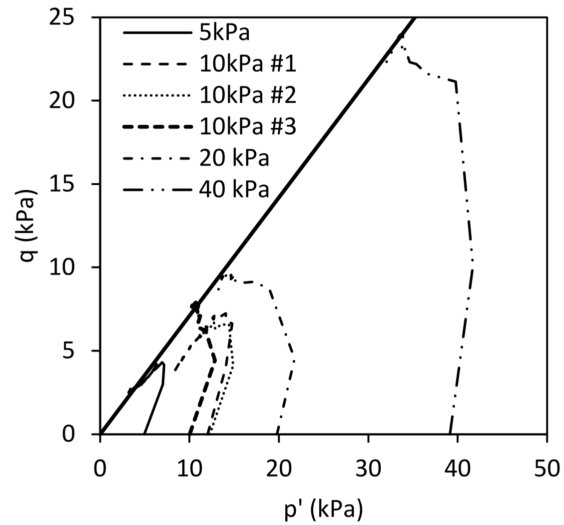

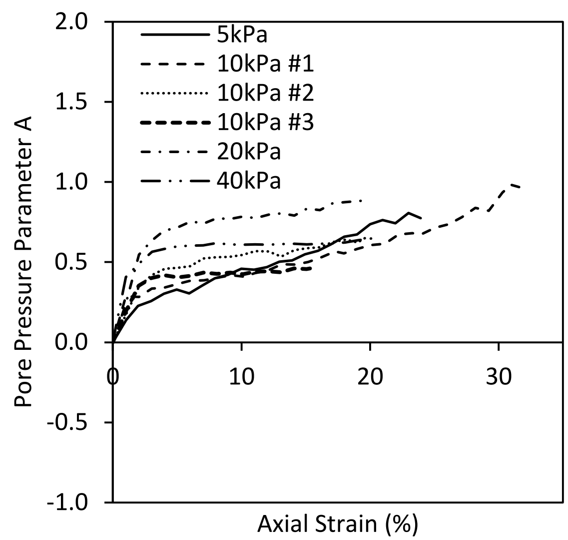

Fine-Garnet Mixtures Summary

Target σ_c' (kPa)	σ_c' (kPa)	σ_{1f}' (kPa)	σ_{3f}' (kPa)	ϕ_p'	ε_{af} (%)	A_f	σ_{1cs}' (kPa)	σ_{3cs}' (kPa)	ϕ_{cs}'	ε_{ae} (%)	A_e	e_r
5	6.78	80.2	17.5	39.9	6.0	-0.13	163.7	35.6	40.0	25.7	-0.18	0.75
10	13.39	100.1	21.2	40.6	2.5	-0.08	375.0	90.0	37.8	21.6	-0.25	0.91
20	22.71	112.9	23.9	40.6	2.8	0.01	333.5	71.2	40.4	24.4	-0.16	0.91
40	43.97	229.7	49.2	40.3	2.4	-0.02	759.4	189.9	36.9	25.0	-0.25	0.71
			Average	40.4					38.8			

Analysis conducted using a failure criterion of reaching the K_f line in p'-q space

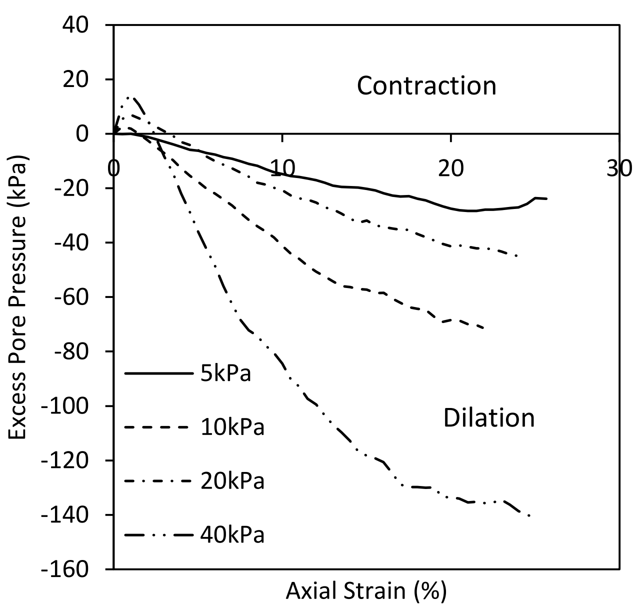

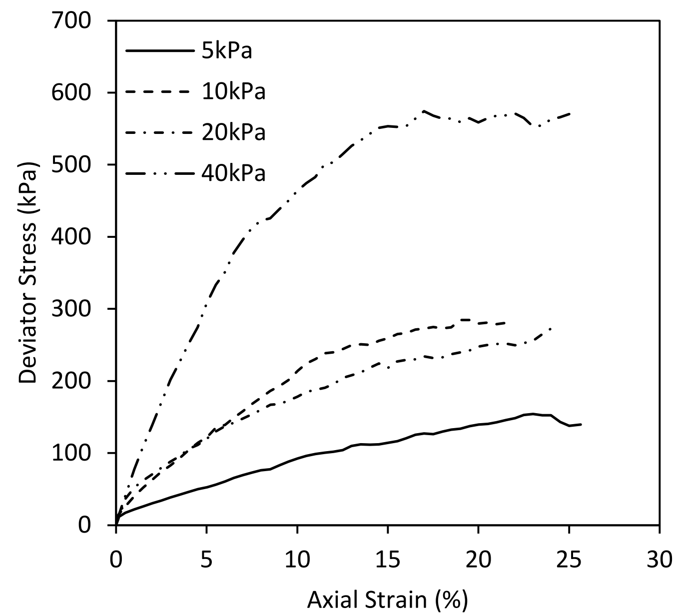

Fine-Garnet Mixtures Summary (Continued)

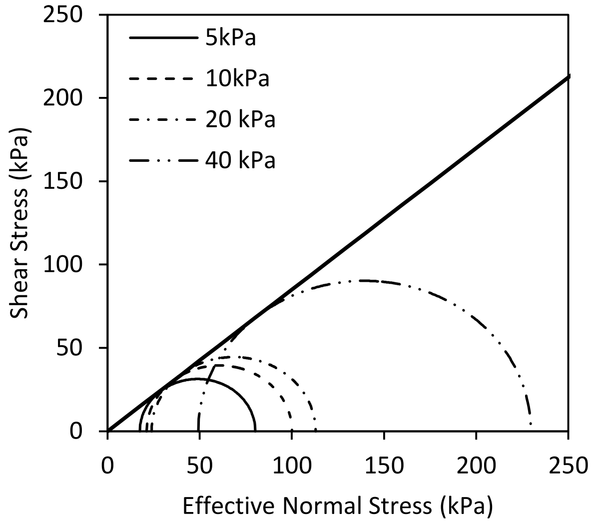

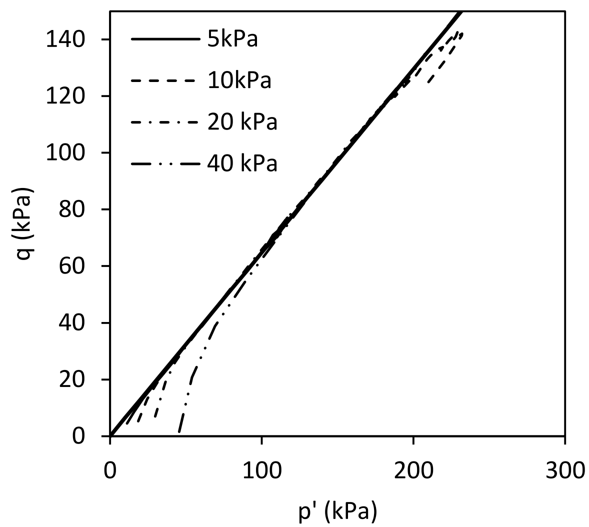

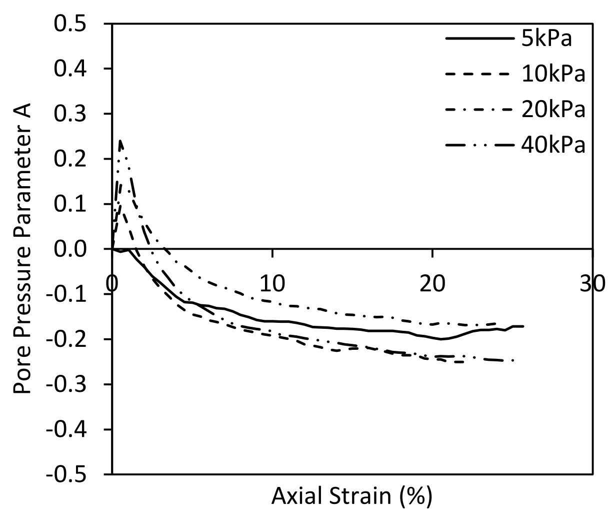

Coarse-Garnet Mixtures Summary

Target σ_c' (kPa)	σ_c' (kPa)	σ_{1f}' (kPa)	σ_{3f}' (kPa)	ϕ_p'	ε_{af} (%)	A_f	σ_{1cs}' (kPa)	σ_{3cs}' (kPa)	ϕ_{cs}'	ε_{ae} (%)	A_e	e_r
5	8.31	91.7	18.6	41.5	3.8	-0.11	191.3	42.3	39.7	24.9	-0.19	0.63
10	12.94	120.1	28.8	37.8	21.8	-0.12	117.8	30.3	36.2	24.8	-0.14	0.61
20	23.14	97.3	24.0	37.1	5.4	0.02	126.0	33.7	35.3	28.4	-0.05	0.62
40	40.56	146.0	31.4	40.3	3.8	0.10	186.7	42.1	39.2	30.0	0.03	0.63
			Average	39.2					37.6			

Analysis conducted using a failure criterion of reaching the K_f line in p'-q space

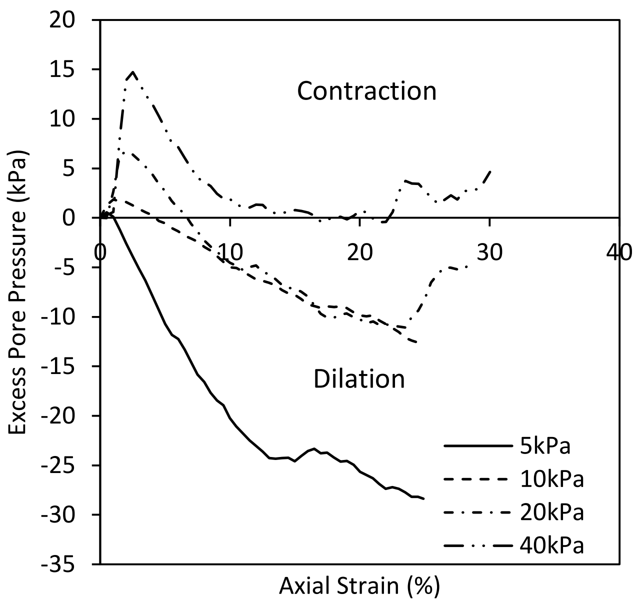

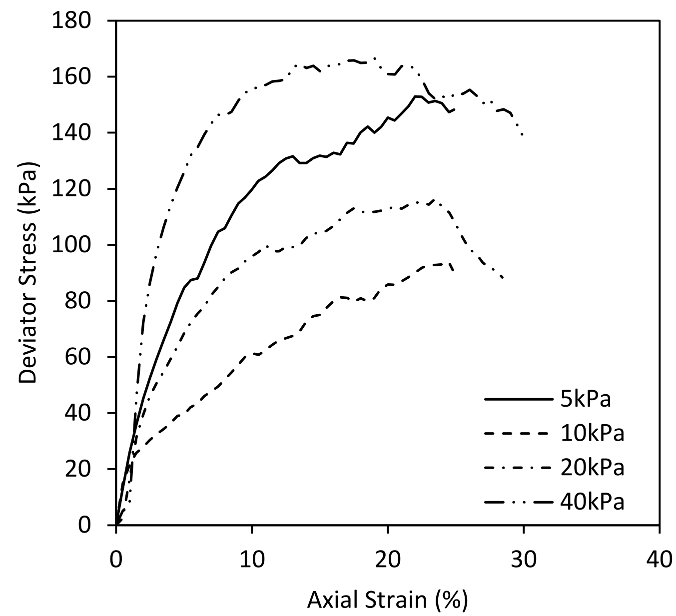

Coarse-Garnet Mixtures Summary (Continued)

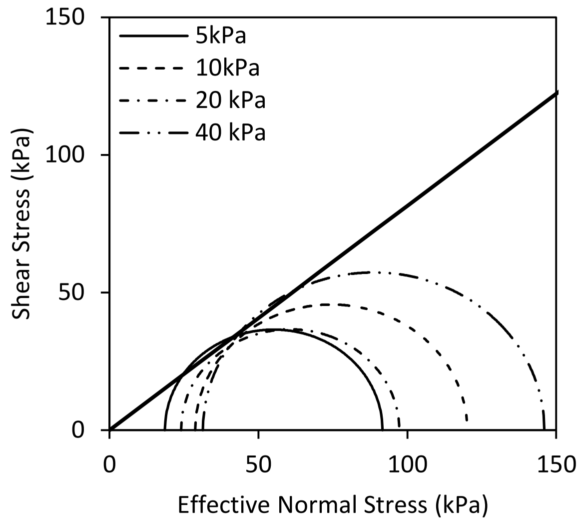

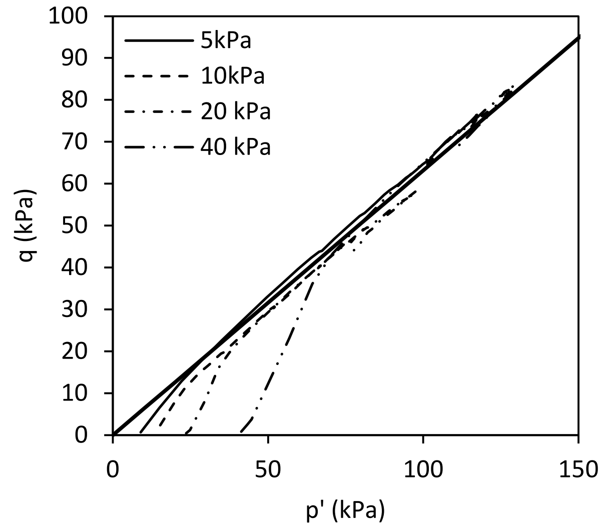

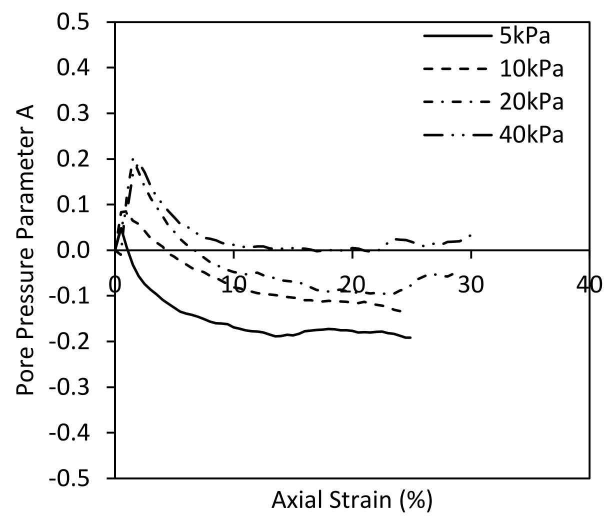

Copper Mixtures Summary

Target σ_c' (kPa)	σ_c' (kPa)	σ_{1f}' (kPa)	σ_{3f}' (kPa)	ϕ_p'	ε_{af} (%)	A_f	σ_{1cs}' (kPa)	σ_{3cs}' (kPa)	ϕ_{cs}'	ε_{ae} (%)	A_e	e_r
5	7.96	79.5	17.9	39.2	3.3	-0.13	252.8	61.2	37.6	23.3	-0.25	0.83
10	12.75	139.6	28.8	41.1	4.0	-0.13	397.8	83.2	39.1	23.4	-0.23	0.75
20	23.66	204.0	45.0	39.7	4.7	-0.12	328.5	77.2	38.3	19.5	-0.20	0.76
40	43.27	255.2	58.4	38.9	5.7	-0.07	427.0	105.2	37.2	22.1	-0.18	0.77
			Average	39.7					38.1			

Analysis conducted using a failure criterion of reaching the K_f line in p'-q space

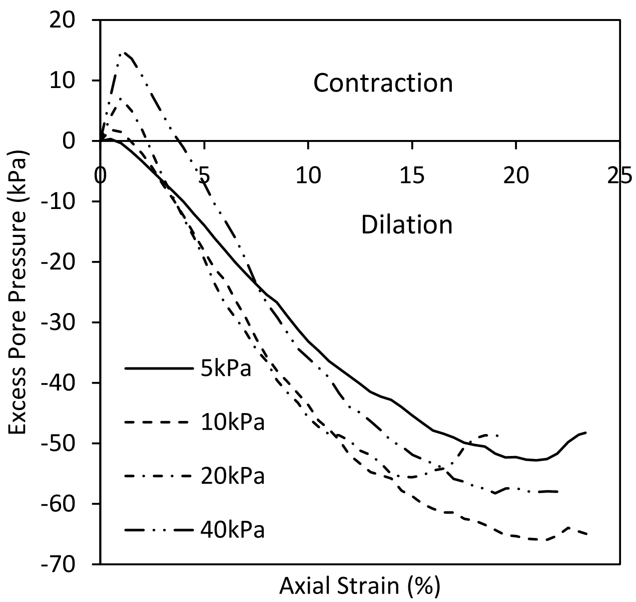

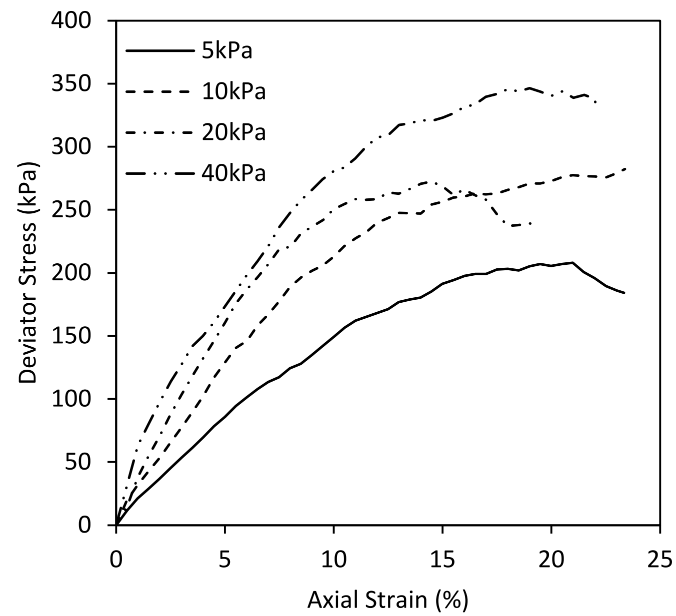

Copper Mixtures Summary (Continued)

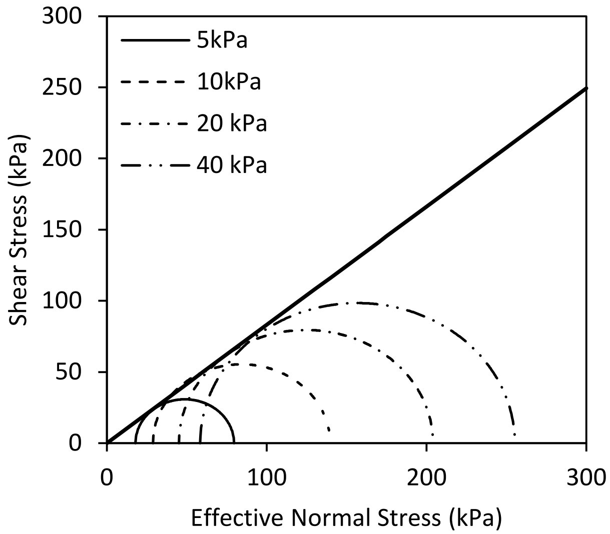

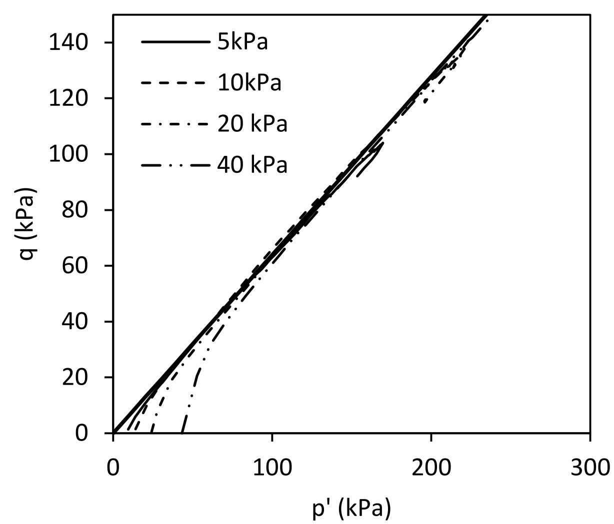

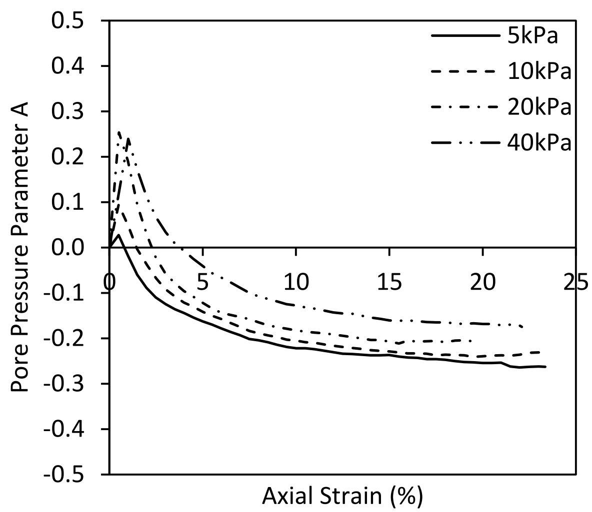

Soda Ash Mixtures Summary

Target σ_c' (kPa)	σ_c' (kPa)	σ_{1f}' (kPa)	σ_{3f}' (kPa)	ϕ_p'	ε_{af} (%)	A_f	σ_{1cs}' (kPa)	σ_{3cs}' (kPa)	ϕ_{cs}'	ε_{ae} (%)	A_e	e_r
5	8.38	79.3	19.3	37.5	6.5	-0.14	105.1	23.1	39.8	19.4	-0.12	0.78
10	12.13	131.5	32.7	37.0	9.7	-0.17	176.6	47.1	35.4	21.6	-0.23	0.64
20	22.76	89.7	22.3	37.0	4.1	0.04	148.1	41.2	34.4	19.0	-0.13	0.81
40	43.38	138.6	33.7	37.5	7.7	0.12	170.3	43.8	36.2	24.2	0.04	0.78
			Average	37.3					36.5			

Analysis conducted using a failure criterion of reaching the K_f line in p'-q space

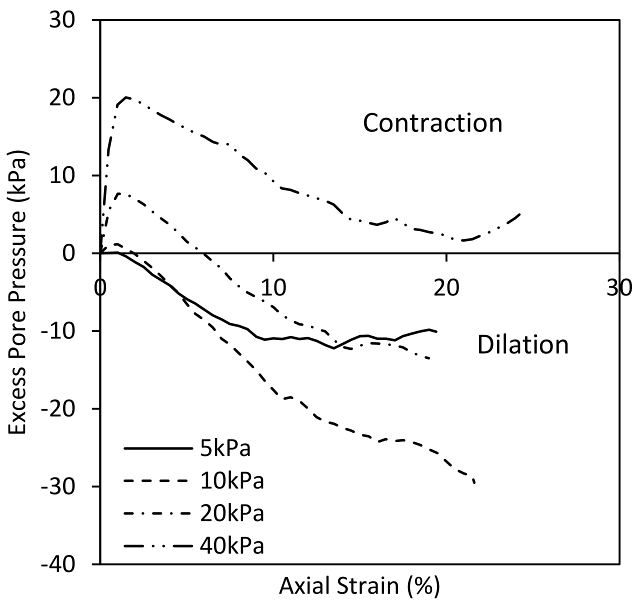

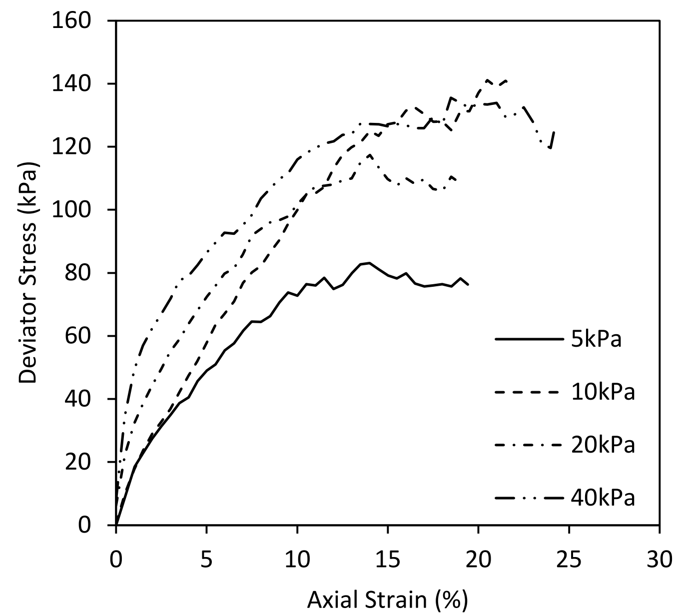

Soda Ash Mixtures Summary (Continued)

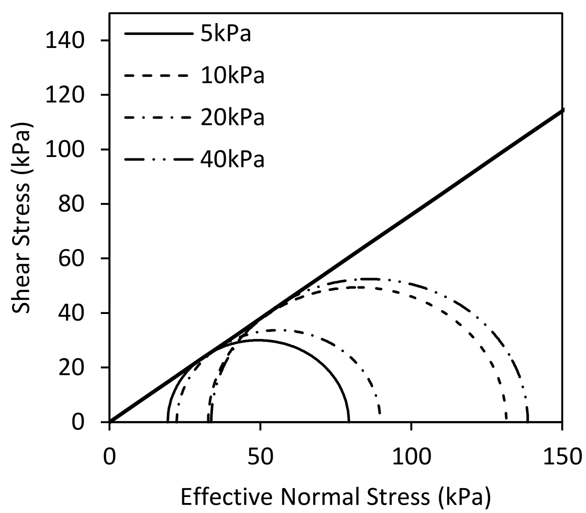

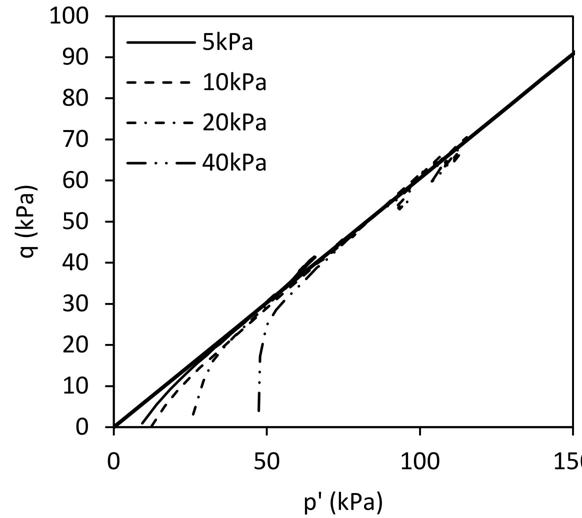

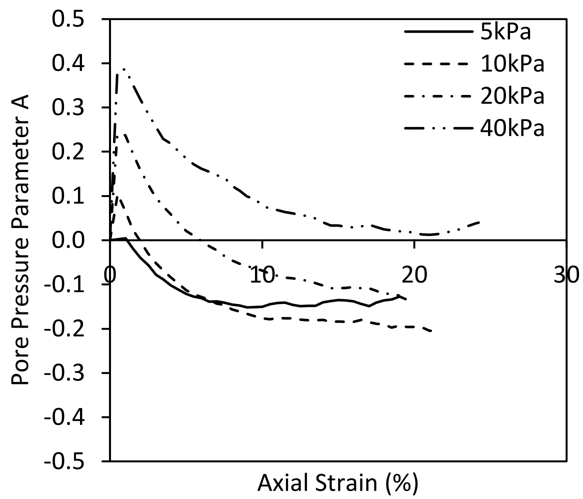

APPENDIX F: DETERMINING MIXTURE RATIO FOR FINE-GRAINED GARNET MIXTURES

The mixture ratio (*R*) for the first three triaxial compression specimens of fine-grained garnet tailings mixed with waste rock (tests performed at effective confining stresses of 5, 10, and 20 kPa) was determined differently than for the other waste rock and tailings (WR&T) specimens due to a lack of data for mass of tailings and mass of waste rock. The mixture ratio for the other WR&T mixtures was calculated by dividing the mass of waste rock by the mass of tailings (as stated in Section 2.4). However, the exact masses of waste rock and tailings present in the fine-garnet mixture specimens after preparation were not recorded. To determine the actual *R* of the specimens, the mixture is assumed to be at the optimum mixture ratio (R_{opt}) when the material is placed into the specimen mold. This assumption was verified for copper tailings and waste rock mixtures by calculating *R* after mixing and before placement into the mold. The total mass of the mixture specimen placed in the mold and the mass of the tailings slurry displaced by the WR&T mixture was recorded for each mixture specimen, including the first three fine-garnet mixture specimens. Using the total specimen mass in the mold and the mass of tailings slurry remaining in the mold after displacement, the mixture ratio was re-calculated assuming the mixture was placed at R_{opt}.

The mass of tailings (M_t) in the specimen placed in the mold can be calculated using Eq. F.1:

$$M_t = \frac{M_b}{R_{opt} + w_t + 1} \qquad \text{Eq. (F.1)}$$

where M_b = bulk mass of the specimen (includes waste rock, tailings, and water) and w_t = water content of the tailings. The mass of waste rock (M_r) can then be determined using M_t and R_{opt} as follows:

$$M_r = R_{opt} \cdot M_t \qquad \text{Eq. (F.2)}$$

The actual value of R can be found by adding the net amount of tailings slurry remaining in the mold:

$$R = \frac{M_t \pm M_{t,slurry}}{M_r} \qquad \text{Eq. (F.3)}$$

where $M_{t,slurry}$ = mass of tailings in displacement slurry added to or removed from the specimen mold. The error introduced by assuming the placed WR&T mixture is at R_{opt} is negligible as stated previously. The mixture ratio calculated for copper tailings and waste rock mixtures differed from R_{opt} by at most 0.17, which corresponds to an error of approximately 5 %.